E. ARKAN

IZMIR KATIP CELEBI UNIVERSITY

2019

IZMIR KATIP CELEBI UNIVERSITY

GRADUATE SCHOOL OF NATURAL AND APPLIED SCIENCES

DEVELOPMENT OF NOVEL DONOR AND ACCEPTOR SAM MOLECULES FOR PHOTOVOLTAIC APPLICATIONS

Ph.D. THESIS

Emre ARKAN

Department of Materials Science and Engineering

AUGUST 2019

IZMIR KATIP CELEBI UNIVERSITY
GRADUATE SCHOOL OF NATURAL AND APPLIED SCIENCES

DEVELOPMENT OF NOVEL DONOR AND ACCEPTOR SAM MOLECULES FOR PHOTOVOLTAIC APPLICATIONS

Ph.D. THESIS

Emre ARKAN
(D120111002)

Department of Materials Science and Engineering

Thesis Advisor: Prof. Dr. Şerafettin DEMİÇ

AUGUST 2019

İZMİR KATİP ÇELEBİ ÜNİVERSİTESİ

FEN BİLİMLERİ ENSTİTÜSÜ

FOTOVOLTAİK UYGULAMALAR İÇİN YENİ NESİL DONÖR VE AKSEPTÖR KENDİLİĞİNDEN ORGANİZE TEK KATMAN MOLEKÜLLERİN GELİŞTİRİLMESİ

DOKTORA TEZİ

Emre ARKAN
(D120111002)

Malzeme Bilimi ve Mühendisliği Ana Bilim Dalı

Tez Danışmanı: Prof. Dr. Şerafettin DEMİÇ

AĞUSTOS 2019

Emre ARKAN, a **/PhD** student of **IKCU Graduate School Of Natural And Applied Sciences**, successfully defended the thesis entitled "**DEVELOPMENT OF NOVEL DONOR AND ACCEPTOR SAM MOLECULES FOR PHOTOVOLTAIC APPLICATIONS**", which he prepared after fulfilling the requirements specified in the associated legislations, before the jury whose signatures are below.

Thesis Advisor :

Prof. Dr. Şerafettin DEMİÇ .....
İzmir Katip Çelebi University

Jury Members :

Assoc. Prof. Dr. Mustafa CAN .....
İzmir Katip Çelebi University

Prof. Dr. Ceylan ZAFER .....
Ege University

Assoc. Prof. Dr. Faruk ÖZEL .....
Karamanoğlu Mehmetbey University

Assoc. Prof. Dr. Fethullah GÜNEŞ .....
İzmir Katip Çelebi University

Date of Submission : 01.07.2019
Date of Defense : 01.08.2019

To my family,

FOREWORD

I would like to grant special appreciation to my supervisor Professor Dr. Şerafettin Demiç for giving me such a great thesis opportunity. He was always ready to listen to me when I had inquiries regarding my thesis work. I gained the scientific working principle from him. He always guided me during the thesis period and also gave valuable suggestions regarding my career.

I want to express profound thanks to Assoc. Prof. Dr. Mustafa Can. He was all the time available for my questions. He was very helpful and friendly. Our discussions were indeed beneficial for the progress and improvement of the thesis work. He always followed my thesis work and also the thesis report from the very beginning to the end.

I am very much thankful to Assoc. Prof. Dr. Cem Tozlu for supporting my thesis work. He opened his laboratory to me and collaborates with us for device fabrication part of thesis. Moreover, he was available all the time for the deep discussion in device physics as well as has guided me to properly shape my thesis.

I am very much thankful to my friends Eyüp Yalçın and Muhittin Ünal for their kind and valuable help as well as for making my lab work joyful and exciting.

Exclusive gratitude goes to my wife; Mesude Zeliha Arkan, whose existence always reminds me importance of the life. Even though we had been away from each other in some part of our life, her presence is more than enough for me to get motivated and being successful.

I am also grateful to my parents. They have been always with for all my life that I became who I am today. They have always believed and motivated me to set out on my own path. So far, I have learned a lot from them and I believe that I will keep learning from them in the rest of my life.

August 2019 Emre ARKAN

TABLE OF CONTENTS

Page

ABBREVIATIONS

ITO	**:** Indium Tin Oxide
SAM	**:** Self Assembled Monolayer
V_{OC}	**:** Open Circuit Voltage
J_{SC}	**:** Short Circuit Current Density
FF	**:** Fill Factor
NMR	**:** Nuclear Magnetic Resonance
CV	**:** Cyclic Voltammetry
AFM	**:** Atomic Force Microscopy
KPFM	**:** Kelvin Probe Force Microscopy
CPD	**:** Contact Potential Difference
SEM	**:** Scanning Electron Microscopy
XPS	**:** X-Ray Photoelectron Spectroscopy
XRD	**:** X-Ray Difraction
HTM	**:** Hole Transport Material
HTL	**:** Hole Transport Layer
ETM	**:** Electron Transport Material
PCE	**:** Power Conversion Efficiency
OPV	**:** Organic Photovoltaic
BHJ	**:** Bulk Heterojunction
DSSC	**:** Dye Sensitized Solar Cell
PSC	**:** Perovskite Solar Cell
PEDOT:PSS	**:** poly(3,4-ethylenedioxythiophene):poly(styrenesulfonate)
PCBM	**:** Phenyl-C61-Butyric Acid Methyl Ester
TLC	**:** Thin Layer Chromotography
MAI	**:** Methyl Ammonium Iodide
WF	**:** Work Function
HOMO	**:** Highest Occupied Molecular Orbital
$MAPbI_3$	**:** Methyl Ammonium Lead Iodide
EQE	**:** External Quantum Efficiency
PTFE	**:** Poly Tetra Fluoro Ethylene

LIST OF TABLES

Page

LIST OF FIGURES

Page

DEVELOPMENT OF NOVEL DONOR AND ACCEPTOR SAM MOLECULES FOR PHOTOVOLTAIC APPLICATIONS

ABSTRACT

Surface modification of indium tin oxide (ITO) is a crucial factor to alter the energy level barrier between ITO and perovskite that has direct influence on the charge extraction and recombination at interface. This phenomenon has further direct effect on device parameters such as open circuit voltage (V_{OC}), fill factor (FF), and short circuit current density (J_{SC}).

This study was base on the synthesis of six novel SAM molecules to be used in fabrication of p-i-n type perovskite solar cells. Since proposed SAMs are of push-pull type molecular nature, contiguous thiophene rings were used as conjugated units in spacer group due to the fact that thiophene has lower delocalization energy and provide superior conjugation than that of benzene. Moreover, donor and acceptor type terminal groups were chosen in the structure of SAM molecules to synergistically examine their effect on device performance.

The molecular structure of the synthesized molecules were proven by NMR spectroscopy and surface characteristics of modified ITO were achieved by various techniques including Kelvin Probe Force Microscopy (KPFM), atomic force microscopy (AFM), cyclic voltammetry (CV), X-ray photoelectron spectroscopy (XPS), X-ray diffraction (XRD), scanning electron microscopy (SEM). The most promising work function alignment was obtained when ITO surface was modified with a SAM molecule having the strongest donor terminal group.

Inverted perovskite solar cell devices were fabricated on surface modified ITO electrodes. The results of modification obtained with such molecular system reveal permanent changes in the work function of ITO, significant enhancement in hole collection and improvement in short circuit photocurrent density in perovskite based solar cells without further requirement of any materials to be used as HTM.

FOTOVOLTAİK UYGULAMALAR İÇİN YENİ NESİL DONÖR VE AKSEPTÖR KENDİLİĞİNDEN ORGANİZE TEK KATMAN MOLEKÜLLERİN GELİŞTİRİLMESİ

ÖZET

İndiyum kalay oksidin (ITO) yüzey modifikasyonu, perovskit ve ITO arasındaki enerji bariyerinin düzenlenmesi ile arayüzeydeki yüklerin ekstraksiyonu ve rekombinasyona direkt etkisi olan önemli bir faktördür. Bu olayın açık devre voltajı (V_{OC}), doldurma faktörü ve kısa devre akım yoğunluğu (J_{SC}) gibi cihaz parametreleri üzerinde doğrudan tesiri vardır.

Bu çalışma, p-i-n tipi perovskit güneş hücrelerinin üretiminde kullanılacak altı yeni KOT (SAM) molekülünün sentezine dayanmaktadır. Önerilen SAM'ler push-pull tipinde moleküler yapıya sahip olduklarından, bitişik tiyofen halkaları, tiyofenin daha düşük bir lokalizasyon enerjisine sahip olması ve benzenden daha üstün bir konjugasyon sağlaması nedeniyle ara gruptaki konjuge birimler olarak kullanılmıştır. Ayrıca, cihaz performansındaki sinerjik etkilerini incelemek üzere SAM molekülü yapısında elektron verici ve elektron çekici uç gruplar eklenmiştir.

Sentezlenen bileşiklerin moleküler yapıları NMR spektroskopisi ile aydınlatılmış ve modifiye edilmiş ITO'nun yüzey analizleri kelvin probe kuvvet mikroskobu (KPFM), atomik kuvvet mikroskobu (AFM), döngüsel voltametri (CV), X-ışını fotoelektron spektroskopisi (XPS), X-ışını kırınımı (XRD) ve taramalı elektron mikroskobu (SEM) ile yapılmıştır. ITO yüzeyi en güçlü elektron verici grup ile modifiye edildiğinde en dikkate çeken iş fonksiyonu elde edilmiştir.

Yüzeyi SAM molekülleri ile modifiye edilmiş ITO kaplı cam elektrotlar, p-i-n türü perovskit güneş hücrelerin üretiminde kullanılmıştır. Bu moleküler sistem ile modifikasyonun sonuçları olarak perovskit güneş hücresinde ek bir inorganik metal okside veya yarı iletken polimere ihtiyaç kalmadan ITO'nun iş fonksiyonunda kalıcı değişiklikler, boşluk toplamada önemli bir artış ve kısa devre akımında iyileşme ortaya çıkmıştır.

1. INTRODUCTION

Energy and environment are two interdependent crucial subjects in the 21th century and strongly related to the new global economic policy. Civilization of human beings has brought non-ignorable achievements in industrial progress nevertheless, the great efforts for building a civilization caused a dramatic decrease in non-renewable energy sources —and unfortunately— left an irrecoverable alteration in climate behind. Since the earth population has reached virtually 7.5 billion, more and more people utilize large amounts of energy than ever before everyday to make their lives healthier, richer, more proper and productive. As a result, over the last century, there is a dramatic augment in global energy consumption which finally achieved an apparent record of 8919 MTOE (million tonnes of oil equivalent) in the year of 2011 [1]. It is worse that the main portion of energy production, that is almost 66.4%, is still based on non-renewable energy sources such as coal crude oil and natural gas [2], where fossil based energy production has caused definite irreversible environmental impacts including air pollution and global warming. The report of International Panel on Climate Change (IPCC) states that global average temperature of Earth has increased by 0.5-0.8 ^{o}C since 1850 [3].

Without any decrease in global energy consumption, three major options are proposed to reduce CO_2 emission as a long-term alternative that are: nuclear power, carbon sequestration and sustainable energy [4]. As for the first method, today, almost 440 nuclear power reactors are operable around the world and they supply more than 11% of global energy demand. However, it offers temporary and inconvenient solution because of limited amount of uranium reserve and potential risks on reactors' operation. The second method, carbon sequestration, helps us to utilize energy from fossil fuels as long as we care about emissions and store them in accessible cavities in the earth. But unfortunately this method is regarded as an unsustainable solution and is an untested method in large scale which makes it uncertain to be worked with for future. As for the third method, sustainable energy, it can supply all required energy provided that we put remarkable effort to develop

existing and new technologies and therefore it is considered as the most favorable and also a long-term solution to be used [4]. From the point of view of energy consumption values, the levels are differently rising all around the world [5]. A notable example would be European countries where consumption levels are relatively stable. Namely, it is estimated to be kept around similar levels for the next 20 years according to the U.S. Energy Information Administration (EIA) [6]. In a long futural, the main requirement is to stop the worldwide increase in energy consumption that necessitates depletion in the world's energy exploitation at least in some regions or countries. Such depletion can be principally achieved through consuming the generated energy in a more effective way. In addition to the European Union (EU), some individual governments have also planned more advanced targets corresponding to their self-energy consumption and production. Namely, the following requirements have to be fulfilled until 2020 [7].

i. Emission of chemicals (i.e. Carbon dioxide, nitrogen oxides, methane etc.) that cause greenhouse have to be reduced by 20%
ii. 20% of energy demand should be supplied by renewable energy sources.
iii. Energy efficiency should be enhanced by 20% within the EU.

Besides to the above-mentioned expectation, EU has set more long-term goals that is greenhouse emission has to be decreased by 80% as well as consumption of energy has to be diminished by 30% until 2050. Further advanced objectives by five Nordic countries have been declared so that decrease in greenhouse emission is to be reached 85% [8].

Besides the aim of decreasing the consumption, the demand for new sources to generate more sustainable energy is also regarded as an essential dilemma. Thus, the phrase of ''sustainable energy source'' carries multiple meanings: that is, CO_2-free and renewable. Main group of such energy sources comprises geothermal energy, biomass-based energy, hydroelectric power, wave power, wind power and particularly sun energy. Although some of these technologies are quite advanced and being benefited by a few EU states like Nordic countries, remaining part of the world still insist on fossil fuels for energy production, unfortunately [8]. This unfavorable incident explains why research in renewable energy sources has been proposed as a crucial fact for sustainable future.

From the perspective of renewable energy, solar energy is defined as the merely unlimited source with huge potential [3]. It is produced as a consequence of constant fusion reaction inside the Sun and generated power is roughly 3.8×10^{23} kW/s. Upper atmosphere of the Earth only receives 1.7×10^{17} kW/s of radiated power. After the reflection of atmosphere and absorption of clouds, ultimate solar energy received by landmass and oceans is about 8.0×10^{16} kW/s, an enormous source of energy [9]. According to the International Energy Agency (IEA), the world's annual energy consumption is same as solar energy absorbed by earth in one hour, in 2012. Therefore, solar cells have recently illustrated a remarkably rapid growth due to its substantial potential [10]. In particular, solar cells with capacity of 139 GW had been installed all around the world until the beginning of 2014 [3]. Through solar cell technologies, absorbed radiation, without any material consumption, can be converted to the most useful form of energy, electricity.

1.1 Photovoltaic Cells

Photovoltaic devices are recognized as the easiest way to convert solar energy directly into electricity. Daryl Chapin et al. developed the first practical p-n junction PVs at Bell Laboratory in 1954, known as the first generation solar cell, and reached power conversion efficiency (PCE) of 6% [11]. The working mechanism of solar cell is quite simple. When the solar cell is illuminated, the front and back sides obtain different charges and this fact turns solar cell into a battery. Basically, there are two principles to explain this effect. The first one is associated with electrons in solar cell that absorbs incoming light. Namely, the electrons are promoted to a higher energy level while leaving oppositely charged particles behind them. These oppositely charged particles move in inverse directions related to the formation of electric field in solar cell's panels. Hence, inversely charged front and back sides are emerged. Whenever these oppositely charged sides are connected to each other via a conductor, a continuous electric current flow takes place. When the electricity is utilized by a load, the electrons come back to solar cell, through the current flow but at lower energy levels, and the circulation become repeatable. This phenomenon is continuously repeated as long as solar cell is subjected to illumination [4].

In today's commercial system, over 90% of solar market is dominated by crystalline or polycrystalline silicon (Si) modules. The essential reasons of this domination are

related to their high power conversion efficiency and good long-term stability. Moreover, a substantial amount of silicon is reserved in Earth's crust as a main component which makes it an abundant source for human being at present. On the other hand, obtaining ideal efficiency levels in silicon entails manufacturing of high purity semiconductor materials. Hence, in contrast to conventional technology, silicon based solar cells cost ten times higher to generate same amount of electricity. In addition to all, while a complete solar cell module is being fabricated, individual Si wafers have to be produced first and then all wafers should be soldered together to constitute a module [4]. That is a cumbersome montage process which not only makes fabrication more sophisticated but also increase manufacture cost.

Other types of photovoltaic systems are thin film solar cells, also regarded as second-generation solar cells. It relies on preparation of numerous thin films with various thicknesses of 10μm or less and deposition on inexpensive substrates is possible, fortunately. Therefore, this technology is superior over silicon-based counterparts in terms of production of one-piece solar modules by monolithic integration that cause crucial decrease in production costs. To date, three major technology are proposed for large scale production of solar cells, such as amorphous silicon (a-silicon), cadmium telluride (CdTe) and copper indium gallium diselenide Cu(In,Ga)Se_2 (CIGS) [4]. But, even though too much effort had been put by both industry and researchers, specifically on CdTe based thin fill solar cells, industrial activity was ceased during 2002 owing to less market acceptance related to toxic component of Cd [12].

Organic photovoltaic cell or Organic Photovoltaics (OPVs) are categorized as the third generation solar cells. Essentially, they are excitonic solar cells while their physical features are distinctive from that of inorganic ones [13]. Over the time, scientists have gained deeper knowledge via conducted researches and incremental improvement in power conversion efficiency (PCE) has been achieved. In particular, great academic and industrial interest has been grown on OPVs after development of solution process because polymer materials and small molecules become adaptable to frequently utilized industrial techniques such as printing lines and wet coating [14]. Fortunately, this development essentially enables us to fabricate cost effective, flexible and thin plastic based OPVs. More good is that, in a recent time, transparent electrodes and semi-transparent solar cells with extensive absorption expending to

UV region have also been introduced which has become to be utilized as building materials [15; 16].

1.1.1 Organic photovoltaics

The beginning of OPVs starts with usage of anthracene molecules for fabrication of solar cells by Kallman and Pope in 1959 [17]. After discovery and treatment of conductive polymers to attain conductivities through doping in 1970, OPVs were acquired further interest [18]. This invention brought Nobel Prize in Chemistry to Heeger, MacDiarmid and Shirakawa in 2000 [19]. Tang and co-workers proposed another method as a milestone in which donor and acceptor molecules combined together [20]. Another turning point was gained by Sariciftci et.al by application of C60 ([60] Fullerene) as a new acceptor group and improvement of different device structure in 1992. Further developments have been focused on types of device architecture, processing conditions, and engineering of new materials [21].

As for device architecture, organic Photovoltaic cells can be essentially classified as ‘‘Bilayer Organic Solar cell, Bulk heterojunction Solar Cell and Dye-Sensitized Solar Cell’’.

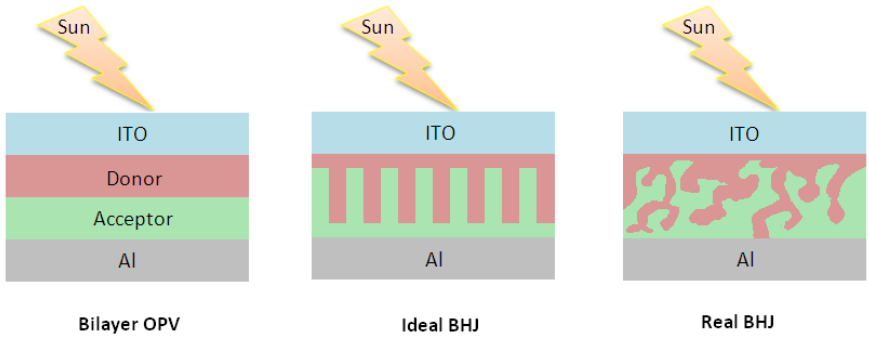

Figure 1. 1: A bilayer OPV, ideal bulk heterojunction and real bulk heterojunction solar cells.

In a bilayer solar cell, donor (p-type) and acceptor (n-type) materials are successively coated layer by layer. Theoretically, 10-20 nm distances at donor-acceptor interface is needed for electron-hole pair to separate the interface of layers. The longer distance gives rise to the quenching of photon, low quantum yield, and depletion of photocurrent [22].

In initial scientific studies, bilayer organic solar cells were dominated in turn by metal phthalocyanine as a donor material and C60 molecule as an acceptor material

where their respective PCE was about 3.6%. Nonetheless, it was realized that obtained results were not repeatable [23]. Therefore, the most reliable PCE for this architecture was roughly accepted as 2.0-2.5% [24].

Different p-type organic materials were applied aiming further increases in PCE of bilayer organic solar cells. Specifically, C60/CuPc system was enriched with intercalation of tin phthalocyanine in order to extend the photon absorption into the infrared region of solar spectrum. However, final PCE could not exceed 1% [25]. In another report, donor material was altered where boron- subphthalocyanine was used rather than Cu/Pc to enhance open circuit voltage (V_{OC}) [26]. Whereas achieved V_{OC} in this arrangement was twice larger than that of the obtained in C60/CuPc system. Yet, the ultimate PCE was solely remained at 2.1% because of diminishes in short-circuit current density (J_{SC}). Nevertheless, further optimizations carried out as a result of which this architecture resulted in PCE of 3% [27].

Using different n-type materials was to another strategy to enhance performance of the bilayer solar cell. For example, fullerene derivatives such as Pyrrolidinofullerenes were tested as an acceptor layer. This substance carries remarkable benefits like being applicable to spin coating; nevertheless, organic moieties on the structure considerably impair electron transport ability of fullerenes for which a PCE was remained around 1.6% [28; 29].

It is probably the most outstanding approach to increase the performance of bilayer architecture through changing phthalocyanine with another organic donor. It was found that application of donor material such as oligothiophene with fullerene acceptor bring PCE to 3.4% that can be accepted as the highest value for bilayer solar cells.

The main difference between bilayer solar and bulk heterojunction (BHJ) solar cell is that the donor and acceptor materials exist as a heterogeneous mixture in active layer of BHJ solar cell. The main reason of this is the miscibility of organic substances in organic solvent and their practical application during fabrication of device. Fortunately, this situation enables us reduce the cost of device fabrication through solvent deposition with present printing techniques which makes heterojunction structure outstanding solar device architecture due to its industrial applicability. BHJ solar cells possess some other benefits compared to bilayer ones. The best example

would be its superiority of PCE that stem from high interface area between donor and acceptor materials. Consequently, excited charge can be effectively separated that provides approximately 100% quantum yields in BHJ solar cell [30].

A short period of time ago, a remarkable development has been occurred in BHJ solar cell studies, namely these BHJ surpassed the barrier of 10% PCE [31]. Even though there is no clear evidence between materials' properties and device performance, some optoelectronic characteristics including absorption and energy levels can be adjusted during synthesis period. It is realized that light absorption and charge separation processes are controlled through conjugated and well-ordered self-organized nanostructures as in case of a photosynthetic system [32]. Therefore, organization of molecular packaging of organic materials is an essential concern in solar cell fabrication for further advanced applications [33; 34]. It can be deduced that besides to electronic structure, numerous parameters embracing morphology of materials has direct influence on device efficiency.

In BHJ solar cells, there are two main semiconductors so-called p-type (donor) and n-type (acceptor) creating interpenetrating networks after simultaneous deposition from solution. This phenomenon gives rise to the transport of charge carriers to their related electrodes. Among various n-type materials, fullerene derivatives, for examples, PC61BM ([6,6]-phenyl-C61-butyric acid methyl ester) and PC71BM are favorable substances due to their remarkable features such as reversible electrochemical reductions, solubility in organic solvent and low-lying energy levels [35]. Also, fullerene has extremely high stability, special π-electron functionality as well as they are outstanding π-conjugated systems. In organic photoelectric conversion, fullerenes play a role that is difficult for other π-electron systems to fill. Therefore fullerenes still have the potential to bring a revolution to solar cells [36].

Recently, donor materials have experienced crucial variation and include both discrete molecules and polymer materials [35; 37; 38]. Application of P3HT as a donor material can be considered as a turning point for OSC because it forms a laminar structure when subjected to elevated temperature. Moreover, its improved charge transfer feature provides high current density and this makes it the most prominent material for many fundamental and theoretical studies. Nevertheless, it has an inadequate absorption in visible region and thereby its maximum PCE remains at roughly 5%. Since the structural configuration of P3HT is not convenient

for chemical modification, studies have been focused on alternative structures instead such as co-polymers, small molecules and organic-inorganic hybrid materials.

As for Dye-Synthesized Solar Cell (DSSC), it became noticeable after O'Regan and Grätzel introduced a promising paper in 1991 and proposed it as a milestone for the fabrication large-scale solar cells based on molecular components[39]. Indeed together with the evolution of DSCCs, conventional solid-state photovoltaic technologies have faced with big challenges by the systems working at nano and molecular level. DSSCs have offered seminal characteristics since small cells and mini modules in this architecture roughly have reached to 12% efficiency. It is also reported to have durable efficiencies of 8-9% with 1000h stability at 80^{o}C. That said DSSCs carry some superior features over other solar cell technologies in terms of low-cost investments, easy fabrication, and relatively better operation under diffused light condition at elevated temperatures. DSSCs are also applicable to the flexible substrate with several shapes, color, and transparency and practical to integrate with varied products develop with new marketable opportunities [40].

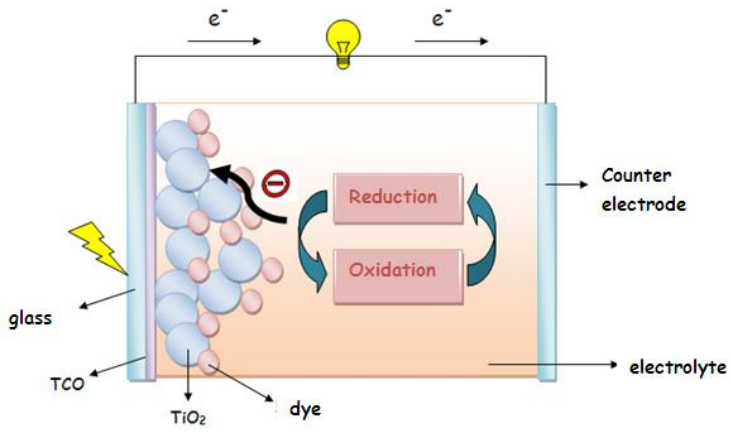

Figure 1. 2: Working principle of Dye Sensitized Solar Cells (DSSC).

Together with all superiorities, unfortunately the use of liquid electrolyte is the main drawback of DSSC architecture due to its temperature stability problem. Namely, electrolyte can freeze at low temperatures that can cause decreases or stops in power generation. As well this situation may finally result in physical damage whilst higher temperature gives rise to electrolyte to expand and therefore cause seal of panels. Moreover, production of DSSCs suffers from cost of the rather expensive ruthenium dye, platinum (catalyst), conducting glass or plastic (contact). Another serious problem of DSSCs is associated with volatile organic compounds in electrolyte

solution that are dangerous for both environment and human health [41]. Saying this, together with all these limitations, efficiency of DSSCs unfortunately roughly remained at 12% [42]. That is the major reason leading researchers to search for alternative methods, more new and effective materials and novel device architectures [43].

1.1.2 Perovskite solar cell

A perovskite structure, indicated as ABX3, has the same crystallographic structure with perovskite mineral ($CaTiO_3$), which was found in Ural Mountains in 1839 and taken Russian mineralogist Lev Perovski's name [44].

The lattice structure of perovskite mineral can be described simply as a cubic unit cell having a calcium atom in the center, titanium atoms at the corners and oxygen atoms at the midpoints. Similar to perovskite mineral, generic form of perovskite can be indicated by ABX_3 and therefore any substance having this arrangement and crystallography similar to perovskite mineral is called as perovskite structure. Moreover, perovskite has a broad application area as a consequence of its tunable properties achieved (superconductivity, colossal magnetoresistance, ferroelectricity,) through using different atoms in the lattice. Its changeable structural, catalytic, magnetic and electrical properties make it attractive playfield for scientists [44].

When the perovskite was first started to be used as a sensitizer in liquid electrolyte based solar cell, it showed efficiencies varying from 3.5 to 6.5% [45; 46]. However, miscibility of perovskite in liquid electrolyte caused a rapid decrease in efficiency. In contrast, perovskite displayed superior features in solid state (ss) solar cells as a consequence of their high absorption coefficients [47]. The first solid-state perovskite solar cell (PSC) was formed in 2012 by using $CsSnI_3$ in a ss-dye sensitized solar cell and reached an efficiency up to 8.5% [48; 49]. However, recent studies are dominated by use of organometal trihalide combination since usage of lead cation as a metal component in main formulation enables us to reach broad absorption spectra, tunable band gap, long charge carrier diffusion lengths and easy manufacturing. In this arrangement (ABX_3), the organic component is generally methylammonium cation (A), big inorganic cation (B) is usually lead (II), the halogen anion (X) is mostly chloride or iodide [47; 50].

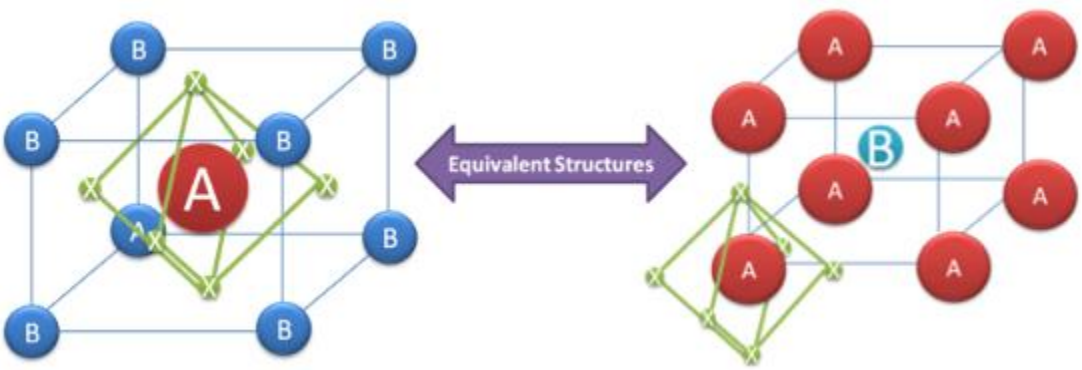

Figure 1. 3: A generic perovskite crystal structure of ABX_3 form.

Significance of perovskite solar cells

The question of 'Why perovskite is important' for both scientific committee and industry can be answered by the following two graphs. The first one is associated with the comparison of power conversion efficiencies between conventional photovoltaic research technologies, thin film technologies and PSCs, over the years. It can be deduced from figure 1.4 that the power conversion efficiency of PSCs have been increased noticeably since they were first taken attention in 2012. Whereas PSCs had showed the same efficiencies with the Cadmium Telluride (CdTe) in the first 4 years of appearance, they have surpassed the all non-concentrator thin film technologies such as CdTe and Copper Indium Gallium Selenide (CIGS) by June 2018 [51].

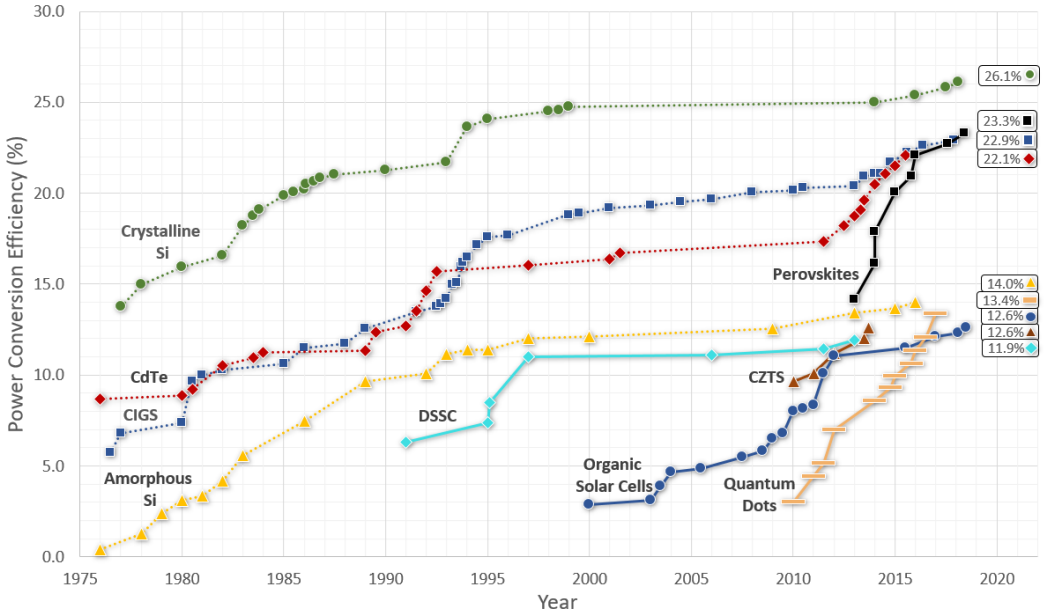

Figure 1. 4: Power conversion efficiency of lab-based "hero cells" by years (NREL).

Figure 1.5 indicates comparison of open circuit voltage and band gap in terms of different types of technologies. This comparison is giving clues about the percentage energy loss of photon in the PSC during the process of light-to-electricity conversion. According to graph, whilst this loss can be reached up to 50% in the both standard excitonic and organic solar cells, PSCs can attain more than 70% photon energy utilization [52]. In addition, it is still probable that this utilization may be further increased. Namely, this value is recently approaching the utilization of the other state of the art technologies, such as GaAs, amorphous Si etc. we note that PSC also carries a potential of being cost-effective [53].

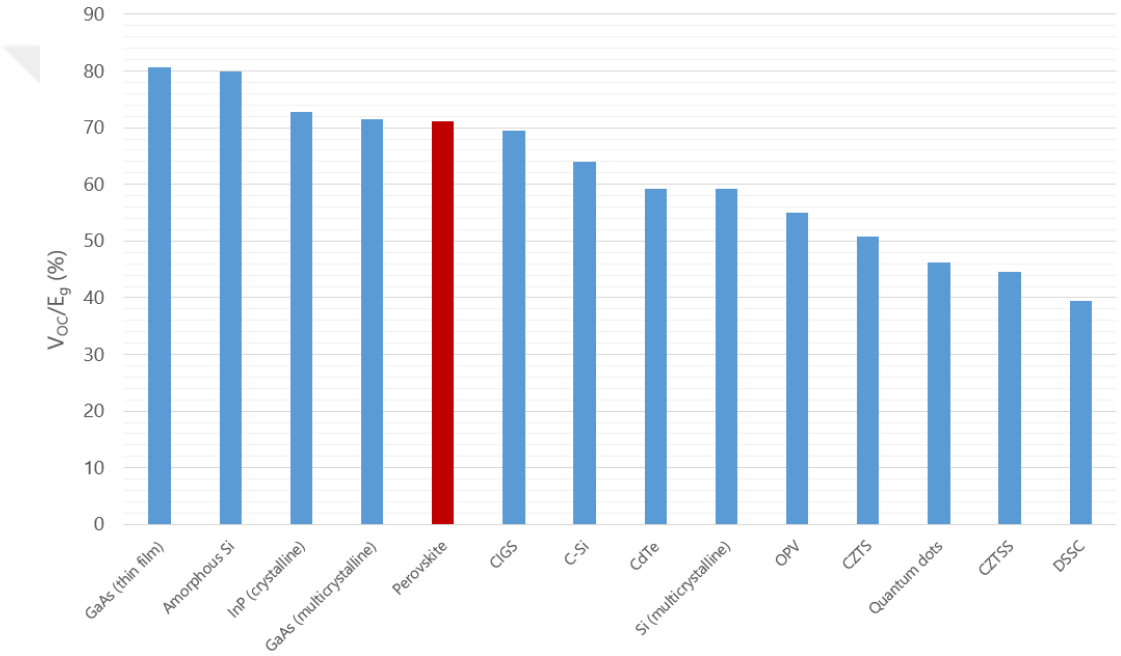

Figure 1. 5: The maximum photon energy utilization (defined as the open circuit voltage V_{OC} divided by the optical band gap E_g) for common single junction solar cells material systems. Calculated from state of the art cells in NREL efficiency tables.

Despite the efficient conversion of sunlight to electricity, PSCs currently have some shortages. The main weakness of PSC is its long-term instability. This is because of the degradations stemming from not only exterior influences such as water, light, oxygen but also due to the intrinsic reasons like deterioration upon heating [52; 54]. So far, many methods have been carried out to enhance the stability. A noteworthy example is the alteration of components. More specifically; application of multiple cation systems embracing rubidium and cesium has resulted in improved efficiency and stability [55; 56].

Stability has also been enhanced with passivation [57] of the surface by using 2D-layered (Ruddlesden-Popper) perovskites with traditional 3D perovskites [58]. Since the first attempt of this method, stability of PSCs pave the way of their lifetimes, namely reaching industrial standards. Hopefully, recent studies have demonstrated the perovskite cells even resisted to 1000-hour moisture and heat test [59; 60].

The architecture of perovskite solar cells (PSCs) can structurally be classified into two main groups referred as 'regular' (n-i-p) and 'inverted' (p-i-n) configurations [61]. In contrast to n-i-p configuration in which the perovskite absorber is placed on top of electron transport materials (ETM), p-i-n structure deposits perovskite layer on the top of the hole transport material (HTM). Since the regular architecture carries some disadvantages particularly associated with its cost due to complex depositing system of HTM (usually spiro-OMETAD and PTAA as a small molecule and polymer, respectively) and charge transport materials such as TiO_2 entailing high processing temperature, inverted configuration has essentially been proposed as an alternative structure. However, regular configuration has still been mostly preferred structure and kept maximum efficiency in PSCs [62].

The inverted architecture, on the other hand possesses outstanding feature of low-temperature processing, which enables fabrication of perovskite configuration on flexible substrates applicable to the roll-to-roll system. Besides, so far, the reported efficiencies has reached about up to 18% in the typical inverted architecture that includes poly(3,4-ethylenedioxythiophene):poly(styrenesulfonate) (PEDOT:PSS) as a HTM and [6,6]-phenyl-C(61)-butyric acid methyl ester ($PC_{60}BM$) or its relevant C_{70} derivative ($PC_{70}BM$) as a ETM [63]. However, although PEDOT:PSS indicates excellent optical characteristics, its acidic and hydroscopic features are main weakness that severely decrease chemical stability at the indium tin oxide (ITO)/PEDOT:PSS interface and therefore decay electron blocking properties after a certain time of storage [63-66]. In this context, modification of electrode surface with organic molecules including self-assembled monolayers (SAMs) has been regarded as an effective substituent to the standard single-carrier transport layers [67].

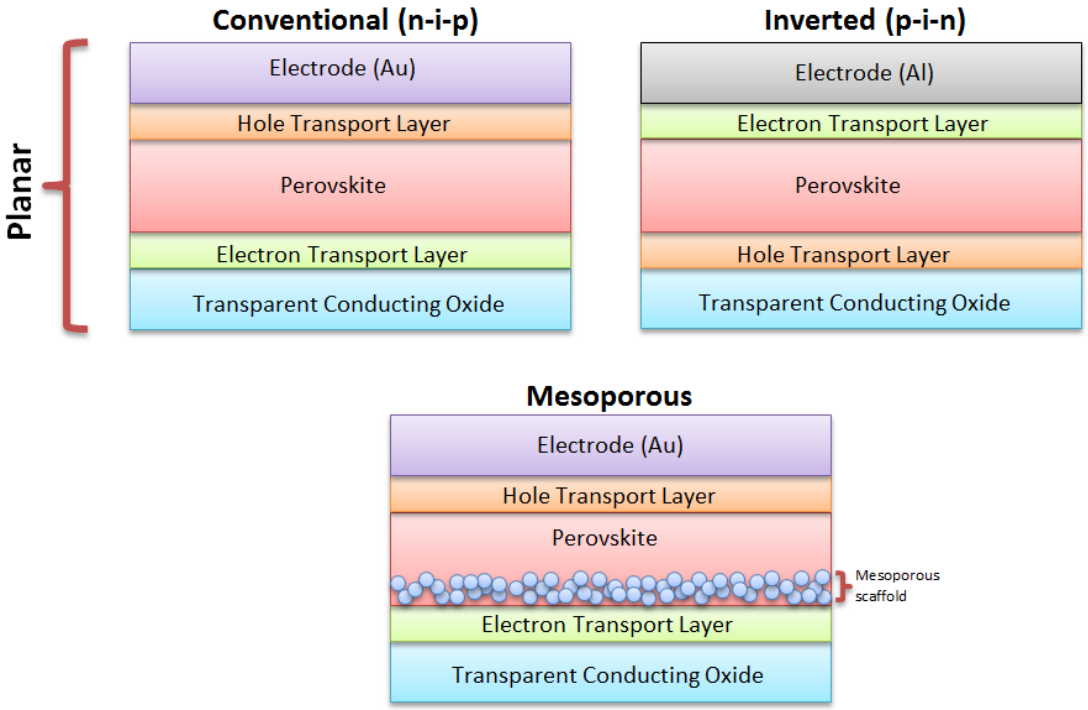

Figure 1. 6: Planar and mesoporous perovskite solar cells.

Indium tin oxide (ITO) is frequently prefered anode electrode in the inverted PSCs due to its transparency in the visible region, ease of patterning and high electrical conductivity. Its rough surface creates some pin holes leading leakage current and interface states causes recombination of charge carriers via trapping centers through transition region. The work function of ITO is reported to change from 4.5 eV to 4.7 eV that is lower than HOMO level of donor material to make an ohmic contact without potential barrier that prevents charge transfer from the active layer to anode layer [68]. Furthermore, open circuit voltage (Voc) strongly depends on interface morphology and matching energy levels at the interface. To obtain higher short circuit current density (Jsc) and fill factor (FF), the charge collection must be maximized by tuning energy level and interface properties. Therefore, interfacial engineering is a significant area to overcome these drawbacks. Usually, PEDOT:PSS (Poly(3,4ethylenedioxylenethiophene):poly(styrenesulfonic acid)) is introduced as buffer layer in inverted PSCs. Unfortunately, acidic nature of PEDOT:PSS can result in etching of ITO surface that is sensitive to acidic environment. Besides, polymer layer in device architecture can be readily oxidized in air leading to deterioration in device performance [69].

1.1.3 Sam molecules

Self-assembly monolayers (SAMs) are generally defined as single layer of molecules lay out on surface of a substrate where molecules perform not only molecular order and packing characteristics but also high degree of orientation. Generally, two basic methods are proposed for monolayer deposition, namely Langmuir-Blodgett and self-assembly technique [70; 71].

Currently, self-assembly monolayer is considered as one of the most exciting topics in research and therefore project support agencies and governments are financing huge amount of money SAM related projects. Since there is striking increase in the number of publications related to SAMs, for example, 273 in 1996, 562 in 1998, 721 in 2000 and 946 in 2002, new projects and application areas are probable to be developed in the near future [72].

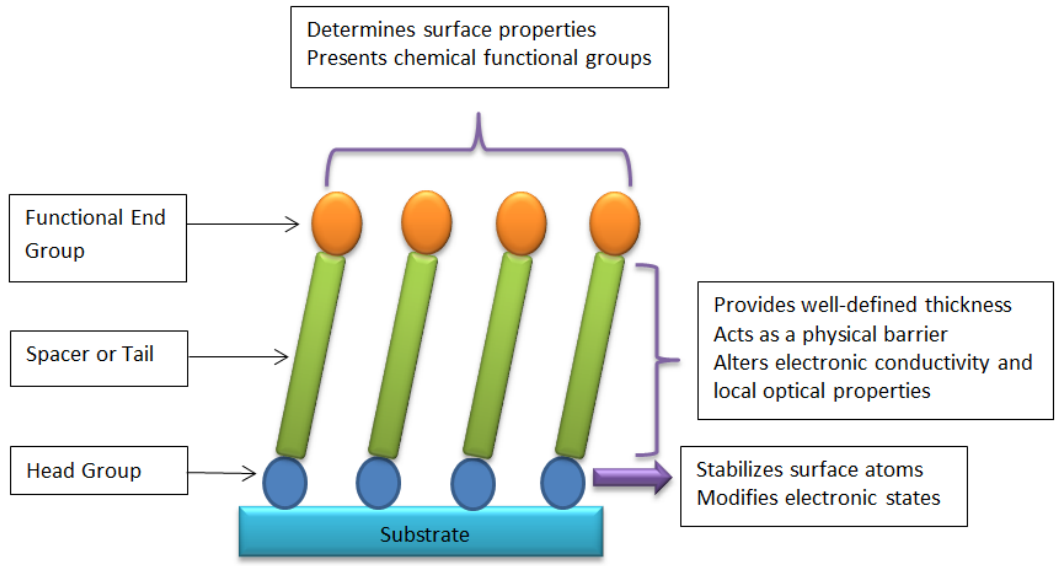

Figure 1. 7: Functional groups of SAM molecules.

SAMs offer proper, simple and flexible surface systems by which interfacial features of metals, metal oxides and semiconductors can be tailored. As it provides affordable and useful surface coating, its application area covers sensors, wetting control, biocompatibility, corrosion prevention etc. The SAM molecules are composed of three main groups, namely head group, tail and functional end group. The head group possesses particular affinity to surface and displaces with adsorbed organic moieties on the surface. Table 1.1 indicates several head groups and their specific affinity to related substrate surfaces [72].

Table 1. 1: Combinations of head groups and substrates used in forming SAMs on metals and metal oxides.

Amphiphiles	**Substarates**
ROH	F_xO_y, Si—H, Si
RCOO— /RCOOH	a-Al_2O_3, F_xO_y, Ni, Ti/TiO_2, Indium tin Oxide
RCOO—OOCR	Si (111):H, Si(100):H
RNH_2	FeS_2, Mica, Stainless Steel, ITO
RCN	Ag, Au
RNC	Pt
RSH	Au, Stainless Steel
RSR	Au
RSSR	Au
R_3P	Au
R_3P=O	Co
RPO_3^{2-}/$RP(O)(OH)_2$	Al, ITO, Mica, TiO_2, ZrO_2
RPO_4^{2-}/ RPO_4H_2	Al, Nb_2O_3, Ta_2O_3
$RSiX_3$ X= H, Cl, OCH_2CH_3	HfO_2, ITO, PtO, TiO_2, ZrO_2

SAMs can be deposited from any liquid or gas phase material on to the substrate's surface by means of chemisorption enabling slow organization of tail group [73]. Sooner, later, may be after a certain period of time from minutes to hours, head group assembles together on the substrate surface and gives rise to formation of closed packed molecular area till single monolayer created on substrate surface. In here, Van der Waals interactions play main role to form tight monolayer packs which reduce the free energy of the surface [74; 75]. The initial illustration of SAM in organic photovoltaic devices was the work of organic electroluminescence in which SAM grafted ITO surface was introduced as the anode electrode. This method enabled both reduction of energy barrier between hole transport materials (HTM) and anode electrode and increased current density [76].

2. CHARACTERIZATION OF SOLAR CELLS

2.1 Current-voltage measurement

The power conversion efficiency (PCE) of solar cell is calculated through measuring the produced power under the illumination of 1.5 AM (100mW/cm^2) that is referred as 1 sun illumination. The electrical power calculations depend on the measurements of current and voltage values of respective device. The current-voltage (I-V) measurement is carried out under sunlight by changing the voltage. A standard I-V curve is indicated in figure 2.1.

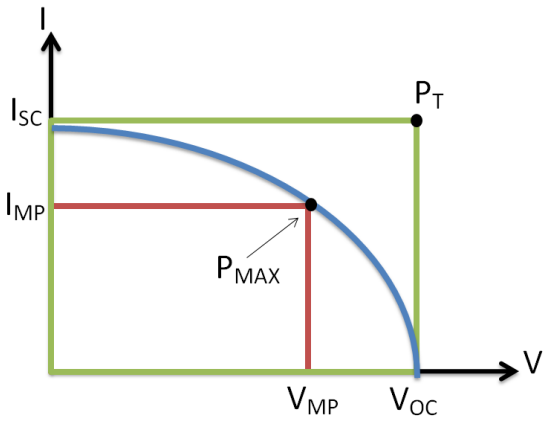

Figure 2. 1: Current-Voltage curve of a solar cell.

In the I-V curve, the maximum point of product is known as (P_{max}). Moreover, ratio between the P_{max} and P_{in} is defined as Power Conversion Efficiency of solar cells and illustrated with the following equation:

$$\eta = P_{max}/P_{in} = FF \times J_{SC} \times V_{OC}/P_{in} \quad (2.1)$$

V_{OC}: open circuit voltage

J_{SC}: short circuit current

FF: fill factor

P_{in}: incident power

The higher PCE requires the higher V_{OC}, J_{SC} and FF whereas P_{in} needs to be reduced.

3. OBJECTIVE OF STUDY

In this study, six novel SAM molecules with various donor and acceptor terminal groups are presented for the modification of ITO surface. The effect of synthesized SAMs on surface characteristics such as wettability and perovskite formation and also on photovoltaic performance of fabricated solar cells are examined. The carboxylic acid is preferred as an attaching group as it is proper building block to form molecular self-assemblies on metallic surface by means of chemisorption. This is the reason that it is particularly useful for the device fabrication in which metal oxides is needed to be utilized [77]. Since proposed SAMs are of push-pull type molecular nature, contiguous thiophene rings were used as conjugated units in spacer group due to the fact that thiophene has lower delocalization energy and provide superior conjugation than that of benzene [78]. Furthermore, effect of modification, with such molecular system, on work function, hole-collection and short circuit photocurrent density are discussed. To the best of our knowledge, this is the first comparative screening study to undertake a longitudinal evaluation of the influence of both donor and acceptor terminal groups on efficiency of inverted type perovskite solar cell.

4. MATERIALS

Methyl 4-bromobenzoate, 3,5-difluorophenylboronic acid, 3,5-dimethoxyphenylboronic acid, *9H*-carbazole-9-(4-phenyl) boronic acid pinacol ester, 4-(diphenylamino)phenylboronic acid, [1,1′-bi(diphenylphospino) ferrocene]dichloropalladium(II) ($Pd(dppf)Cl_2$) and PEDOT:PSS, lead(II) iodide (PbI_2) were purchased from Sigma-Aldrich. 4-Methoxy-*N*-(4-methoxyphenyl)-*N*-(4-(4,4,5,5-tetramethyl-1,3,2-dioxaborolan-2-yl)phenyl)aniline and (5'-bromo-3,4'-dihexyl-[2,2'-bithiophen]-5-yl)boronic acid were bought from SunaTech Inc. All solvents such as 1,2-dimethoxy ethane (DME), tetrahydrofuran (THF), ethanol, anhydrous isopropyl alcohol, toluene, acetone, dimethyl sulfoxide (DMSO) and hydrochloric acid (HCl), potassium hydroxide (KOH) were purchased from Alfa-Aesar. Potassium carbonate (K_2CO_3) was from Riedel de Haen. Methylammonium iodide (MAI) was obtained from Dysol Inc., $PC_{61}BM$ was purchased from Luminescence Technology Corp. (LUMTEC).

Synthesis: All chemicals, including the solvents and reagents as well, were used as received from commercial source without further purification. All glassware was oven-dried and all Suzuki-Coupling reactions were performed under inert (N_2) environment.

5. INSTRUMENTATION AND DEVICE CHARACTERIZATION

^{1}H and ^{13}C NMR (Varian-400 MHz) data were recorded at 25 °C using $CHCl_3$-d and d6-DMSO as solvents and TMS as an internal standard.

The surface morphology of bare ITO and SAM-modified ITO coated substrates were characterized by Nanosurf Easyscan-2 controller atomic force microscopy (AFM). During KPFM measurements, conducting tin cantilever was used to obtain the change in the surface potential and work function of the ITO surfaces before and after modification.

CH Instrument CH440b potentiostat was used to determine electrochemical behavior of SAM-modified ITO coated substrates.

KSV Attension Theta Lite Optical Tensiometer was used for static contact angle measurements by dispensing a water droplet with average volume of 4 μL.

Chemical composition of SAM-modified ITO surface was analyzed with K-AlphaTM+ X-ray Photo-electron Spectrometer (XPS) System.

X-RAY diffraction (XRD) pattern of perovskite was recorded with Rigaku D/Max-2500 diffractometer using Cu Kα radiation (λ = 1.54 Å)

Zeiss Evo 40 model Field Emission Electron Microscopy (FESEM) was used to obtain surface image of perovskite films.

The J-V measurements were performed by using a solar simulator (ABET 11000) and a source meter (Keithley 2400). The curves were registered under 1-sun conditions (100 mW cm^2, AM 1.5G) calibrated with a silicon photodiode (NREL). The average active area of the fabricated devices was 0.07 cm^2.

IPCE spectrum was measured through Stanford SR803 lock-in amplifier under monochromatic illumination.

6. SYNTHESIS METHODS

Synthesis of methyl 4-(5'-bromo-3,4'-dihexyl-[2,2'-bithiophen]-5-yl)benzoate (EA-40)

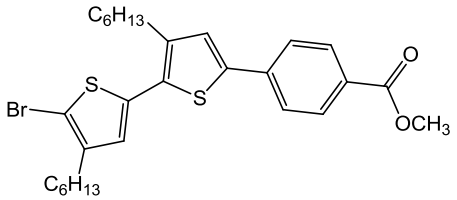

(5'-Bromo-3,4'-dihexyl-[2,2'-bithiophen]-5-yl)boronic acid (250 mg; 0.54 mmol) and methyl 4-bromobenzoate (141 mg; 0.65 mmol)) were dissolved in 20ml DME in Schlenk Flask. Pd(dppf)Cl_2 (22 mg; 0.03 mmol) and K_2CO_3 solution (1 mL; 1 M) were added to the mixture after temperature was reached to 50°C. The reaction mixture was heated to 90°C and refluxed under N_2 atmosphere overnight. The reaction was monitored by TLC to establish completion. The final solution was then extracted with equal volume of CH_2Cl_2 and distilled water. The organic solvent was evaporated and the crude product was purified by column chromatography (CC) (SiO_2, CH_2Cl/n-hexane: 1/1) to afford yellow powder as a product. ^{1}H NMR (400 MHz, $CDCl_3$, ppm); δ 8.02 (t, 1H), 8.00 (t, 1H), 7.21 (s, 1H), 6.83 (s, 1H), 3.91 (s, 3H), 2.72-2.68 (t, 2H), 2.57-2.53 (t, 2H), 1.66-1.58 (m, 4H), 1.41-1.30 (m, 12H), 0.91-0.86 (m,6H). ^{13}C NMR (400 MHz, $CDCl_3$, ppm); δ 166.87, 142.69, 140.82, 138.33, 130.01, 128.53, 126.75, 108.71, 52.33, 31.34, 30.24, 29.52, 29.19, 22.70, 14.00.

Synthesis of 4-(5'-bromo-3,4'-dihexyl-[2,2'-bithiophen]-5-yl)benzoic acid (EA-41)

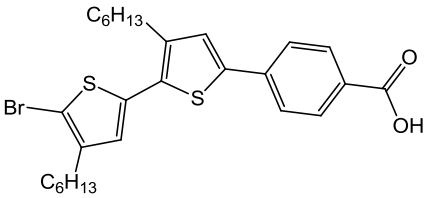

EA-40 (100 mg; 0.18 mmol) was dissolved in 10 mL THF-ethanol mixture (1:1, V:V) in a round-bottom flask. KOH solution (0.5 ml; 1 M) was added to mixture and final solution was refluxed overnight. After all organic solvents were removed under vacuum, distilled water (10 ml) and 1 M HCl solution was added to flask until pH of the solution reached to region between 3-4. Finally, yellow product was precipitated, filtered, washed with distilled water and dried overnight. ^{1}H NMR (400 MHz, $CDCl_3$, ppm); δ 7.80-7.78 (d, 2H), 7.15-7.13 (d, 2H), 6.79 (s, 1H), 6.61 (s, 1H), 2.46-2.42 (t, 4H), 1.28-1.19 (m, 12H), 0.87-0.86 (m, 6H). ^{13}C NMR (400 MHz, $CDCl_3$, ppm); δ 142.25, 140.81, 140.46, 136.49, 130.36, 130.27, 126.52, 126.04, 124.38, 108.37, 77.31, 76.39, 76.67, 31.99, 30.41, 29.64, 29.52, 29.42, 29.32, 28.99, 22.66, 22.61, 14.08, 14.07.

Synthesis of methyl 4-(5'-(3,5-dimethoxyphenyl)-3,4'-dihexyl-[2,2'-bithiophen]-5-yl)benzoate (EA-43)

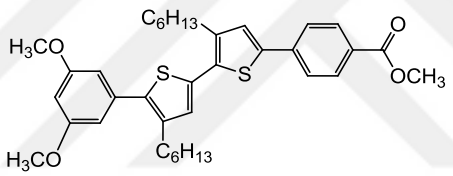

EA-40 (250 mg; 0.54 mmol) and (3,5-dimethoxyphenyl)boronic acid (118.3 g; 0.65 mmol) were dissolved in 20 ml DME in Schlenk Flask. $Pd(dppf)Cl_2$ (22 mg; 0.03 mmol) and K_2CO_3 solution (1 mL; 1 M) were added to the mixture after temperature was reached to 50°C. The reaction mixture was heated to 90°C and refluxed under N_2 atmosphere overnight. The reaction was monitored by TLC to establish completion. The final solution was then extracted with equal volume of CH_2Cl_2 and distilled water. The organic solvent was evaporated and obtained crude product was purified by CC (SiO_2, CH_2Cl/n-hexane: 2/1) to afford yellow powder as a product. ^{1}H NMR (400 MHz, $CDCl_3$, ppm); δ 8.04-8.02 (d, 2H), 7.66-7.63 (d, 2H), 7.26 (d, 2H), 6.63-6.62 (d, 2H), 6.47-6.46 (t, 1H), 3.93 (s, 3H), 3.84 (s, 6H), 2.83-2.79 (t, 2H), 2.71-2.67 (t, 2H), 1.72-1.62 (m, 5H), 1.35-1.26 (m, 12H), 0.91-0.86 (m, 6H). ^{13}C NMR (400 MHz, $CDCl_3$, ppm); δ 166.70, 160.75, 139.27, 138.37, 136.01, 133.86, 130.23, 127.51, 125.00, 107.39, 99.76, 55.38, 52.05, 31.66, 30.91, 29.23, 22.99, 14.05.

Synthesis of 4-(5'-(3,5-dimethoxyphenyl)-3,4'-dihexyl-[2,2'-bithiophen]-5-yl)benzoic acid (EA-49)

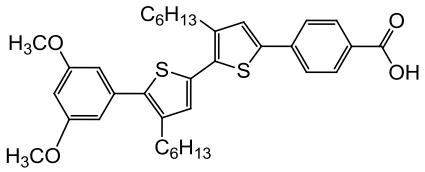

EA-43 (100 mg; 0.17 mmol) was dissolved in 10 mL THF-ethanol mixture (1:1, V:V) in round-bottom flask. KOH solution (0.5 ml; 1 M) was added to mixture and final solution was refluxed overnight. After all organic solvents were removed under vacuum, distilled water (10 ml) and 1 M HCl solution was added to flask until pH of the solution reached to region between 3-4. Finally, dark yellow product was precipitated, filtered, washed with distilled water and dried overnight. ^{1}H NMR (400 MHz, $CDCl_3$, ppm); δ 7.94 (s, 2H), 7.44 (s, 2H), 6.92 (s, 1H), 6.55-6.41 (d, 4H), 3.78 (s, 6H), 2.62-2.58 (t, 4H), 1.24-1.23 (d, 12H), 0.82 (s, 6H). ^{13}C NMR (400 MHz, $CDCl_3$, ppm); δ 160.61, 140.27, 139.12, 136.07, 134.06, 130.73, 128.06, 124.57, 107.16, 99.58, 55.28, 31.62, 30.90, 29.24, 28.83, 22.58, 14.04.

Synthesis of methyl 4-(3,4'-dihexyl-5'-(3,4,5-trimethoxyphenyl)-[2,2'-bithiophen]-5-yl)benzoate (EA-42)

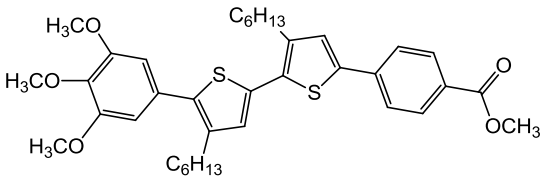

EA-40 (250 mg; 0.54 mmol) and (3,4,5-trimethoxyphenyl)boronic acid (137.8 mg; 0.65 mmol) were dissolved in 20 ml DME in Schlenk Flask. $Pd(dppf)Cl_2$ (22 mg; 0.03 mmol) and K_2CO_3 solution (1 mL; 1 M) were added to the mixture after temperature was reached to 50°C. The reaction mixture was heated to 90°C and refluxed under N_2 atmosphere overnight. The reaction was monitored by TLC to establish completion. The final solution was then extracted with equal volume of CH_2Cl_2 and distilled water. The organic solvent was evaporated and obtained crude product was purified by CC (SiO_2, CH_2Cl/n-hexane: 2/1) to afford yellow powder as a product. ^{1}H NMR (400 MHz, $CDCl_3$, ppm); δ 8.02-8.00 (d, 2H), 7.64-7.62 (d, 2H), 7.25 (s, 2H), 6.66 (s, 2H), 3.90-3.80 (t, 13H), 2.81-2.65 (dt, 4H), 1.71-1.63 (m, 4H),

1.32-1.24 (m, 12H), 0.89-0.85 (q, 6H). ^{13}C NMR (400 MHz, $CDCl_3$, ppm); δ 166.68, 153.14, 140.48, 139.96, 139.02, 138.30, 137.61, 133.67, 132.02, 130.23, 129.69, 128.57, 128.38, 127.50, 124.97, 106.46, 60.93, 56.11, 52.08, 31.70, 31.64, 31.06, 30.56, 29.68, 29.51, 29.26, 29.24, 28.86, 22.60, 14.08, 14.05.

Synthesis of 4-(3,4'-dihexyl-5'-(3,4,5-trimethoxyphenyl)-[2,2'-bithiophen]-5-yl)benzoic acid (EA-46)

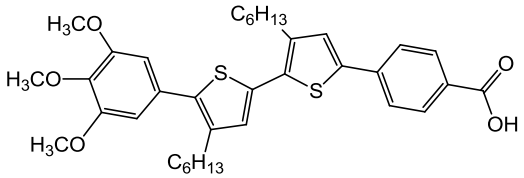

EA-42 (100 mg; 0.16 mmol) was dissolved in 10 mL THF-ethanol mixture (1:1, V:V) in round-bottom flask. KOH solution (0.5 ml; 1 M) was added to reaction mixture and final solution was refluxed overnight. After all organic solvents were removed under vacuum, distilled water (10 ml) and 1M HCl solution was added to flask until pH of the solution reached to region between 3-4. Finally, dark yellow product was precipitated, filtered, washed with distilled water and dried overnight. ^{1}H NMR (400 MHz, $CDCl_3$, ppm); δ 8.07-8.05 (d, 2H), 7.63-7.61 (d, 2H), 7.02 (s, 1H), 6.94-6.81 (dd, 1H), 6.65 (s, 2H), 3.89-3.88 (d, 9H), 2.83-2.75 (m, 2H), 2.67-2.62 (m, 2H), 1.69-1.62 (m, 4H), 1.31-1.23 (m, 12H), 0.89-0.84 (m, 6H). ^{13}C NMR (400 MHz, $CDCl_3$, ppm); δ 153.11, 139.91, 139.03, 137.57, 133.67, 130.81, 129.70, 124.95, 106.43, 60.94, 56.11, 31.69, 31.07, 29.26, 28.85, 22.61, 14.05.

Synthesis of methyl 4-(5'-(3,5-difluorophenyl)-3,4'-dihexyl-[2,2'-bithiophen]-5-yl)benzoate (EA-45)

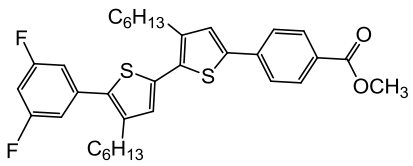

EA-40 (250 mg; 0,54 mmol) and (3,5-difluorophenyl)boronic acid (102.6 mg; 0.65 mmol)) were dissolved in 20ml DME in Schlenk Flask. Pd(dppf)Cl_2 (22 mg; 0.03 mmol) and K_2CO_3 solution (1 mL; 1 M) were added to the mixture after temperature was reached to 50°C. The reaction mixture was heated to 90°C and refluxed under

N_2 atmosphere overnight. The reaction was monitored by TLC to establish completion. The final solution was then extracted with equal volume of CH_2Cl_2 and distilled water. The organic solvent was evaporated and obtained crude product was purified by CC (SiO_2, CH_2Cl/n-hexane: 1/1) to afford yellow powder as a product. ^{1}H NMR (400 MHz, $CDCl_3$, ppm); δ 8.05-8.03 (d, 3H), 7.66-7.64 (d, 4H), 7.07 (s, 2H), 3.93 (s, 3H), 2.83-2.57 (dt, 4H), 1.73-1.69 (t, 2H), 1.62-1.61 (d, 2H), 1.29 (s, 12H), 0.90-0.88 (d, 6H). ^{13}C NMR (400 MHz, $CDCl_3$, ppm); δ 166.71, 142.91, 140.65, 140.09, 138.31, 135.64, 131.94, 130.25, 128.63, 128.54, 127.58, 127.50, 125.02, 52.10, 31.67, 30.73, 30.57, 29.69, 29.61, 29.26, 29.14, 22.62, 22.60, 14.08.

Synthesis of 4-(5'-(3,5-difluorophenyl)-3,4'-dihexyl-[2,2'-bithiophen]-5-yl)benzoic acid (EA51)

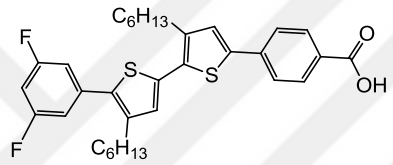

EA-45 was dissolved in 10 mL THF-ethanol mixture (1:1, V:V) in round-bottom flask. KOH solution (0.5 ml; 1M) was added to mixture and final solution was refluxed overnight. After all organic solvents were removed under vacuum, distilled water (10 ml) and 1 M HCl solution was added to flask until pH of the solution reached to region between 3-4. Finally, light yellow product was precipitated, filtered, washed with distilled water and dried overnight. . ^{1}H NMR (400 MHz, $CDCl_3$, ppm); δ 8.03-8.01 (d, 1H), 760-7.58 (d, 1H), 7.45-7.44 (d, 2H), 7.31 (s, 1H), 7.25 (s, 1H), 7.06 (s, 1H), 7.01-6.94 (t, 2H), 2.82-2.79 (t, 2H), 2.60-2.57 (t, 2H), 1.71-1.68 (t, 2H), 1.62-1.60 (d, 2H), 1.25 (s, 12H), 0.87 (s, 6H). ^{13}C NMR (400 MHz, $CDCl_3$, ppm); δ 147.96, 139.24, 135.62, 129.97, 124.92, 124.90, 124.03, 123.69, 118.93, 114.05, 31.92, 31.45, 30.11, 29.70, 29.36, 22.69, 14.12.

Synthesis of methyl 4-(3,4'-dihexyl-5'-(3,4,5-trifluorophenyl)-[2,2'-bithiophen]-5-yl)benzoate (EA-44)

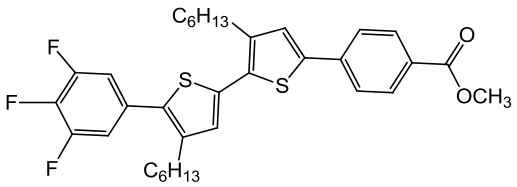

EA-40 (250 mg; 0,54 mmol) and (3,4,5-trifluorophenyl)boronic acid (114.3 mg; 0.65 mmol)) were dissolved in 20ml DME in schlenk flask. $Pd(dppf)Cl_2$ (22 mg; 0.03 mmol) and K_2CO_3 solution (1 mL; 1 M) were added to the mixture after temperature was reached to 50°C. The reaction mixture was heated to 90°C and refluxed under N_2 atmosphere overnight. The reaction was monitored by TLC to establish completion. The final solution was then extracted with equal volume of CH_2Cl_2 and distilled water. The organic solvent was evaporated and obtained crude product was purified by CC (SiO_2, CH_2Cl/n-hexane: 1/1) to afford yellow powder as a product. ^{1}H NMR (400 MHz, $CDCl_3$, ppm); δ 8.05-8.03 (d, 2H), 7.67-7.64 (d, 2H), 7.55-7.53 (d, 1H), 736 (s, 1H), 7.27-7.26 (d, 2H), 3.93 (s, 3H), 2.83-2.80 (t, 2H), 2.61-2.57 (t, 2H), 1.73-1.69 (t, 4H), 1.29 (s, 12H), 0.89-0.88 (d, 6H). ^{13}C NMR (400 MHz, $CDCl_3$, ppm); δ 166.72, 147.03, 142.90, 140.63, 138.29, 135.61, 131.92, 130.25, 127.59, 125.01, 119.04, 52.12, 31.66, 31.41, 30.16, 29.69, 22.61, 14.09.

Synthesis of 4-(3,4'-dihexyl-5'-(3,4,5-trifluorophenyl)-[2,2'-bithiophen]-5-yl)benzoic acid (EA50)

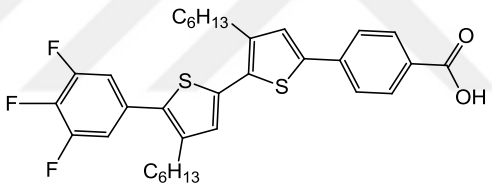

EA-44 (100 mg; 0.17 mmol) was dissolved in 10 mL THF-ethanol mixture (1:1, V:V) in round-bottom flask. KOH solution (0.5 ml; 1 M) was added to reaction mixture and final solution was refluxed overnight. After all organic solvents were removed under vacuum, distilled water (10 ml) and 1M HCl solution was added to flask until pH of the solution reached to region between 3-4. Finally, light yellow product was precipitated, filtered, washed with distilled water and dried overnight. ^{1}H NMR (400 MHz, $CDCl_3$, ppm); δ 8.07 (s, 1H), 7.65 (s, 1H), 7.53-7.51 (d, 1H), 7.37-7.35 (d, 1H), 7.13-7.06 (m, 2H), 6.98-6.94 (d, 1H), 6.82 (s, 1H), 2.85-2.81 (t, 2H), 2.62-2.58 (t, 2H), 1.42 (s, 2H), 1.38 (s, 2H), 1.25 (s, 12H), 0.87 (s, 6H). ^{13}C NMR (400 MHz, $CDCl_3$, ppm); δ 151.01, 135.81, 135.62, 128.22, 124.92, 124.74, 124.43, 31.91, 31.41, 29.68, 29.35, 27.07, 22.68, 14.11.

Synthesis of methyl 4-(5'-(4-(bis(4-methoxyphenyl)amino)phenyl)-3,4'-dihexyl-[2,2'-bithiophen]-5-yl)benzoate (EA-55)

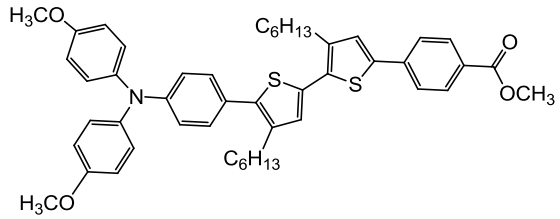

EA-40 (250 mg; 0,54 mmol) and 4-methoxy-N-(4-methoxyphenyl)-N-(4-(4,4,5,5-tetramethyl-1,3,2-dioxaborolan-2-yl)phenyl)aniline (281 mg; 0.65 mmol) were dissolved in 20 ml DME in schlenk flask. Pd(dppf)Cl_2 (22 mg; 0.03 mmol) and K_2CO_3 solution (1 mL; 1 M) were added to the mixture after temperature was reached to 50°C. The reaction mixture was heated to 90°C and refluxed under N_2 atmosphere overnight. The reaction was monitored by TLC to establish completion. The final solution was then extracted with equal volume of CH_2Cl_2 and distilled water. The organic solvent was evaporated and obtained crude product was purified by CC (SiO_2, CH_2Cl/n-hexane: 3/2) to afford orange powder as a product. ^{1}H NMR (400 MHz, $CDCl_3$, ppm); δ 8.02-8.00 (d, 2H), 7.64-7.62 (d, 2H), 7.11-7.09 (d, 4H), 6.94-6.92 (d, 2H), 6.85-6.83 (d, 4H), 3.91 (s, 3H), 3.79 (s, 6H), 2.81-2.77 (t, 4H), 1.70-1.66 (m, 4H), 1.25 (s, 12H), 0.87 (s, 6H). ^{13}C NMR (400 MHz, $CDCl_3$, ppm); δ 167.74, 156.00, 140.55, 140.16, 139.54, 138.47, 138.41, 138.26, 132.81, 132.46, 130.22, 129.59, 128.41, 127.53, 126.85, 125.75, 124.92, 119.70, 114.69, 37.08, 32.76, 31.93, 31.68, 30.96, 30.59, 30.04, 29.71, 29.54, 29.37, 29.28, 29.22, 28.79, 27.09, 22.70, 22.62, 19.72, 14.13.

Synthesis of 4-(5'-(4-(bis(4-methoxyphenyl)amino)phenyl)-3,4'-dihexyl-[2,2'-bithiophen]-5-yl)benzoic acid (EA58)

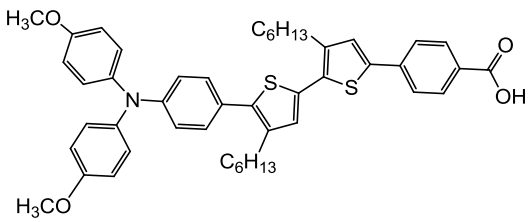

EA-55 (100 mg; 0.13 mmol) was dissolved in 10 mLTHF-ethanol mixture (1:1, V:V) in round-bottom flask. KOH solution (0.5 ml; 1 M) was added to mixture and final solution was refluxed overnight. After all organic solvents were removed under

vacuum, distilled water (10 ml) and 1 M HCl solution was added to flask until pH of the solution reached to region between 3-4. Finally, orange product was precipitated, filtered, washed with distilled water and dried overnight. ^{1}H NMR (400 MHz, $CDCl_3$, ppm); δ 8.09-8.07 (d, 2H), 7.67-7.65 (d, 2H), 7.11-7.08 (dd, 4H), 6.95-6.92 (dd, 2H), 6.86-6.83 (dd, 4H), 3.80-3.79 (d, 6H), 2.81-2.77 (t, 2H), 2.66-2.63 (t, 2H), 1.70-1.62 (m, 4H), 1.25 (s, 12H), 0.87 (s, 6H). ^{13}C NMR (400 MHz, $CDCl_3$, ppm); δ 156.00, 148.07, 140.56, 140.21, 138.54, 138.29, 132.77, 130.86, 129.60, 128.47, 126.85, 125.75, 124.96, 119.72, 114.71, 55.46, 31.92, 31.67, 30.96, 30.57, 29.69, 29.36, 29.28, 29.22, 28.79, 22.63, 14.11.

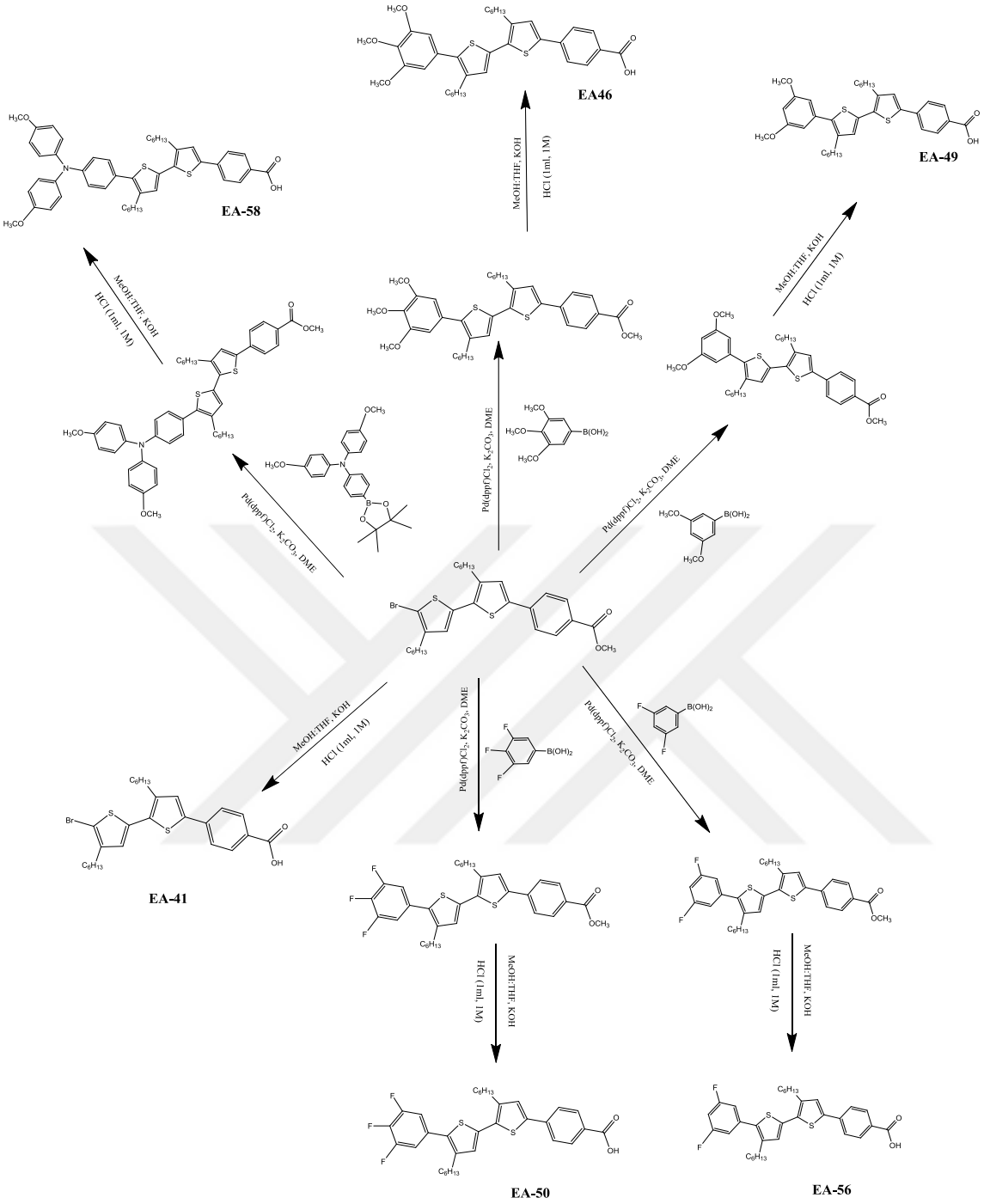

Figure 6. 1: Schematic illustration of synthetic route.

7. DEVICE FABRICATION

Commercially available ITO coated glasses were cleaned by an ultrasonic cleaning bath with usual cleaning process (15 minutes in DI-water, acetone and isopropanol, respectively). After the cleaning process, ITO coated substrates were exposed to UV-ozone treatment for 20 minutes to activate the ITO surface. SAM molecules (EA-58, EA-54 and EA-63) were dissolved in toluene ($4x10^{-4}$ M) and kept stirring in an ultrasonic bath at 50 ^{0}C for 2 h. Then, activated ITO coated substrates were immersed in SAM solution and kept overnight in ambient air. After that, ITO substrates were removed and rinsed with toluene to remove residual SAM molecules that are not strongly bonded to ITO surface. Alternatively, PEDOT:PSS deposited on ITO coated substrate as hole transport material (HTM) by spin coating at 4500 rpm for 45 s and annealed at 120 ^{0}C for 30 minutes. Finally, all substrates were transferred in glovebox to complete the rest of device fabrication.

Perovskite solution was prepared with 460 mg lead iodide (PbI_2) and 50 mg methyl ammonium iodide (MAI). PbI_2 was dissolved in anhydrous DME:DMSO mixture with ratio of 920:80 μL. MAI was dissolved in 1 mL of anhydrous isopropyl alcohol. The solutions were kept stirring at least for 2 h. Before deposition, both PbI_2 and MAI solutions were filtered with a 0.22 μL PTFE filters. The perovskite layer was deposited by spin coating with two-step deposition method. In the first step, 70 μL of PbI_2 was spin-coated at 4000 rpm for 60 s. Just after 60 s. 100 μL of MAI was dripped over the spinning substrate and the substrate was kept spinning for a further 30 s. After obtained perovskite layer, the substrates were annealed at 100 ^{0}C for 10 minutes. Subsequently, 20 mg of PCB_xM was dissolved in 1 mL of anhydrous chlorobenzene. The solution was stirred for 2 h. Then, 70 μL of solution was deposited via spin coating at 2000 rpm for 30 s. Finally, 20 nm calcium and then 100 nm of Ag was deposited by thermal evaporation under high vacuum.

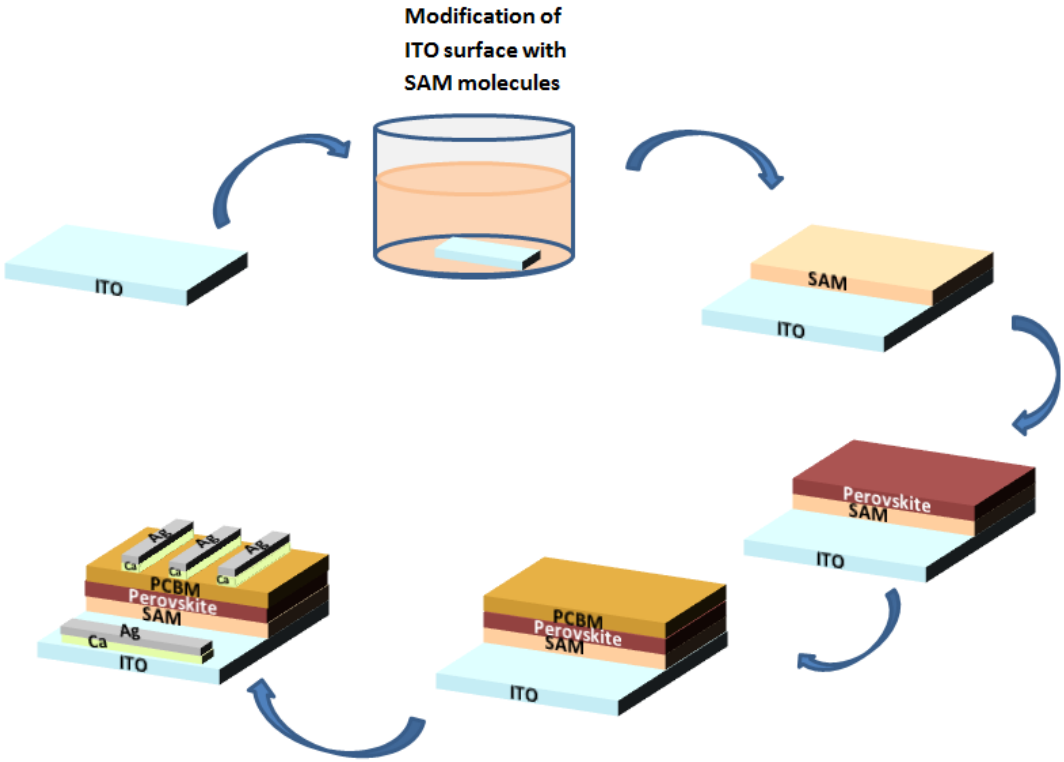

Figure 7. 1: Fabrication of SAM modified Perovskite solar cells.

8. RESULTS AND DISCUSSION

In this study, six molecules with various functional groups have been employed for the surface modification of ITO electrode by self-assembly method. The chemical structure of molecules and *p-i-n* type device configuration are indicated in Figure 8.1. Since the decrease in energy level between work function (*W*) of ITO electrode (W_{ITO}) and HOMO level of $MAPbI_3$ is essential for increasing efficient hole collection, the rationale for the modification of ITO surface with SAMs is to closely match the energy barrier alignment of the ITO/$MAPbI_3$ interface.

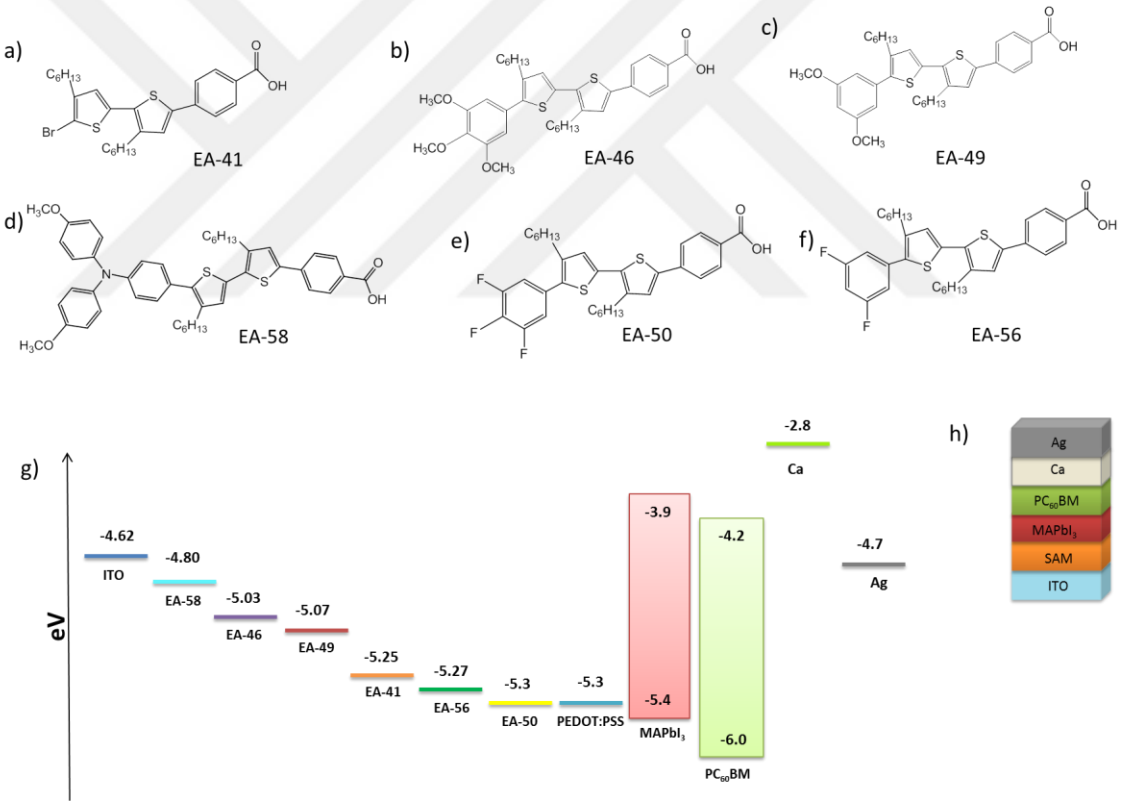

Figure 8. 1: The molecular structure of SAM molecules (a-f), energy levels of PSC materials employed in this study (g), layered structure of SAM based devices (h).

Various terminal groups with electron donating and withdrawing characteristics are intentionally chosen because, to the best of our knowledge, there is no synergistic

approach exists in the literature indicating the effect of a change of terminal group on energy level alignment and performance of perovskite solar cell.

To assess whether and how surface modification has affected W_{ITO}, Kelvin-Probe Force Microscopy (KPFM) measurements before and after surface coverage were implemented (Figure 8.2). The bare ITO shows a *W* value of 4.62eV and surface grafted ITO samples exhibit *W* values of 5.25, 5.03, 5.07, 5.30, 5.27 and 4.80eV for EA-41, EA-46, EA-49, EA-50, EA-56, and EA-58, respectively. In accordance with energy level alignment of electronic states, a suitable photo-carrier collection at the anode side is expected with having closer work function of ITO electrode as having a lower energy barrier than HOMO level of $MAPbI_3$ [79]. It can be concluded from KPFM analysis that surface modification of ITO by SAMs with electron donating terminal groups are more favorable in terms of hole collection with respect to modification by SAMs with electron withdrawing terminal groups.

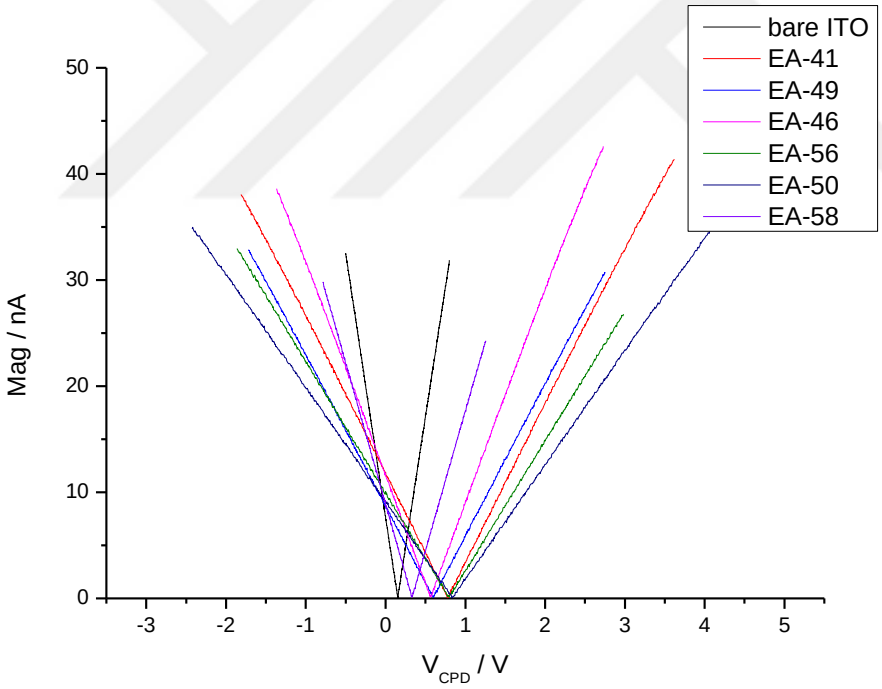

Figure 8. 2: Contact potential differences of bare and SAM coated ITO substrates.

Further information of the key features of SAM molecules with respect to changing terminal groups has been gained by examining their electrochemical behavior on ITO surface through cyclic voltammetry. For the electrochemical analysis, SAM-modified ITO was used as working electrode, platinum wire was chosen as counter electrode, and silver wire was preferred as reference electrode, respectively. Analysis

was carried out in 0.1 M tetrabutylammonium hexafluorophosphate ($TBAPF_6$). As shown in voltammograms (Figure 8.3), the inflection points of surface modified ITO electrodes have been found to be, in turn, 1.0, 0.92, 0.96, 1.05, 1.03, and 0.67 V for EA-41, EA-46, EA-49, EA-50, EA-56, and EA-58. Since triphenylamine backbone has the stronger donor feature compare to single phenyl structure, it can be already expected that EA-58 modified ITO might give inflection at the smallest oxidation potential. Besides, it should be noticed in here that in agreement with previous results, current results demonstrate that existence of methoxy groups on phenyl backbone decreases oxidation potential of SAM molecules and leads to alignment of work function at lower energy level [79]. These are possible explanations for the early inflection point of EA-46, EA-49, and EA-58 grafted ITO electrodes. This evidence also is in line with CPD (contact potential difference) values gained from KPFM plots and elucidates why EA-46, EA-49, and EA-58 modified ITO surfaces have the lower *W* values in comparison to remaining SAM modified ITO electrodes. Moreover, energy level alignment of modified ITO electrodes was calculated again by Nernst equation and obtained results are summarized in Table 8.1. Energy level values found in CV follows same trend with values obtained in KPFM.

$$E_{HOMO} = -(E_{1/2(OX)} + 4.4)eV \quad (8.1)$$

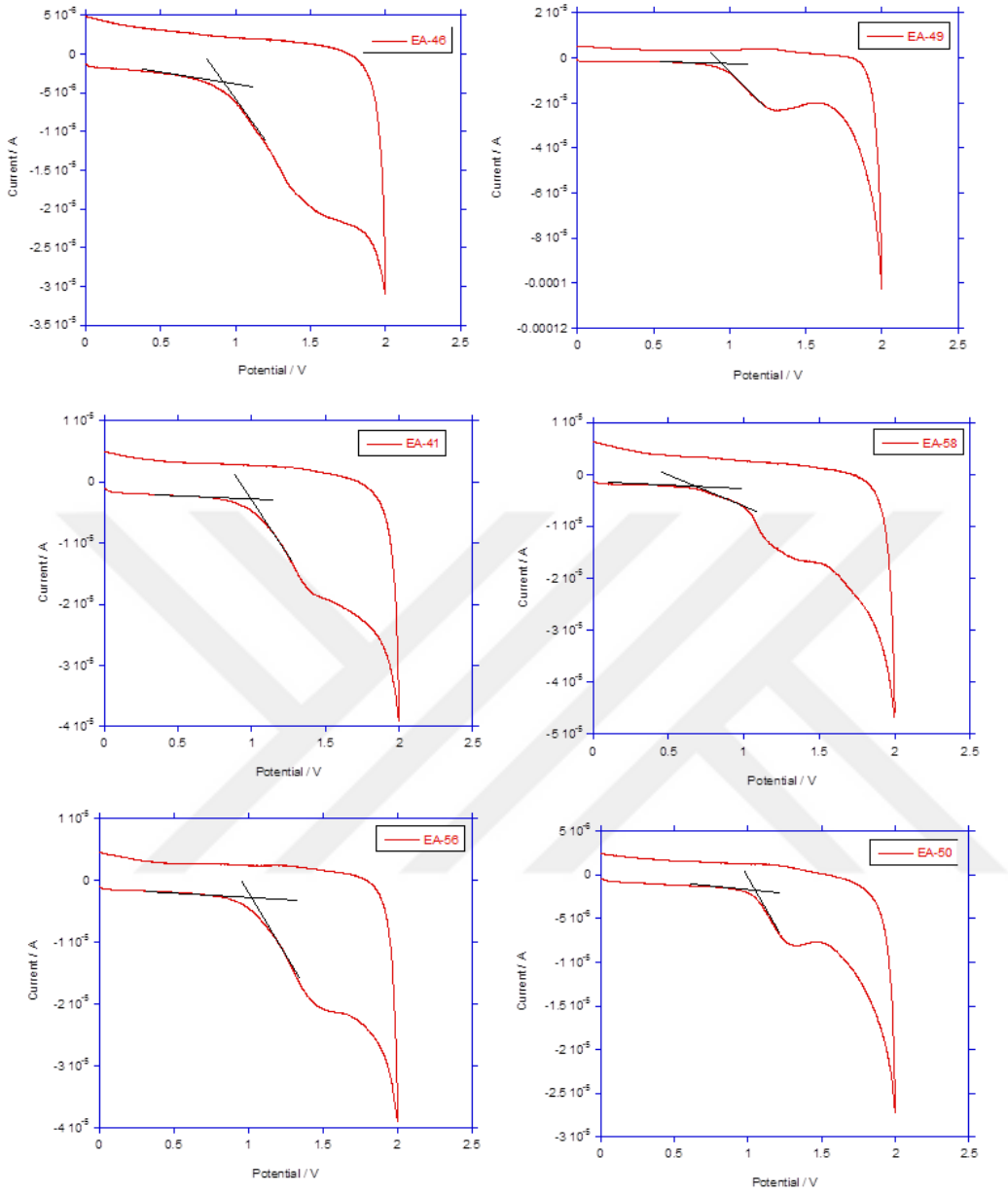

Figure 8. 3: Cyclic voltammograms of bare and SAM coated ITO substrates.

The contact angle and surface texture are two important parameters, where wetting behavior and topographical properties need to be defined, to evaluate modification of any surface by SAMs. Thus, sessile water droplet experiment was performed to reveal the changes in contact angle values of bare and modified ITO samples. As it is already known, bare-ITO surface has hydrophilic character. But, Figure 8.4 shows that surface modification by SAMs has led to increase contact angle values and loaded hydrophobic character to ITO surface. Along with wettability values, surface topography and roughness are synergistically examined because these phenomena

are corresponding to wetting properties of sample surface (Figure 8.5). As an overall description, any rough surface becomes more hydrophobic when chemically modified by hydrophobic moieties [80]. As indicated in Table 8.1, root-mean-square (RMS) values of ITO surfaces are increased after surface modification by SAM molecules due to the physical and chemical interactions with SAMs that gave rise to formation of extra layer or aggregation on ITO surface [81]. These surface roughness values and their association with contact angle measurements once again bear out that ITO surface are covered by SAM molecules.

Figure 8. 4: Changes in water contact angle with regard to bare and different SAM coated ITO substrates.

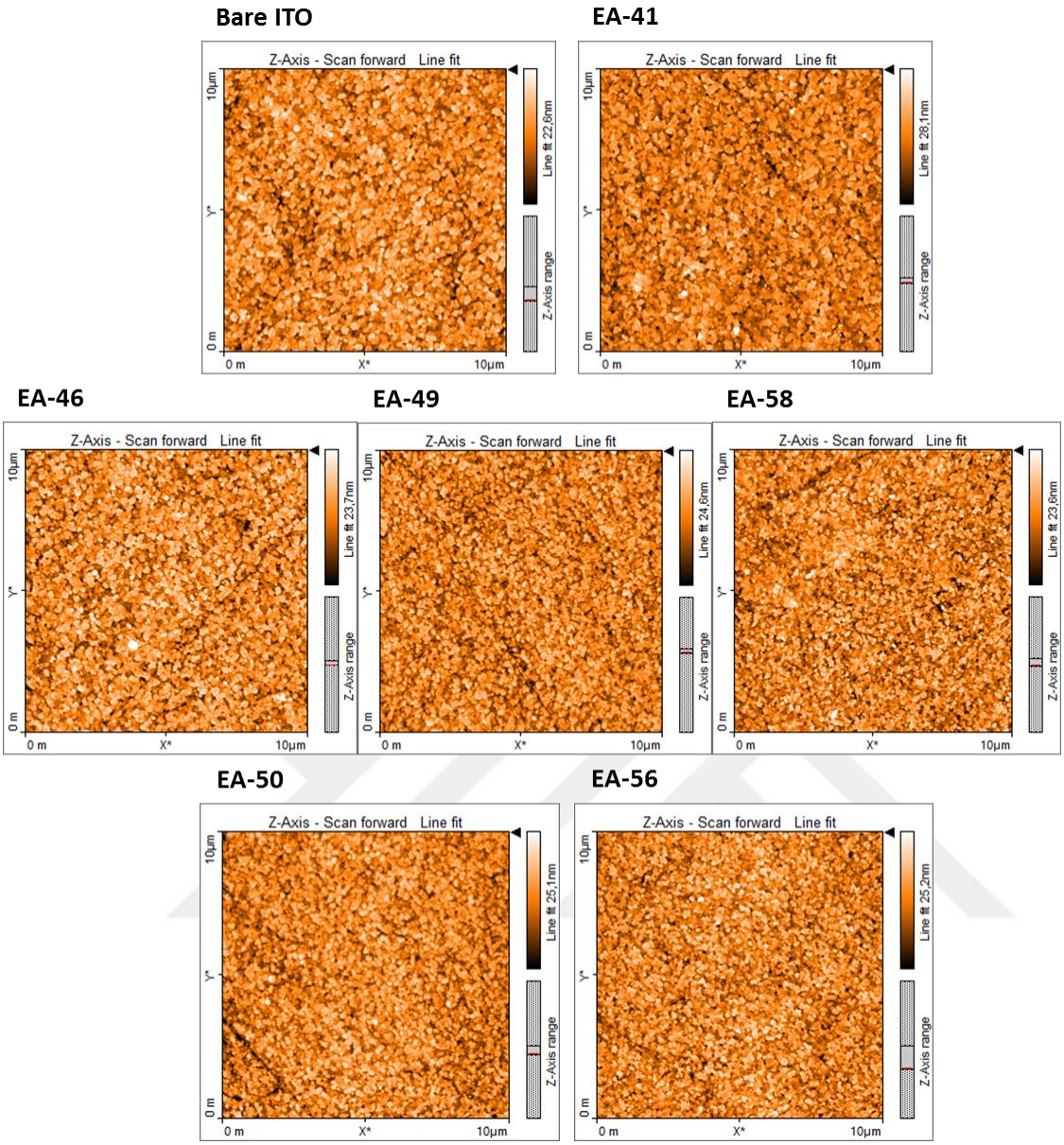

Figure 8. 5: Topographical AFM images of bare and SAM coated ITO substrates.

Table 8. 1: Comparison of bare and modified ITO surface proporties with different techniques.

	Work Function (CV) (eV)	Work Function (KPFM) (eV)	Contact Angle	RMS (nm)
Bare ITO	-	4.62	53.93^{o}	3.73
EA-41	5.40	5.25	93.49 ^{o}	4.38
EA-46	5.32	5.03	93.68 ^{o}	4.45
EA-49	5.36	5.07	99.15 ^{o}	3.99
EA-58	5.07	4.80	95.18 ^{o}	4.16
EA-50	5.45	5.30	93.49 ^{o}	4.06
EA-56	5.43	5.27	94.07 ^{o}	4.27

The surface chemical composition of modified ITO surfaces coated with EA-58, EA-41, EA-46, EA-49, EA-50 and EA-56 SAM molecules were analyzed by X-ray photoelectron spectroscopy (XPS). Figure 8.6 shows the high-resolution survey spectra of C1s and O1s to analyze the atomic bonds formed on ITO surface for **ITO/EA-58** and **ITO/EA-41.** C1s spectra fitted by three peaks corresponding to carbon in different chemical environment. The binding energy peaks of C1s for **ITO/EA-58** at 285.63, 286.37, 289.32 eV and for **ITO/EA-41** at 285.70, 286.32 and 289.24 eV are assigned to C—C/C—H, C—O—C and O—C=O, respectively. The peaks assigned O—C=O (ester bonding) at 289.32 and 289.24 eV indicates the formation of covalent bonds between COOH (carboxylic acid) head group of **EA-58** (Fig. 8.6a) and **EA-41** (Fig. 8.6c) molecules and —OH (hydroxyl groups) existent on the ITO surface [67; 82; 83].

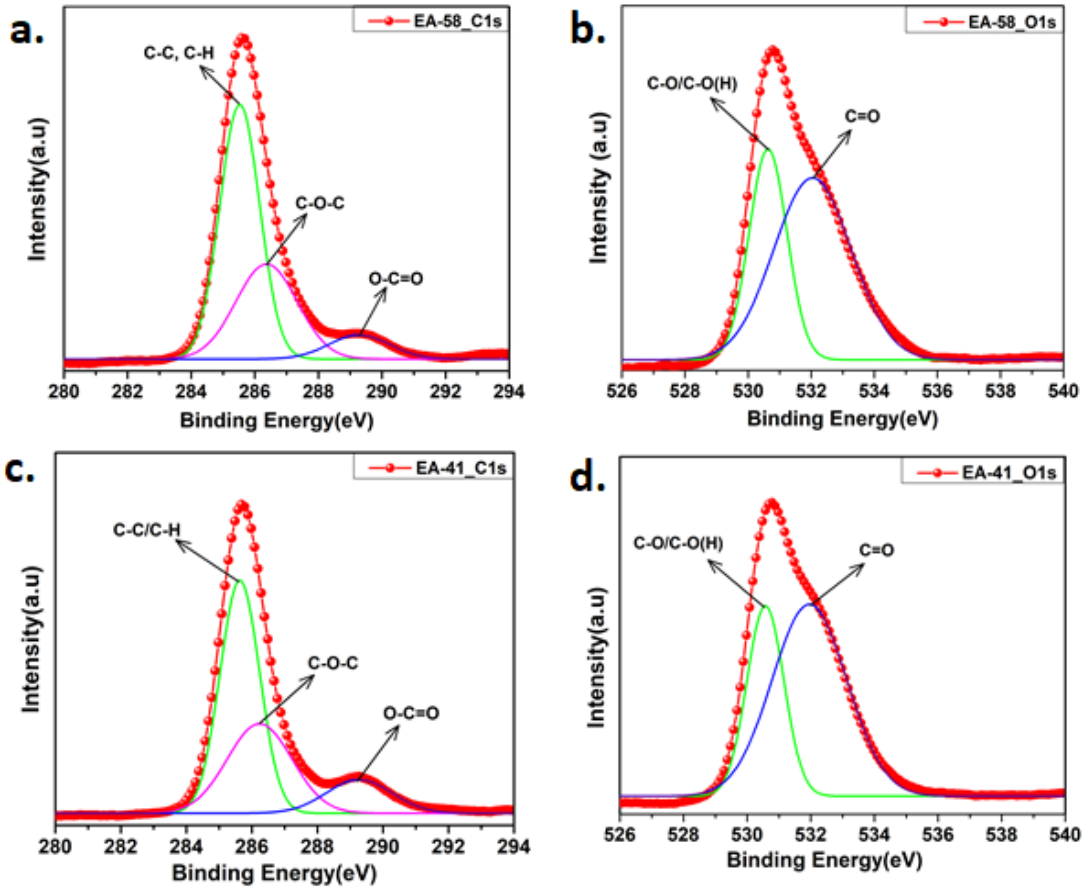

Figure 8. 6: The XPS high resolution survey spectrum of C1s (a, c) and O1s (b, d) for ITO/EA-58 and ITO/EA-41.

O1s high-resolution survey spectrum shows two main components for **ITO/EA-58** (Fig.8.6b). The O1s of **ITO/EA-58** peaks observed at 530.90 and 532.07 eV are associated with lattice oxide in $ln_xSn_yO_z$ (C—O/C—O(H)) and carbonyl group (C=O), respectively. Approximately, the same peaks are obtained from **ITO/EA-41** coated surface with values of 530.77 and 531.96 eV (Fig.8.6d) [67; 84]. The high-resolution survey spectra of C1s and O1s for **ITO/EA-46, ITO/EA-49** and **ITO/EA-50, ITO/EA-56** were shown in Figure 8.7 and Figure 8.8, respectively. As in **ITO/EA-58** and **ITO/EA-41**, same functional groups and almost the same peaks are obtained from C1s and O1s high-resolution survey spectra of **ITO/EA46, ITO/EA-49, ITO/EA-50** and **ITO/EA-56,** respectively. Corresponding binding energies of functional groups for **ITO/EA-58**, **ITO/EA-41, ITO/EA-46, ITO/EA-49, ITO/EA-50** and **ITO/56** are listed as in Table 8.2.

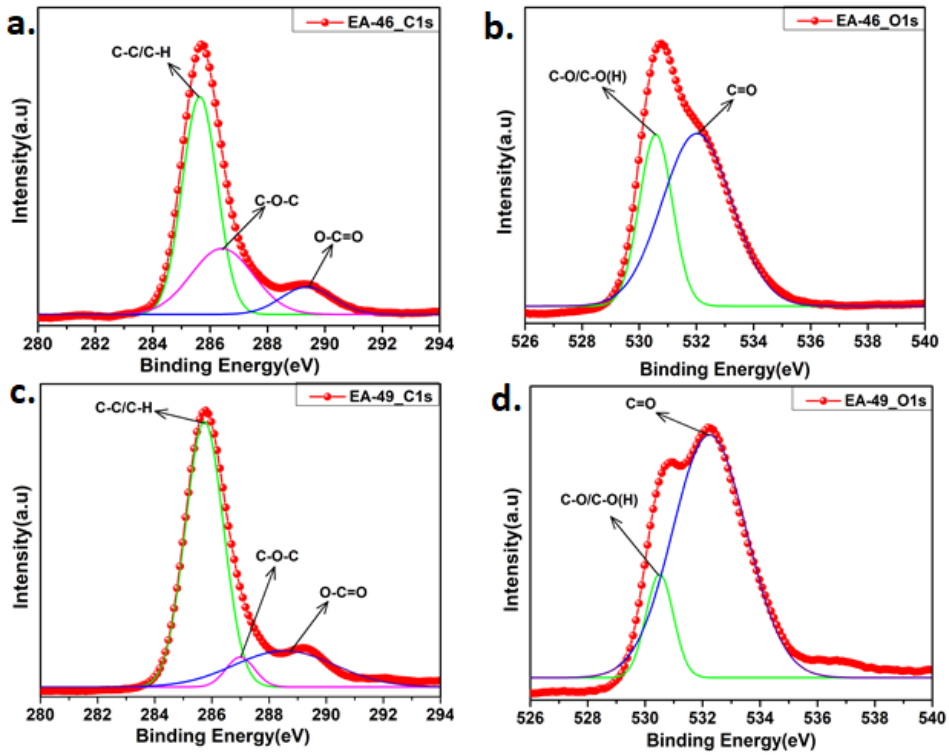

Figure 8. 7: The XPS high resolution survey spectra of C1s (a, c) and O1 (b, d) for ITO/EA-46 and ITO/EA-49.

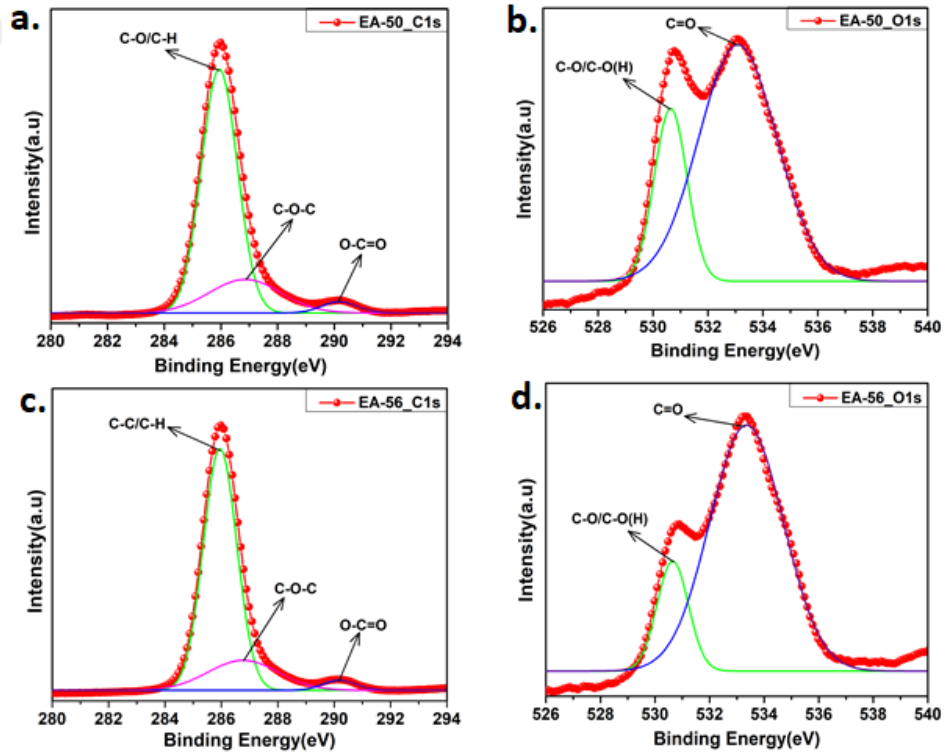

Figure 8. 8: The XPS high resolution survey spectra of C1s (a, c) and O1s (b, d) for ITO/EA-50 and ITO/EA-56.

Fig. 8.9, Fig. 8.10 and Fig. 8.11 show the wide survey spectra of ITO/EA-58, ITO/EA-41, ITO/EA-46, ITO/EA-49, ITO/EA-50 and ITO/EA-56, respectively. Almost at the same binding energies C, O, N, F, S, ln and Sn elements are identified on these six ITO/SAM surfaces by XPS. The binding energies in turn at ~487 and ~496 eV indicates the Sn3d5/2 and Sn3d3/2 while the peaks at ~446 and ~ 454 eV confirm the ln3d5/2 and ln3d3/2, respectively [85; 86]. In addition, the binding energies in turn at ~164, ~285, ~401, ~532 and ~690 eV are attributed to S2p, C1s, N1s, O1s and F1s elements [87; 88].

The XPS measurements were also performed on bare ITO before ITO substrates modified with SAM molecules (Fig. 8.12). In this measurement, the absence of N, S and F confirms ITO substrates successfully covered by SAM molecules.

Table 8. 2: The functional groups and their related binding energy for ITO/EA-58, ITO/EA-41, ITO/EA-46, ITO/EA49, ITO/EA-50 and ITO/EA-56.

Samples	O1s (eV)		C1s (eV)			N1s (eV)	S2p (eV)	F1s (eV)
	C-O/C-O(H)	C=O	C—C/C—H	C—O—C	O—C=O			
ITO/EA-58	530.90	532.07	285.63	286.37	289.32	401.28	169.10	-
ITO/EA-41	530.77	531.96	285.70	286.32	289.24	-	169.82	-
ITO/EA-46	530.56	532.07	285.66	286.39	289.32	-	169.58	-
ITO/EA-49	530.52	532.27	285.75	266.90	289.20	-	165.25	-
ITO/EA-50	530.66	533.08	285.93	286.78	290.17	-	164.89	689.77
ITO/EA-56	530.64	533.35	285.93	286.78	290.17	-	164.36	689.31

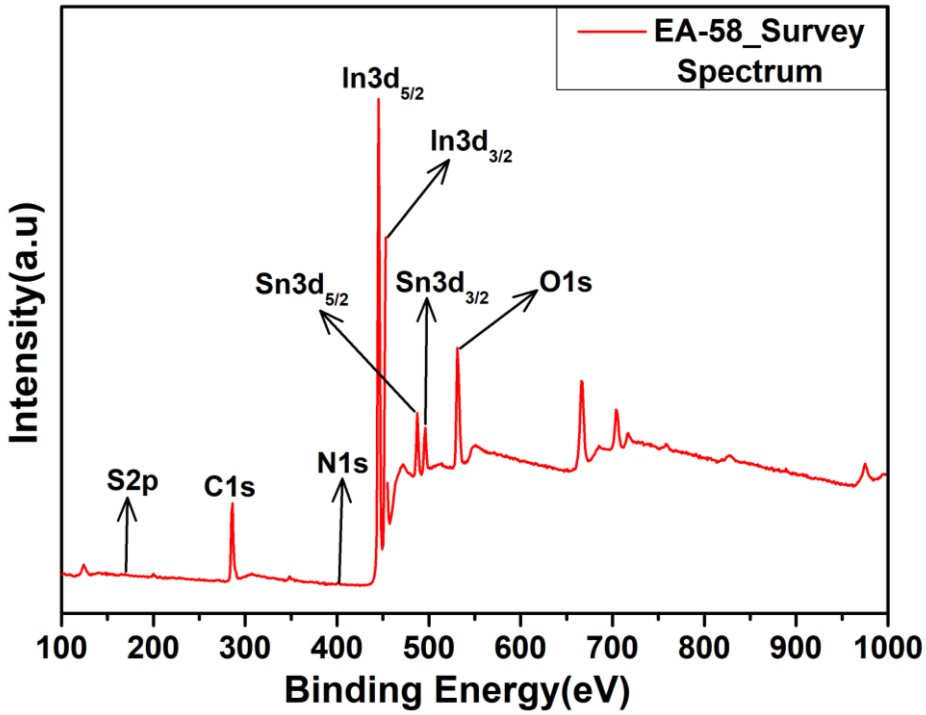

Figure 8. 9: The XPS wide survey spectrum of ITO/EA-58.

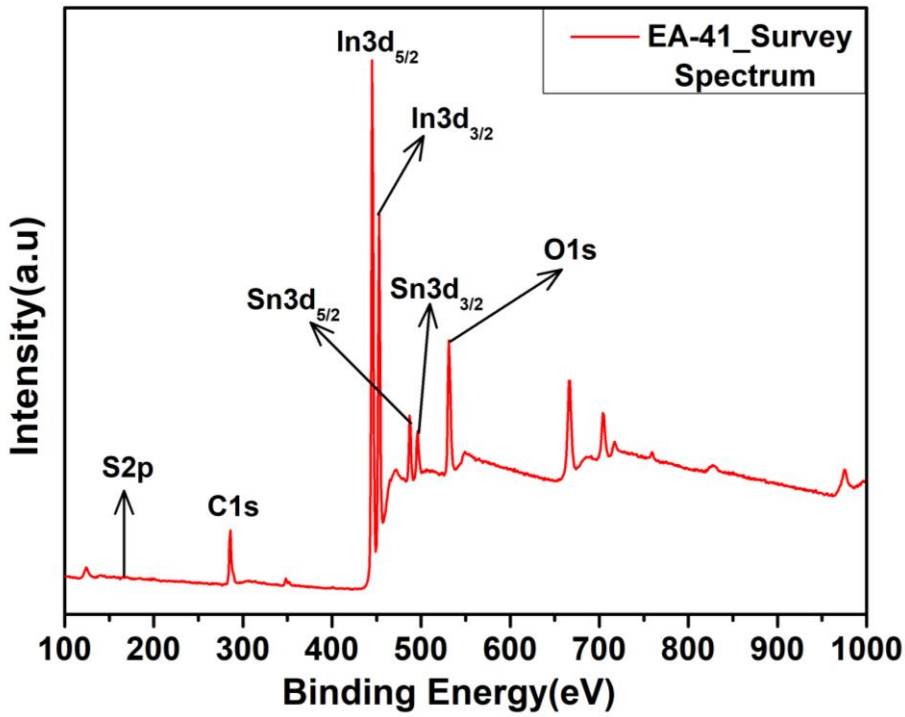

Figure 8. 10: The XPS wide survey spectrum of ITO/EA-41, ITO/EA-46 and ITO/EA-49.

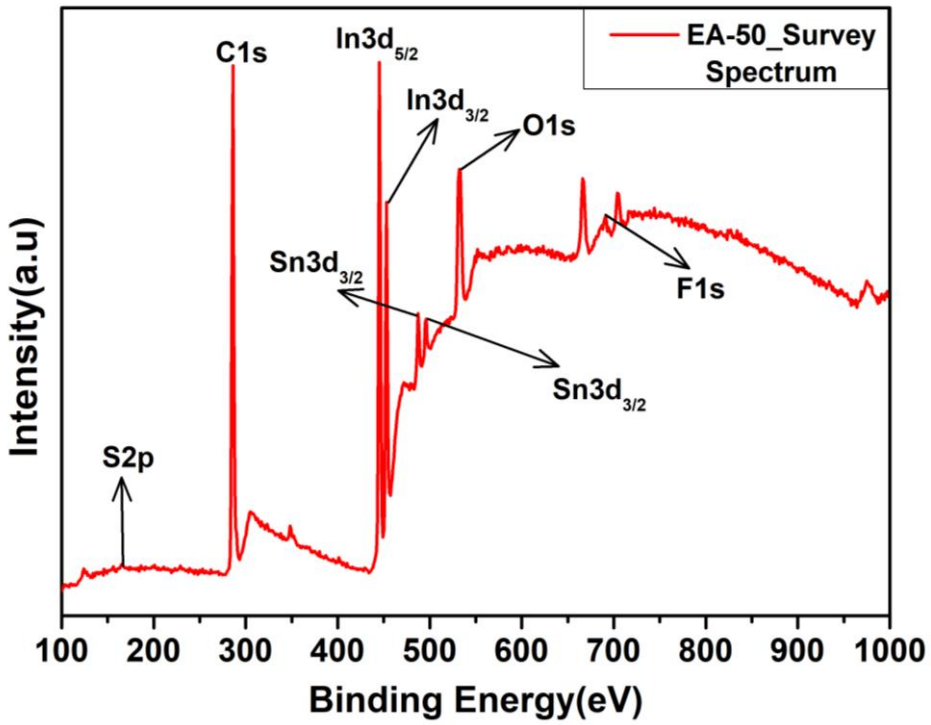

Figure 8. 11: The XPS wide survey spectrum of ITO/EA-50 and ITO/EA-56.

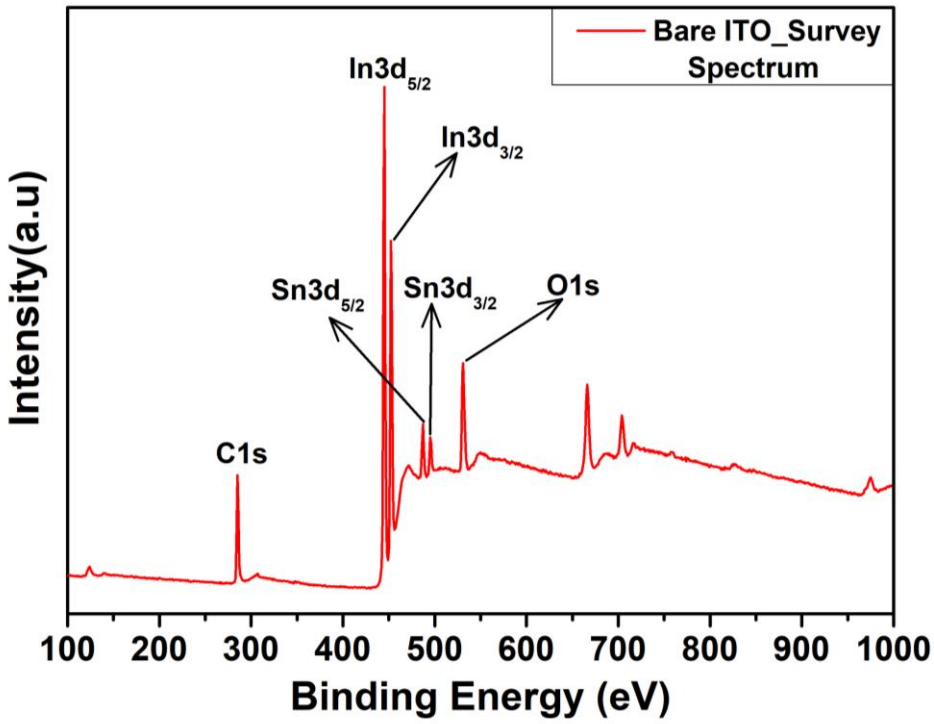

Figure 8. 12: The XPS wide survey spectrum of bare-ITO.

Photophysical properties of synthesized SAMs on ITO surface have been examined by using UV-spectrophotometer and obtained spectra are indicated in figure 8.13 The SAM molecules have shown absorption bands in the range of 300-700 nm corresponding to π-π* transitions including localized conjugated skeleton and intramolecular charge transfer between terminal groups and head groups of molecules. EA-41 and EA-49 have shown absorption at UV range of solar spectrum; therefore, they haven't prevented visible light reaching to perovskite layer. EA-49 has indicated absorption band covering the region between 326-417 nm, but EA-46 has shown broader absorption band extending from 300 to 462 nm compare to EA-49. As indicated in CV measurement, one more methoxy moiety on terminal group of EA-46 has caused increase in HOMO level of molecule that also has caused 20nm red shift in absorption maximum with respect to EA-49. Moreover, triphenylamine group on EA-58 has given rise to the highest increase in HOMO level that has provided absorption from 300 to 513 nm. Nevertheless, its absorption is lower than 600 nm and therefore it only absorbed light within some part of visible region. On the other hand, EA-50 and EA-56 carrying fluorine terminal groups have shown absorption reaching to 670 nm that could be resulted in limited absorption of perovskite within visible region.

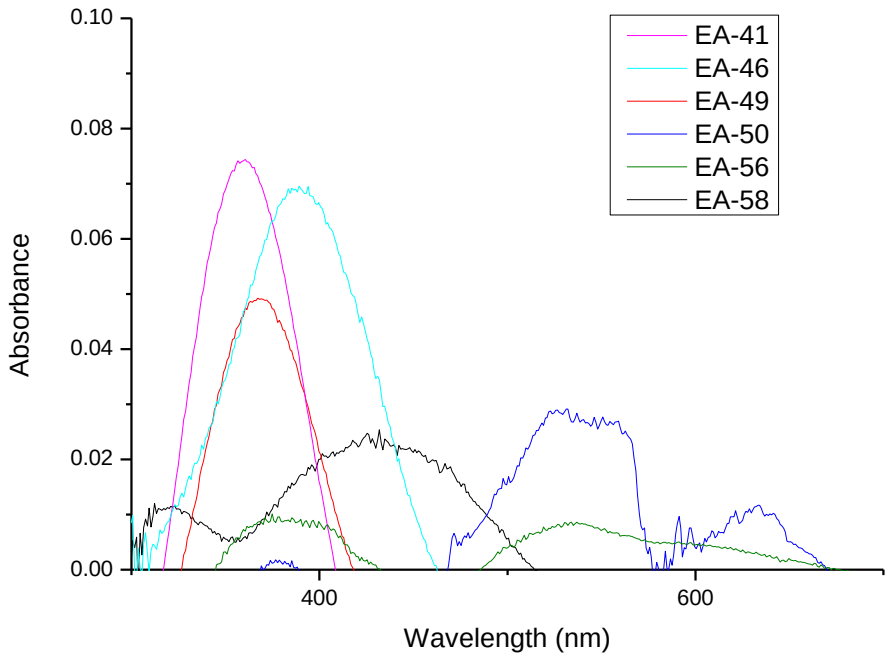

Figure 8. 13: Absorption curves of SAM modified ITO surfaces.

As shown in figure 8.14, XRD is used to characterize the structure of $CH_3NH_3PbI_3$ perovskite. The diffraction peaks at 14.22^0, 20.15^0, 23.63^0, 24.64^0, 28.59^0, 30.31^0, 32.03^0 and $40,82^0$ are correspond to (110), (112), (211), (202), (220), (213), (222) and (224) planes of tetragonal phase $CH_3NH_3PbI_3$ perovskite, respectively [89-93]. The diffraction peak appearing at 12.83^0 belongs to the residual PbI_2(*). Moreover, diffraction peaks at 38.97^0, 39.87^0, 42.95^0 and 43.50^0 are related to PbI_2-MAI-DMF intermediate phase [93].

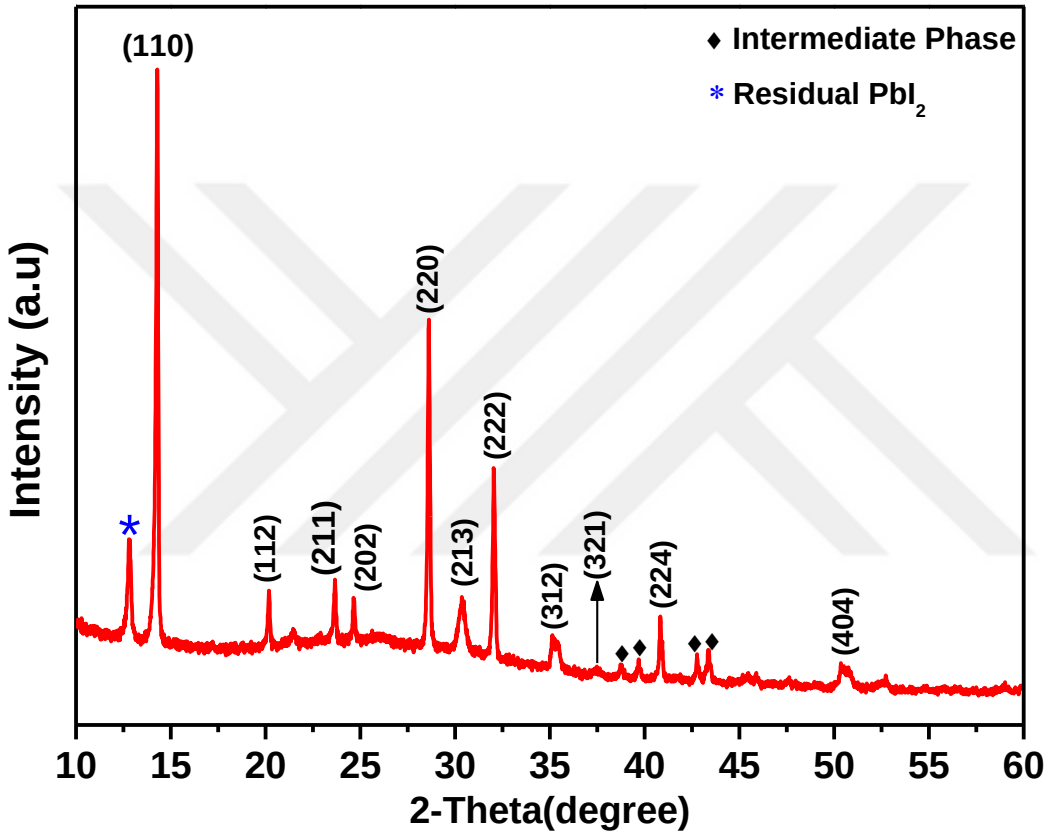

Figure 8. 14: XRD pattern of $CH_3NH_3PbI_3$ perovskite film.

The quality of the perovskite film has a crucial effect on performance of perovskite solar cells. The film quality is determined by grain size, crystallinity, surface coverage etc. [94]. Figure 8.15 shows the morphology of the perovskite films deposited on bare ITO (a), ITO/PEDOT:PSS (b), ITO/EA-58 (c), ITO/EA-41 (d) and ITO/EA-46 (e), ITO/EA-49 (f), ITO/EA-50 (g) and ITO/EA-56 (h). It is clear from these images that after modification of ITO with PEDOT:PSS and SAM molecules, bigger grain size, pinhole-free, high compact and full surface coverage films (which is desirable for perovskite solar cells) were obtained.

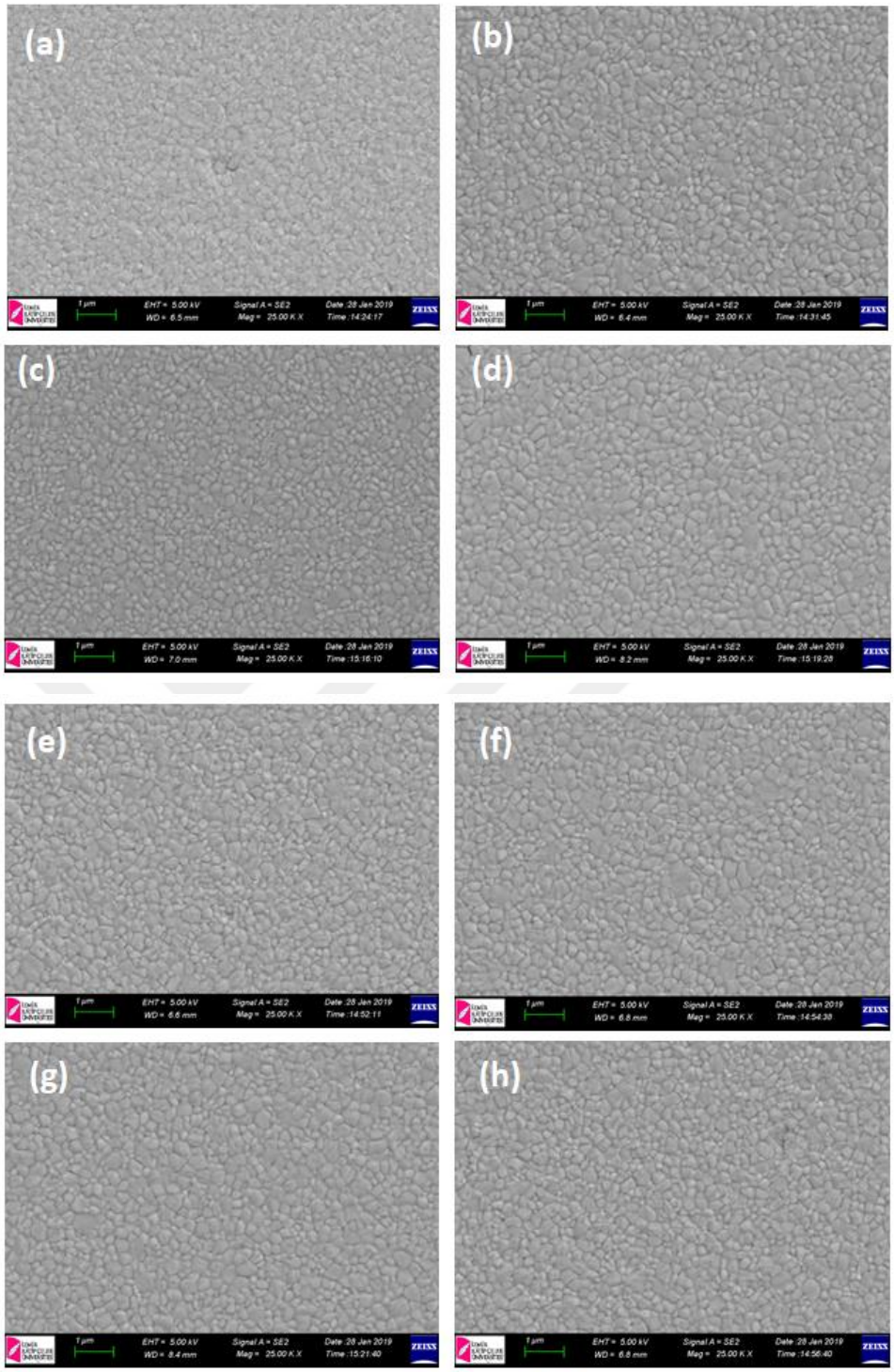

Figure 8. 15: SEM images of perovskite film deposited on bare ITO (a), ITO/PEDOT:PSS (b), ITO/EA-58 (c), ITO/EA-41 (d), ITO/EA-46 (e), ITO/EA-49 (f), ITO/EA-50 (g) and ITO/EA-56 (h).

8.1 Solar Cell Performance

The interface modification between ITO and perovskite is essential for the change of energy level alignment that also effect the charge extraction and recombination at

interface. This situation can influence some device parameters such as the V_{OC}, FF, and J_{SC} [79]. Beyond the re-arrangement of energy barrier, metal oxide surfaces include dangling bonds due to some active groups such as hydrogen, hydroxyl that result in formation of deep trap states and therefore increase charge recombination velocity. Besides, lead containing perovskite films possess empty orbits of Pb^{2+} that can form several chemical bonds with electron donating groups such as pyridine, amino, hydroxyl and can cause trapping and de-trapping on the carriers by inducing electron density change in perovskite film. SAMs modification can saturate active sites on surface and passivate trap states on both metal oxide and perovskite film surfaces as well as improve charge extraction efficiency and enhance the FF [95]. Interactions of end groups of SAM molecules with perovskite structure is shown in figure 8.16.

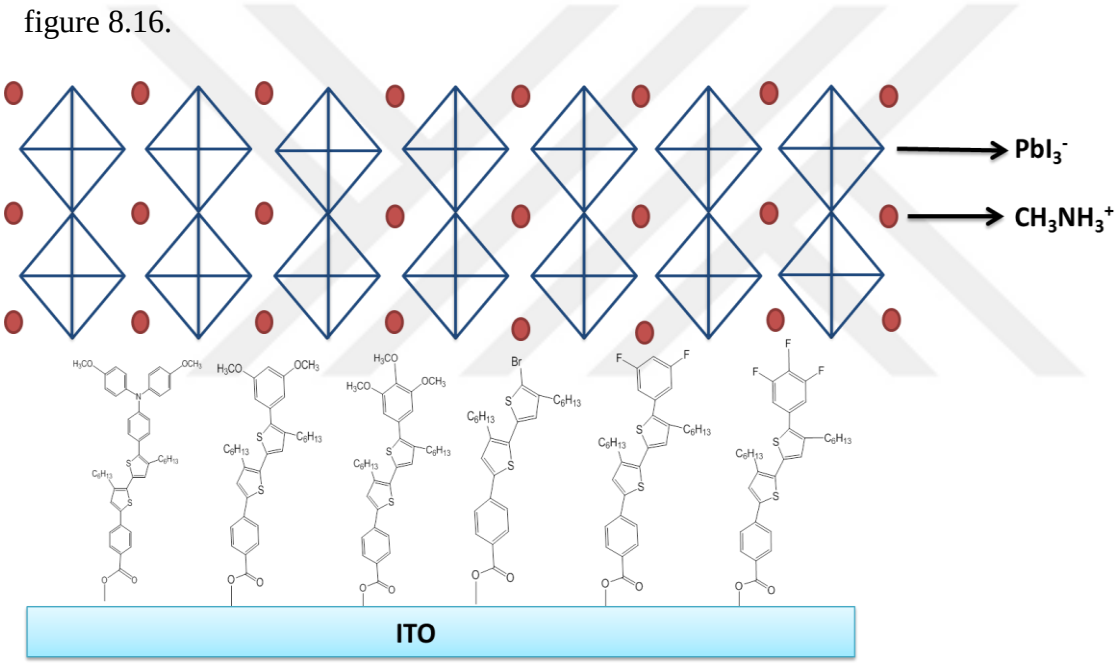

Figure 8. 16: Interactions of end groups of SAM molecules with perovskite structure.

Figure 8.16 shows current-voltage (I-V) characteristics of solar cells fabricated on bare, SAMs modified and PEDOT:PSS (reference cell) coated ITOs. The highest efficiency is obtained with EA-58 modified cell due to appropriate energy barrier that led to rectification in J_{SC} and FF values. As for EA-49, it has higher PCE than both EA-46 and reference cell because of the its better energy alignment, which give rise to rectification in V_{OC} while its J_{SC} and FF values are comparable with one observed with PEDOT:PSS. Moreover, in agreement with literature, it can be

concluded that methoxy terminal group can passivate the trap state in the perovskite layer through coordination bond that can improve optoelectronic properties of perovskite film and therefore result in enhancement in efficiency of device [95; 96].

Additionally, the obtained PCE of EA-41 is more favorable than that of reference cell. As in case of EA-49 treatment, improvement in V_{OC} as well as intimate interaction between halogen terminal atom and $MAPbI_3$ are closely related to enhanced PCE. It should be pointed out that bromine atom can be used to participate to perovskite structure [95; 97].

On the other hand, EA-50 and EA-56, bearing electron-withdrawing terminal groups, indicate relatively lower PCE compared to other cells. Formation of hydrogen bond between organic constituent of perovskite and fluorine containing molecule has already been introduced to literature [98]. In accordance with this finding, it can be deduced that formation of hydrogen bond (C—H-F—C) might withdraw the electron density towards ITO surface and reduce effective charge seperation and therefore having resulted in deterioration of PCE. Moreover, effect of degree of fluorination on dipole moment has already been studied. As a general statement, the higher the number of fluorine atoms on terminal group, the bigger the dipole moment directing to ITO surface [79]. This phenomenon has given rise to the bigger change in work function and therefore resulted in improper energy level alignment with perovskite layer. This could be another explanation of decrease in PCE .

It is commonly observed that I-V curve of the perovskite solar cell display hysteresis. Thus, to understand influence of SAMs' modification on device performance, their effect on hysteresis was investigated. Different from bare-ITO, all SAMs except for EA-50 present less or negligible hysteresis with respect to reference cell that is in accordance with photovoltaic parameters regardless of scan direction (Figure 8.17). The reduced hysteresis might be consequence of efficient hole collection due to decreased interstitial defects of perovskite layer within or near to the interface of materials, which could act as traps for holes and electrons [95; 99]. This interpretation is also in agreement with the theory stating that hysteresis is influenced by the requirement for trap filling and decreased by lower trap density in PSCs [100].

Figure 8.18 compares the external quantum efficiency (EQE) spectra for PSCs with and without modification. As it can be seen, the highest EQE peaks of the best

device (EA-58) can achieve to ~83% and it has a stronger EQE response than reference cell in the wavelength ranges of 350-750 nm, also, its integrated J_{SC} (19.10 mA/cm^2) from the EQE spectra matches well to that of obtained J_{SC} (18.62 mA/cm^2) from I-V measurements. Moreover, EA-41 and EA-49 demonstrates the better response in the wavelength region between 350-750 nm with respect to PEDOT:PSS and they achieve EQE peaks of 78.03 % and 79.51%, respectively. Their integrated J_{SC} values are well match with those obtained from I-V measurements (Table 8.3). These superior results could be consequence of the better charge extraction and recombination reduction representing efficiency of optimal interfacial chemical interactions for efficient photon-to-electron conversion for $MAPbI_3$ based PSC [79; 96]. Among the remaining SAMs, EA-50 has comparable EQE spectrum response and J_{SC} value with reference cell whereas EA-46 and EA-56 have less favorable results than PEDOT:PSS. J_{SC} results obtained in I-V curves and EQE are indicated in Figure 8.17 and Figure 8.18 as well as all data related to device parameters is summarized in table 8.3.

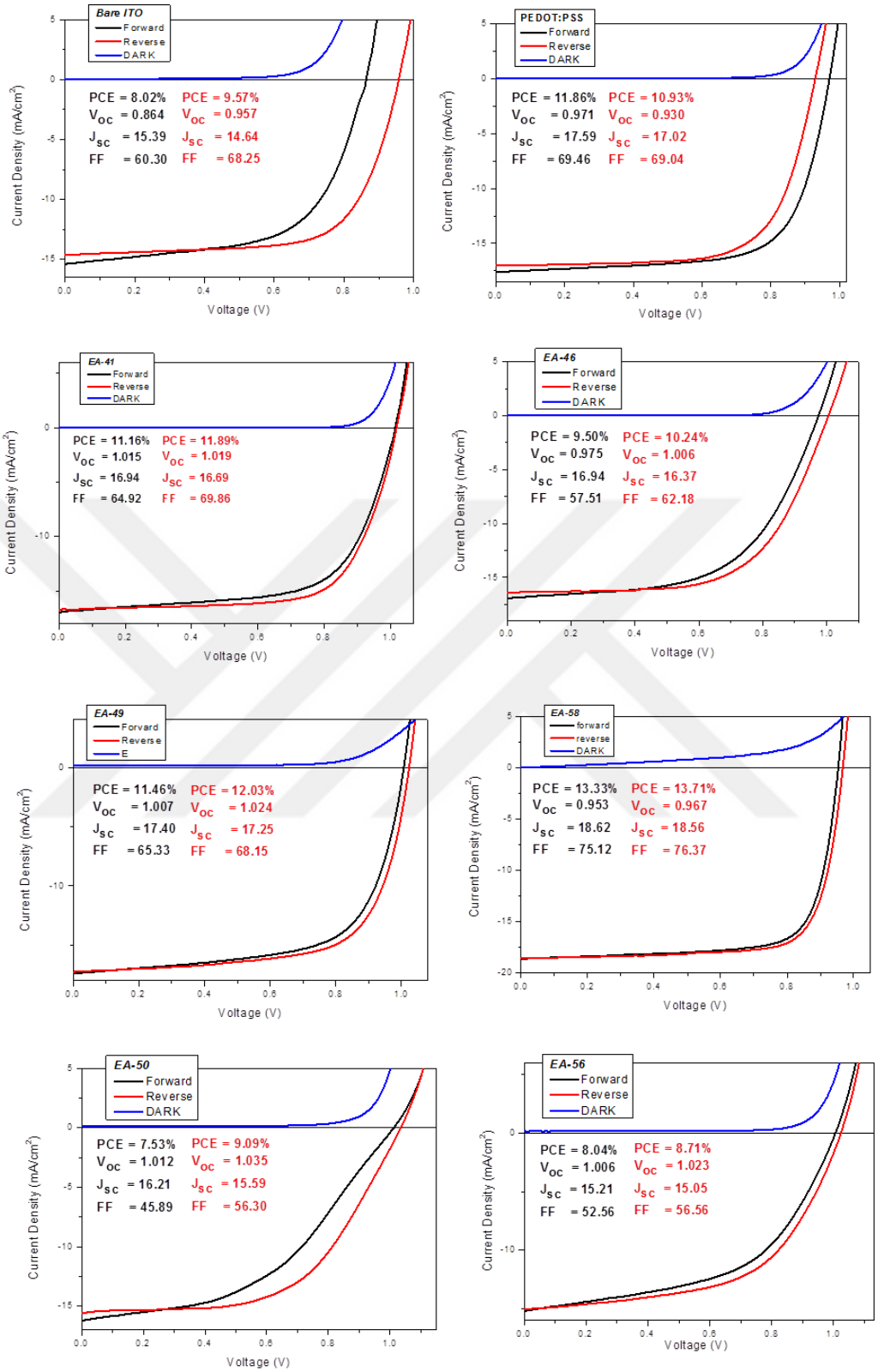

Figure 8. 17: Current density-Voltage curves of bare and modified cells.

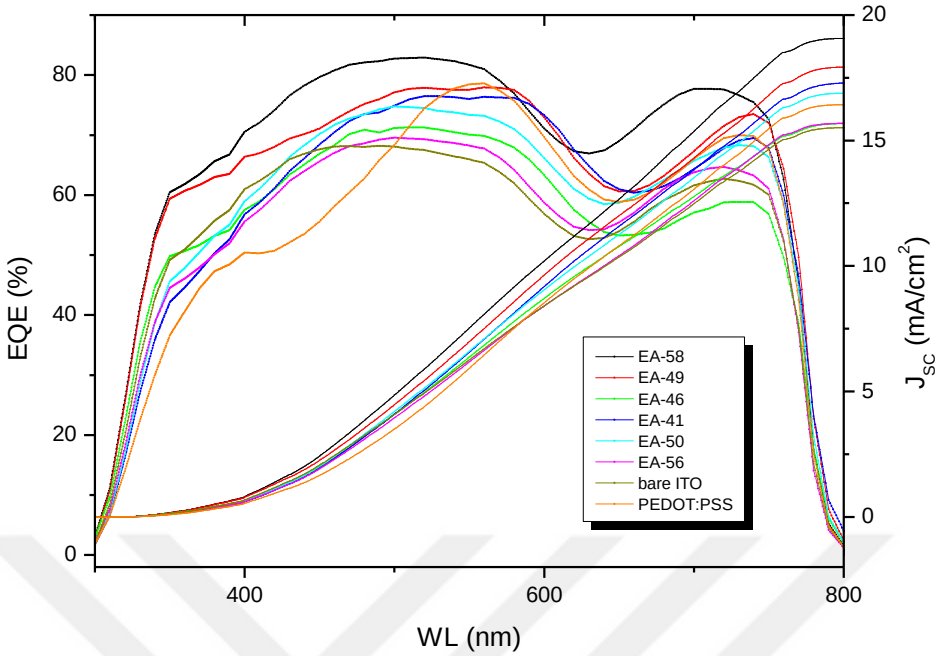

Figure 8. 18: EQE spectra of the devices.

Table 8. 3: Photovoltaic parameters of devices.

	V_{OC} (V)		J_{SC} (mA/cm^2)			FF		PCE (%)		Resistance (Ωcm^2)	
	forward	**reverse**	**forward**	**reverse**	**integrated**	**forward**	**reverse**	**forward**	**reverse**	**Rs**	**Rsh**
Bare ITO	0.864	0.957	15.39	14.64	15.53	60.30	68.25	8.02	9.57	8.69	335.64
PEDOT:PSS	0.971	0.930	17.59	17.02	16.44	69.46	69.04	11.86	10.93	5.89	681.37
EA-41	1.015	1.019	16.94	16.69	17.33	64.92	69.86	11.16	11.89	9.53	479.32
EA-46	0.975	1.006	16.94	16.37	15.70	57.51	62.18	9.50	10.24	13.15	2271.43
EA-49	1.007	1.024	17.40	17.25	17.95	65.33	68.15	11.46	12.03	5.93	760.04
EA-50	1.012	1.035	16.21	15.59	16.91	45.89	56.30	7.53	9.09	20.95	1242.64
EA-56	1.006	1.023	15.21	15.05	15.70	52.56	56.56	8.04	8.71	13.54	248.91
EA-58	0.953	0.967	18.62	18.56	19.10	75.12	76.37	13.33	13.71	3.59	849.61

9. CONCLUSION AND FUTURE PERSPECTIVE

In this doctoral thesis, novel six molecules with various terminal groups were synthesized and utilized for the surface modification of ITO electrodes. Afterwards, surface grafted substrates were used for the fabrication of $MAPbI_3$ based inverted PSCs.

The synthesis of surface modifiers was achieved through Suzuki coupling reaction of donor and acceptor type moieties of thiophene linkers with bromine to result in methyl ester as intermediate structures. Final molecules were obtained by converting methyl ester to carboxylic acid via acidification reaction. The success of each reaction step was proven by NMR spectroscopy.

SAM molecules were adsorbed on ITO surface by dip-coating. KPFM, CV, contact angle, AFM, and XPS analysis were carried out to determine surface modification by SAM molecules. Different oxidation potentials, various contact angle values, AFM roughness parameters and XPS results showed that SAM molecules are chemically adsorbed on ITO surface, succesfully. Moreover, the change in work function after surface grafting was calculated through CPD (contact potential difference) values gained from KPFM plots.

$MAPbI_3$ based perovskite film was performed by two-step solution process. Formation of perovskite lattice was borne out by XRD pattern. Quality of obtained perovskite films was analyzed by SEM. SEM images indicated that SAM modifications gave rise to bigger grain size, pinhole-free, high compact and full surface coverage films that are desirable for perovskite solar cells.

Among all synthesized SAM molecules, and devices fabricated from these structures, following results were obtained.

- SAMs with acceptor terminal groups resulted in higher increase in energy level alignment with respect to SAMs with donor terminal groups.
- SAMs with donor terminal groups indicated superior device parameters than SAMs with acceptor terminal groups. Furthermore, depending on energy level

alignment as well as saturation of dangling bond and trap states, all SAMs with donor terminal groups, except EA-46, showed comparable or more favorable PCE performance than the reference cell. EA-58 indicated the highest PCE value reaching to non-negligible value of 13.71%.

- SAM with halide terminal group (EA-41) has advantage of intimate interaction with $MAPbI_3$ and can be utilized as participant of perovskite structure. This makes it a rival molecular structure with respect to PEDOT:PSS.
- SAMs with acceptor terminal groups are less favorable in terms of device performance. It can be concluded from device parameters that formation of hydrogen bond (C—H-F—C) might withdraw the electron density towards ITO surface and reduce efficient charge extraction and effective hole transport and therefore having resulted in deterioration of PCE.
- All proposed SAMs except EA-50 showed comparable or improved hysteresis compare to PEDOT:PSS and this is possibly due to the passivation of trap states in both ITO surface and perovskite interface.

This thesis proved that it is feasible to customize ITO surface with SAM molecules with a versatile approach. This study guides us to design new SAM structures showing good performance in photovoltaic applications.

Remarkably, as a future perspective, the performance of the SAMs proposed in this study can be examined by changing device configuration from PSC to OSC. This approach can give us an opportunity to evaluate interaction of SAMs with pure organic photosensitizers rather than organic-inorganic hybrid structure.

Another further perspective obtained from this study is that this modification process can also be applied to other substrate materials. ETMs such as TiO_2 and SnO_2 can be used to assess the effect of modification on their work functions and finally on their device parameters in *n-i-p* type device architecture. As a general exception, molecular modification with dipole moment from substrate to perovskite film can be more favorable in ETM but it is vice versa in HTL. Therefore, comparative screening study can be conducted to elucidate the effect of variation in terminal organic group on device performance.

As can be seen throughout the work, donor structures with organic extension, which has intimate interaction with perovskite film, have shown superior performance than

acceptor moieties in inverted PSC. Further strategy of the prospective SAM should be based on designing of the stronger donor with organic or halide extension that can pretend as participate into $MAPbI_3$ film such as amine and iodine. This approach may be more clear indicative behavior of SAM at HTL and $MAPbI_3$ interface.

REFERENCES

[1] IEA, I., (2013), Key World Energy Statistics, 2013. International Energy Agency publication.

[2] Bo, X. (2015). *Advanced Organic Hole Transport Materials for Solution-Processed Photovoltaic Devices.* KTH Royal Institute of Technology.

[3] Yang, L. (2014). *Hole Transport Materials for Solid-State Mesoscopic Solar Cells.* Acta Universitatis Upsaliensis.

[4] Lundberg, O. (2003). *Band gap profiling and high speed deposition of Cu (In, Ga) Se2 for thin film solar cells.* Acta Universitatis Upsaliensis.

[5] Lindqvist, C.**,** (2014), *Stability of Bulk-Heterojunction Blends for Solar Cell Applications*. Chalmers University of Technology.

[6] Outlook, A.E., (2016), Early Release: Annotated Summary of Two Cases. DOE/EIA-440 0373ER.

[7] Barroso, J.M. (2007)Europe's energy policy and the third industrial revolution. in *speech by President of the European Commission at Loyola de Palacio energy conference, Madrid*.

[8] Hoeven, M., (2013). Nordic energy technology perspectives: Pathways to a carbon neutral energy future. *2013 Nordic Energy Technology Perspectives OECD/IEA. Tech. Rep*.

[9] Bárány, A.&Grigonytė, D., (2015). Measuring fossil fuel subsidies. *ECFIN Economic Brief*, 40(40): p. 1-13.

[10] Morata, F.&Sandoval, I.S.**,** (2012), *European energy policy: An environmental approach*. Edward Elgar Publishing.

[11] Chapin, D.M., Fuller, C.&Pearson, G., (1954). A new silicon p-n junction photocell for converting solar radiation into electrical power. *Journal of Applied Physics*, 25(5): p. 676-677.

[12] Green, M.A., Emery, K., King, D.L., Igari, S.&Warta, W., (2003). Solar cell efficiency tables (version 22). *Progress in Photovoltaics: Research and Applications*, 11(5): p. 347-352.

[13] Gregg, B.A., (2003), Excitonic solar cells. ACS Publications.

[14] Yu, G., Gao, J., Hummelen, J.C., Wudl, F.&Heeger, A.J., (1995). Polymer photovoltaic cells: enhanced efficiencies via a network of internal donor-acceptor heterojunctions. *Science*, 270(5243): p. 1789-1791.

[15] Zhu, R., Chung, C.-H., Cha, K.C., Yang, W., Zheng, Y.B., Zhou, H., Song, T.-B., Chen, C.-C., Weiss, P.S.&Li, G., (2011). Fused silver nanowires with metal oxide nanoparticles and organic polymers for highly transparent conductors. *ACS nano*, 5(12): p. 9877-9882.

[16] Chen, K.-S., Salinas, J.-F., Yip, H.-L., Huo, L., Hou, J.&Jen, A.K.-Y., (2012). Semi-transparent polymer solar cells with 6% PCE, 25% average visible transmittance and a color rendering index close to 100 for power generating window applications. *Energy & Environmental Science*, 5(11): p. 9551-9557.

[17] Kallmann, H.&Pope, M., (1959). Photovoltaic effect in organic crystals. *The Journal of Chemical Physics,* 30(2): p. 585-586.
[18] Shirakawa, H., Louis, E.J., MacDiarmid, A.G., Chiang, C.K.&Heeger, A.J., (1977). Synthesis of electrically conducting organic polymers: halogen derivatives of polyacetylene,(CH) x. *Journal of the Chemical Society, Chemical Communications,* (16): p. 578-580.
[19] Anselmo, A.S. (2011). *The morphology of polyfluorene: fullerene blend films for photovoltaic applications.* Karlstad University.
[20] Tang, C.W., (1986). Two-layer organic photovoltaic cell. *Applied physics letters,* 48(2): p. 183-185.
[21] Sariciftci, N.S., Smilowitz, L., Heeger, A.J.&Wudl, F., (1992). Photoinduced electron transfer from a conducting polymer to buckminsterfullerene. *Science,* 258(5087): p. 1474-1476.
[22] Winder, C.&Sariciftci, N.S., (2004). Low bandgap polymers for photon harvesting in bulk heterojunction solar cells. *Journal of Materials Chemistry,* 14(7): p. 1077-1086.
[23] Peumans, P.&Forrest, S., (2001). Very-high-efficiency double-heterostructure copper phthalocyanine/C 60 photovoltaic cells. *Applied Physics Letters,* 79(1): p. 126-128.
[24] Drechsel, J., Männig, B., Kozlowski, F., Gebeyehu, D., Werner, A., Koch, M., Leo, K.&Pfeiffer, M., (2004). High efficiency organic solar cells based on single or multiple PIN structures. *Thin Solid Films,* 451: p. 515-517.
[25] Rand, B.P., Xue, J., Yang, F.&Forrest, S.R., (2005). Organic solar cells with sensitivity extending into the near infrared. *Applied Physics Letters,* 87(23): p. 233508.
[26] Mutolo, K.L., Mayo, E.I., Rand, B.P., Forrest, S.R.&Thompson, M.E., (2006). Enhanced open-circuit voltage in subphthalocyanine/C60 organic photovoltaic cells. *Journal of the American Chemical Society,* 128(25): p. 8108-8109.
[27] Gommans, H., Cheyns, D., Aernouts, T., Girotto, C., Poortmans, J.&Heremans, P., (2007). Electro-Optical Study of Subphthalocyanine in a Bilayer Organic Solar Cell. *Advanced functional materials,* 17(15): p. 2653-2658.
[28] Koeppe, R., Sariciftci, N.S., Troshin, P.A.&Lyubovskaya, R.N., (2005). Complexation of pyrrolidinofullerenes and zinc-phthalocyanine in a bilayer organic solar cell structure. *Applied Physics Letters,* 87(24): p. 244102.
[29] Troshin, P.A., Koeppe, R., Peregudov, A.S., Peregudova, S.M., Egginger, M., Lyubovskaya, R.N.&Sariciftci, N.S., (2007). Supramolecular association of pyrrolidinofullerenes bearing chelating pyridyl groups and zinc phthalocyanine for organic solar cells. *Chemistry of Materials,* 19(22): p. 5363-5372.
[30] Troshin, P., Lyubovskaya, R.&Razumov, V., (2008). Organic solar cells: structure, materials, critical characteristics, and outlook. *Nanotechnologies in Russia,* 3(5-6): p. 242.
[31] You, J., Dou, L., Yoshimura, K., Kato, T., Ohya, K., Moriarty, T., Emery, K., Chen, C.-C., Gao, J.&Li, G., (2013). A polymer tandem solar cell with 10.6% power conversion efficiency. *Nature communications,* 4: p. 1446.
[32] Zitzler-Kunkel, A., Lenze, M.R., Meerholz, K.&Würthner, F., (2013). Enhanced photocurrent generation by folding-driven H-aggregate formation. *Chemical Science,* 4(5): p. 2071-2075.

[33] Bhosale, R., Míšek, J., Sakai, N.&Matile, S., (2010). Supramolecular n/p-heterojunction photosystems with oriented multicolored antiparallel redox gradients (OMARG-SHJs). *Chemical Society Reviews,* 39(1): p. 138-149.
[34] Bassani, D.M., Jonusauskaite, L., Lavie-Cambot, A., McClenaghan, N.D., Pozzo, J.-L., Ray, D.&Vives, G., (2010). Harnessing supramolecular interactions in organic solid-state devices: Current status and future potential. *Coordination Chemistry Reviews,* 254(19-20): p. 2429-2445.
[35] Brunetti, F.G., Kumar, R.&Wudl, F., (2010). Organic electronics from perylene to organic photovoltaics: painting a brief history with a broad brush. *Journal of Materials Chemistry,* 20(15): p. 2934-2948.
[36] Matsuo, Y., Kawai, J., Inada, H., Nakagawa, T., Ota, H., Otsubo, S.&Nakamura, E., (2013). Addition of dihydromethano group to fullerenes to improve the performance of bulk heterojunction organic solar cells. *Advanced Materials,* 25(43): p. 6266-6269.
[37] Gendron, D.&Leclerc, M., (2011). New conjugated polymers for plastic solar cells. *Energy & Environmental Science,* 4(4): p. 1225-1237.
[38] Li, G., Zhu, R.&Yang, Y., (2012). Polymer solar cells. *Nature photonics,* 6(3): p. 153.
[39] O'regan, B.&Grätzel, M., (1991). A low-cost, high-efficiency solar cell based on dye-sensitized colloidal TiO2 films. *nature,* 353(6346): p. 737.
[40] Hagfeldt, A., Boschloo, G., Sun, L., Kloo, L.&Pettersson, H., (2010). Dye-sensitized solar cells. *Chemical reviews,* 110(11): p. 6595-6663.
[41] Sharma, K., Sharma, V.&Sharma, S., (2018). Dye-sensitized solar cells: fundamentals and current status. *Nanoscale research letters,* 13(1): p. 381.
[42] Yao, Z., Zhang, M., Li, R., Yang, L., Qiao, Y.&Wang, P., (2015). A Metal-Free N-Annulated Thienocyclopentaperylene Dye: Power Conversion Efficiency of 12% for Dye-Sensitized Solar Cells. *Angewandte Chemie International Edition,* 54(20): p. 5994-5998.
[43] Nattestad, A., Mozer, A.J., Fischer, M.K., Cheng, Y.-B., Mishra, A., Bäuerle, P.&Bach, U., (2010). Highly efficient photocathodes for dye-sensitized tandem solar cells. *Nature materials,* 9(1): p. 31.
[44] Stojanovic, B.**,** (2018), *Magnetic, Ferroelectric, and Multiferroic Metal Oxides*. Elsevier.
[45] Kojima, A., Teshima, K., Shirai, Y.&Miyasaka, T., (2009). Organometal halide perovskites as visible-light sensitizers for photovoltaic cells. *Journal of the American Chemical Society,* 131(17): p. 6050-6051.
[46] Im, J.-H., Lee, C.-R., Lee, J.-W., Park, S.-W.&Park, N.-G., (2011). 6.5% efficient perovskite quantum-dot-sensitized solar cell. *Nanoscale,* 3(10): p. 4088-4093.
[47] Kim, H.-S., Lee, C.-R., Im, J.-H., Lee, K.-B., Moehl, T., Marchioro, A., Moon, S.-J., Humphry-Baker, R., Yum, J.-H.&Moser, J.E., (2012). Lead iodide perovskite sensitized all-solid-state submicron thin film mesoscopic solar cell with efficiency exceeding 9%. *Scientific reports,* 2: p. 591.
[48] Lee, B., He, J., Chang, R.P.&Kanatzidis, M.G., (2012). All-solid-state dye-sensitized solar cells with high efficiency. *Nature,* 485(7399): p. 486.
[49] Snaith, H.J., (2012). How should you measure your excitonic solar cells? *Energy & Environmental Science,* 5(4): p. 6513-6520.
[50] Lee, M.M., Teuscher, J., Miyasaka, T., Murakami, T.N.&Snaith, H.J., (2012). Efficient hybrid solar cells based on meso-superstructured organometal halide perovskites. *Science,* 338(6107): p. 643-647.

[51] Saliba, M., (2018). Perovskite solar cells must come of age. *Science,* 359(6374): p. 388-389.
[52] Snaith, H.J., (2018). Present status and future prospects of perovskite photovoltaics. *Nature materials,* 17(5): p. 372.
[53] Ibn-Mohammed, T., Koh, S., Reaney, I., Acquaye, A., Schileo, G., Mustapha, K.&Greenough, R., (2017). Perovskite solar cells: An integrated hybrid lifecycle assessment and review in comparison with other photovoltaic technologies. *Renewable and Sustainable Energy Reviews,* 80: p. 1321-1344.
[54] Berhe, T.A., Su, W.-N., Chen, C.-H., Pan, C.-J., Cheng, J.-H., Chen, H.-M., Tsai, M.-C., Chen, L.-Y., Dubale, A.A.&Hwang, B.-J., (2016). Organometal halide perovskite solar cells: degradation and stability. *Energy & Environmental Science,* 9(2): p. 323-356.
[55] Saliba, M., Matsui, T., Seo, J.-Y., Domanski, K., Correa-Baena, J.-P., Nazeeruddin, M.K., Zakeeruddin, S.M., Tress, W., Abate, A.&Hagfeldt, A., (2016). Cesium-containing triple cation perovskite solar cells: improved stability, reproducibility and high efficiency. *Energy & environmental science,* 9(6): p. 1989-1997.
[56] Yang, W.S., Noh, J.H., Jeon, N.J., Kim, Y.C., Ryu, S., Seo, J.&Seok, S.I., (2015). High-performance photovoltaic perovskite layers fabricated through intramolecular exchange. *Science,* 348(6240): p. 1234-1237.
[57] Abdi-Jalebi, M., Andaji-Garmaroudi, Z., Pearson, A.J., Divitini, G., Cacovich, S., Philippe, B., Rensmo, H., Ducati, C., Friend, R.H.&Stranks, S.D., (2018). Potassium-and Rubidium-Passivated Alloyed Perovskite Films: Optoelectronic Properties and Moisture Stability. *ACS energy letters,* 3(11): p. 2671-2678.
[58] Wang, Z., Lin, Q., Chmiel, F.P., Sakai, N., Herz, L.M.&Snaith, H.J., (2017). Efficient ambient-air-stable solar cells with 2D–3D heterostructured butylammonium-caesium-formamidinium lead halide perovskites. *Nature Energy,* 2(9): p. 17135.
[59] Wong-Stringer, M., Game, O.S., Smith, J.A., Routledge, T.J., Alqurashy, B.A., Freestone, B.G., Parnell, A.J., Vaenas, N., Kumar, V.&Alawad, M.O., (2018). High-Performance Multilayer Encapsulation for Perovskite Photovoltaics. *Advanced Energy Materials,* 8(24): p. 1801234.
[60] Bush, K.A., Palmstrom, A.F., Zhengshan, J.Y., Boccard, M., Cheacharoen, R., Mailoa, J.P., McMeekin, D.P., Hoye, R.L., Bailie, C.D.&Leijtens, T., (2017). 23.6%-efficient monolithic perovskite/silicon tandem solar cells with improved stability. *Nature Energy,* 2(4): p. 17009.
[61] Noh, J.H.&Seok, S.I., (2015). Steps toward efficient inorganic–organic hybrid perovskite solar cells. *MRS Bulletin,* 40(8): p. 648-653.
[62] Hu, Q., Wu, J., Jiang, C., Liu, T., Que, X., Zhu, R.&Gong, Q., (2014). Engineering of electron-selective contact for perovskite solar cells with efficiency exceeding 15%. *ACS nano,* 8(10): p. 10161-10167.
[63] Guo, S., Lai, C., Wu, C., Cen, G., Weiner, M.W., Aisen, P., Weiner, M., Petersen, R., Jack Jr, C.R.&Jagust, W., (2017). Conversion discriminative analysis on mild cognitive impairment using multiple cortical features from MR Images. *Frontiers in aging neuroscience,* 9: p. 146.
[64] Sapochak, L.S., Padmaperuma, A.B., Cai, X., Male, J.L.&Burrows, P.E., (2008). Inductive effects of diphenylphosphoryl moieties on carbazole host materials: design rules for blue electrophosphorescent organic light-emitting devices. *The Journal of Physical Chemistry C,* 112(21): p. 7989-7996.

[65] Yan, H., Lee, P., Armstrong, N.R., Graham, A., Evmenenko, G.A., Dutta, P.&Marks, T.J., (2005). High-performance hole-transport layers for polymer light-emitting diodes. Implementation of organosiloxane cross-linking chemistry in polymeric electroluminescent devices. *Journal of the American Chemical Society,* 127(9): p. 3172-3183.

[66] Wong, K., Yip, H., Luo, Y., Wong, K., Lau, W., Low, K., Chow, H., Gao, Z., Yeung, W.&Chang, C., (2002). Blocking reactions between indium-tin oxide and poly (3, 4-ethylene dioxythiophene): poly (styrene sulphonate) with a self-assembly monolayer. *Applied physics letters,* 80(15): p. 2788-2790.

[67] Yalcin, E., Can, M., Rodriguez-Seco, C., Aktas, E., Pudi, R., Cambarau, W., Demic, S.&Palomares, E., (2019). Semiconductor self-assembled monolayers as selective contacts for efficient PiN perovskite solar cells. *Energy & Environmental Science,* 12(1): p. 230-237.

[68] Sharma, A., Kippelen, B., Hotchkiss, P.J.&Marder, S.R., (2008). Stabilization of the work function of indium tin oxide using organic surface modifiers in organic light-emitting diodes. *Applied Physics Letters,* 93(16): p. 391.

[69] Girtan, M.&Rusu, M., (2010). Role of ITO and PEDOT: PSS in stability/degradation of polymer: fullerene bulk heterojunctions solar cells. *Solar Energy Materials and Solar Cells,* 94(3): p. 446-450.

[70] Blodgett, K.B., (1935). Films built by depositing successive monomolecular layers on a solid surface. *Journal of the American Chemical Society,* 57(6): p. 1007-1022.

[71] Blodgett, K.B.&Langmuir, I., (1937). Built-up films of barium stearate and their optical properties. *Physical Review,* 51(11): p. 964.

[72] Durmaz, F. (2006). *A modular approach to functional self-assembled monolayers.* ETH Zurich.

[73] Schwartz, D.K., (2001). Mechanisms and kinetics of self-assembled monolayer formation. *Annual Review of Physical Chemistry,* 52(1): p. 107-137.

[74] Love, J.C., Estroff, L.A., Kriebel, J.K., Nuzzo, R.G.&Whitesides, G.M., (2005). Self-assembled monolayers of thiolates on metals as a form of nanotechnology. *Chemical reviews,* 105(4): p. 1103-1170.

[75] Kaifer, A.E.&Gómez-Kaifer, M**.,** (1999), *Supramolecular electrochemistry*. Wiley Online Library.

[76] Hatton, R.A., Day, S.R., Chesters, M.A.&Willis, M.R., (2001). Organic electroluminescent devices: enhanced carrier injection using an organosilane self assembled monolayer (SAM) derivatized ITO electrode. *Thin Solid Films,* 394(1-2): p. 291-296.

[77] Jadhav, S.A., (2011). Self-assembled monolayers (SAMs) of carboxylic acids: an overview. *Central European Journal of Chemistry,* 9(3): p. 369-378.

[78] Jen, A.K., Rao, V.P., Wong, K.&Drost, K.J., (1993). Functionalized thiophenes: second-order nonlinear optical materials. *Journal of the Chemical Society, Chemical Communications,* (1): p. 90-92.

[79] Akın Kara, D., Kara, K., Oylumluoglu, G., Yigit, M.Z., Can, M., Kim, J.J., Burnett, E.K., Gonzalez Arellano, D.L., Buyukcelebi, S.m.&Ozel, F., (2018). Enhanced Device Efficiency and Long-Term Stability via Boronic Acid-Based Self-Assembled Monolayer Modification of Indium Tin Oxide in a Planar Perovskite Solar Cell. *ACS applied materials & interfaces,* 10(35): p. 30000-30007.

[80] Wenzel, R.N., (1936). Resistance of solid surfaces to wetting by water. *Industrial & Engineering Chemistry,* 28(8): p. 988-994.

[81] Can, M., Havare, A.K., Aydın, H., Yagmurcukardes, N., Demic, S., Icli, S.&Okur, S., (2014). Electrical properties of SAM-modified ITO surface using aromatic small molecules with double bond carboxylic acid groups for OLED applications. *Applied Surface Science,* 314: p. 1082-1086.

[82] Prieto, P., Nistor, V., Nouneh, K., Oyama, M., Abd-Lefdil, M.&Díaz, R., (2012). XPS study of silver, nickel and bimetallic silver–nickel nanoparticles prepared by seed-mediated growth. *Applied Surface Science,* 258(22): p. 8807-8813.

[83] Carroll, K.J., Reveles, J.U., Shultz, M.D., Khanna, S.N.&Carpenter, E.E., (2011). Preparation of elemental Cu and Ni nanoparticles by the polyol method: an experimental and theoretical approach. *The Journal of Physical Chemistry C,* 115(6): p. 2656-2664.

[84] Montagne, F., Polesel-Maris, J., Pugin, R.&Heinzelmann, H., (2008). Poly (N-isopropylacrylamide) thin films densely grafted onto gold surface: preparation, characterization, and dynamic AFM study of temperature-induced chain conformational changes. *Langmuir,* 25(2): p. 983-991.

[85] Raju, M.S.&Bhattacharya, S., (2017). Structural and optical properties of nanocrystalline pure and indium doped tin oxide powders synthesized in a single step by flame spray pyrolysis. *Materials Research Express,* 4(7): p. 075034.

[86] Liu, Y., Palmieri, A., He, J., Meng, Y., Beauregard, N., Suib, S.L.&Mustain, W.E., (2016). Highly conductive In-SnO 2/RGO nano-heterostructures with improved lithium-ion battery performance. *Scientific reports,* 6: p. 25860.

[87] Xu, R., Xiao, L., Luo, L., Yuan, Q., Qin, D., Hu, G.&Gan, W., (2016). Nitrogen, sulfur dual-doped mesoporous carbon modified glassy carbon electrode for simultaneous determination of hydroquinone and catechol. *Journal of The Electrochemical Society,* 163(13): p. B617-B623.

[88] Yang, D., Yang, R., Wang, K., Wu, C., Zhu, X., Feng, J., Ren, X., Fang, G., Priya, S.&Liu, S.F., (2018). High efficiency planar-type perovskite solar cells with negligible hysteresis using EDTA-complexed SnO 2. *Nature communications,* 9(1): p. 3239.

[89] Yu, J., Chen, X., Wang, Y., Zhou, H., Xue, M., Xu, Y., Li, Z., Ye, C., Zhang, J.&Van Aken, P.A., (2016). A high-performance self-powered broadband photodetector based on a CH 3 NH 3 PbI 3 perovskite/ZnO nanorod array heterostructure. *Journal of Materials Chemistry C,* 4(30): p. 7302-7308.

[90] Zou, X., Fan, H., Tian, Y.&Yan, S., (2014). Synthesis of Cu 2 O/ZnO hetero-nanorod arrays with enhanced visible light-driven photocatalytic activity. *CrystEngComm,* 16(6): p. 1149-1156.

[91] Fan, X., Cui, C., Fang, G., Wang, J., Li, S., Cheng, F., Long, H.&Li, Y., (2012). Efficient polymer solar cells based on poly (3-hexylthiophene): indene-C70 bisadduct with a MoO3 buffer layer. *Advanced Functional Materials,* 22(3): p. 585-590.

[92] Heo, J.H., Im, S.H., Noh, J.H., Mandal, T.N., Lim, C.-S., Chang, J.A., Lee, Y.H., Kim, H.-j., Sarkar, A.&Nazeeruddin, M.K., (2013). Efficient inorganic–organic hybrid heterojunction solar cells containing perovskite compound and polymeric hole conductors. *Nature photonics,* 7(6): p. 486.

[93] Guo, X., McCleese, C., Kolodziej, C., Samia, A.C., Zhao, Y.&Burda, C., (2016). Identification and characterization of the intermediate phase in hybrid organic–inorganic MAPbI 3 perovskite. *Dalton Transactions,* 45(9): p. 3806-3813.

[94] Song, T.-B., Chen, Q., Zhou, H., Jiang, C., Wang, H.-H., Yang, Y.M., Liu, Y., You, J.&Yang, Y., (2015). Perovskite solar cells: film formation and properties. *Journal of Materials Chemistry A,* 3(17): p. 9032-9050.

[95] Simeone, D., Ribis, J.&Luneville, L., (2018). Continuum approaches for modeling radiation-induced self-organization in materials: From the rate theory to the phase field approach. *Journal of Materials Research,* 33(4): p. 440-454.

[96] Zuo, L., Chen, Q., De Marco, N., Hsieh, Y.-T., Chen, H., Sun, P., Chang, S.-Y., Zhao, H., Dong, S.&Yang, Y., (2016). Tailoring the interfacial chemical interaction for high-efficiency perovskite solar cells. *Nano letters,* 17(1): p. 269-275.

[97] Kim, H.B., Im, I., Yoon, Y., Do Sung, S., Kim, E., Kim, J.&Lee, W.I., (2015). Enhancement of photovoltaic properties of CH 3 NH 3 PbBr 3 heterojunction solar cells by modifying mesoporous TiO 2 surfaces with carboxyl groups. *Journal of Materials Chemistry A,* 3(17): p. 9264-9270.

[98] Jia, G., Shi, Z.-J., Xia, Y.-D., Wei, Q., Chen, Y.-H., Xing, G.-C.&Huang, W., (2018). Super air stable quasi-2D organic-inorganic hybrid perovskites for visible light-emitting diodes. *Optics express,* 26(2): p. A66-A74.

[99] Li, Y., Zhao, Y., Chen, Q., Yang, Y., Liu, Y., Hong, Z., Liu, Z., Hsieh, Y.-T., Meng, L.&Li, Y., (2015). Multifunctional fullerene derivative for interface engineering in perovskite solar cells. *Journal of the American Chemical Society,* 137(49): p. 15540-15547.

[100] Snaith, H.J., Abate, A., Ball, J.M., Eperon, G.E., Leijtens, T., Noel, N.K., Stranks, S.D., Wang, J.T.-W., Wojciechowski, K.&Zhang, W., (2014). Anomalous hysteresis in perovskite solar cells. *J. Phys. Chem. Lett,* 5(9): p. 1511-1515.

APPENDIX

1-) ^{1}H NMR of methyl 4-(5'-bromo-3,4'-dihexyl-[2,2'-bithiophen]-5-yl)benzoate

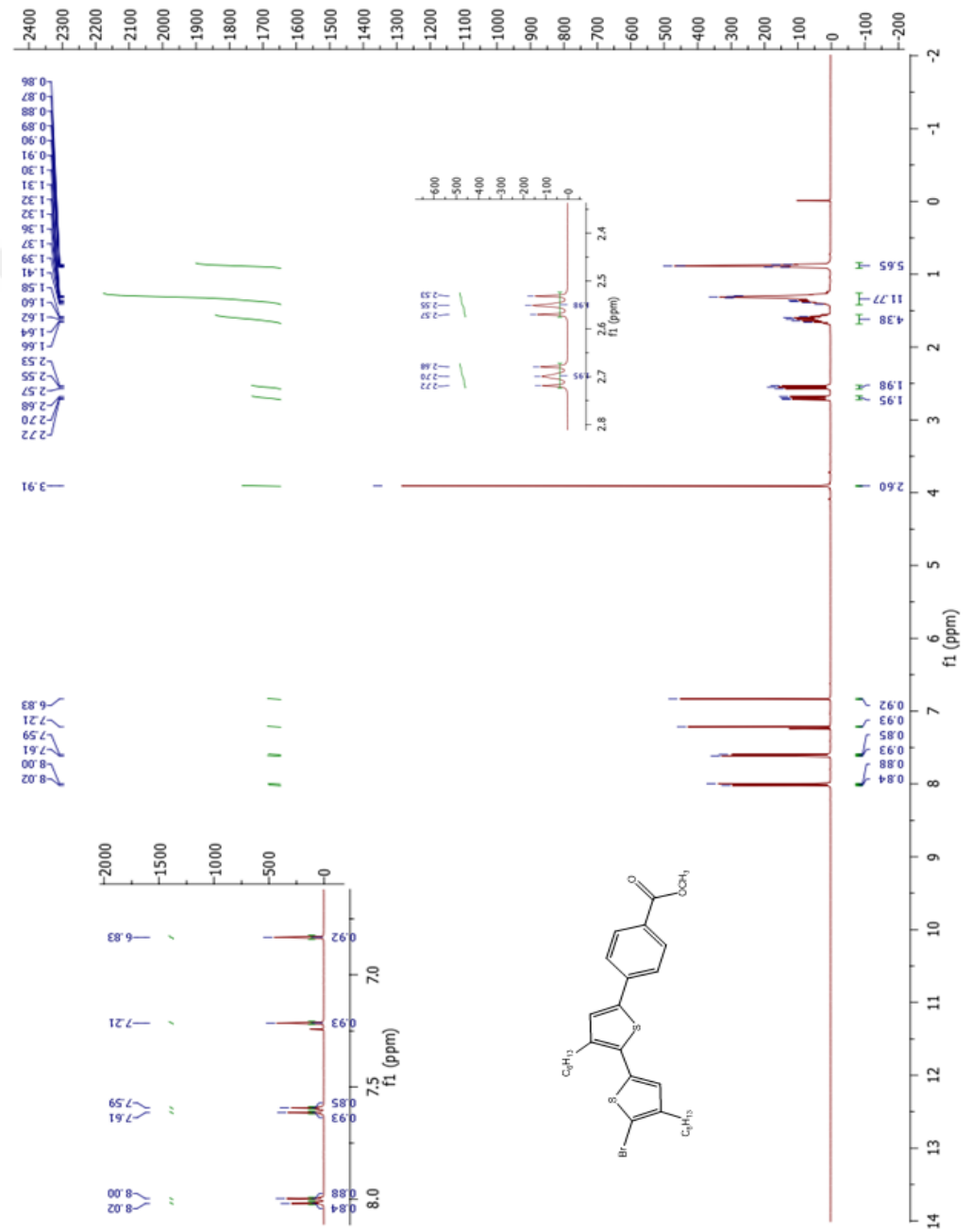

2-) ^{13}C NMR of methyl 4-(5'-bromo-3,4'-dihexyl-[2,2'-bithiophen]-5-yl)benzoate

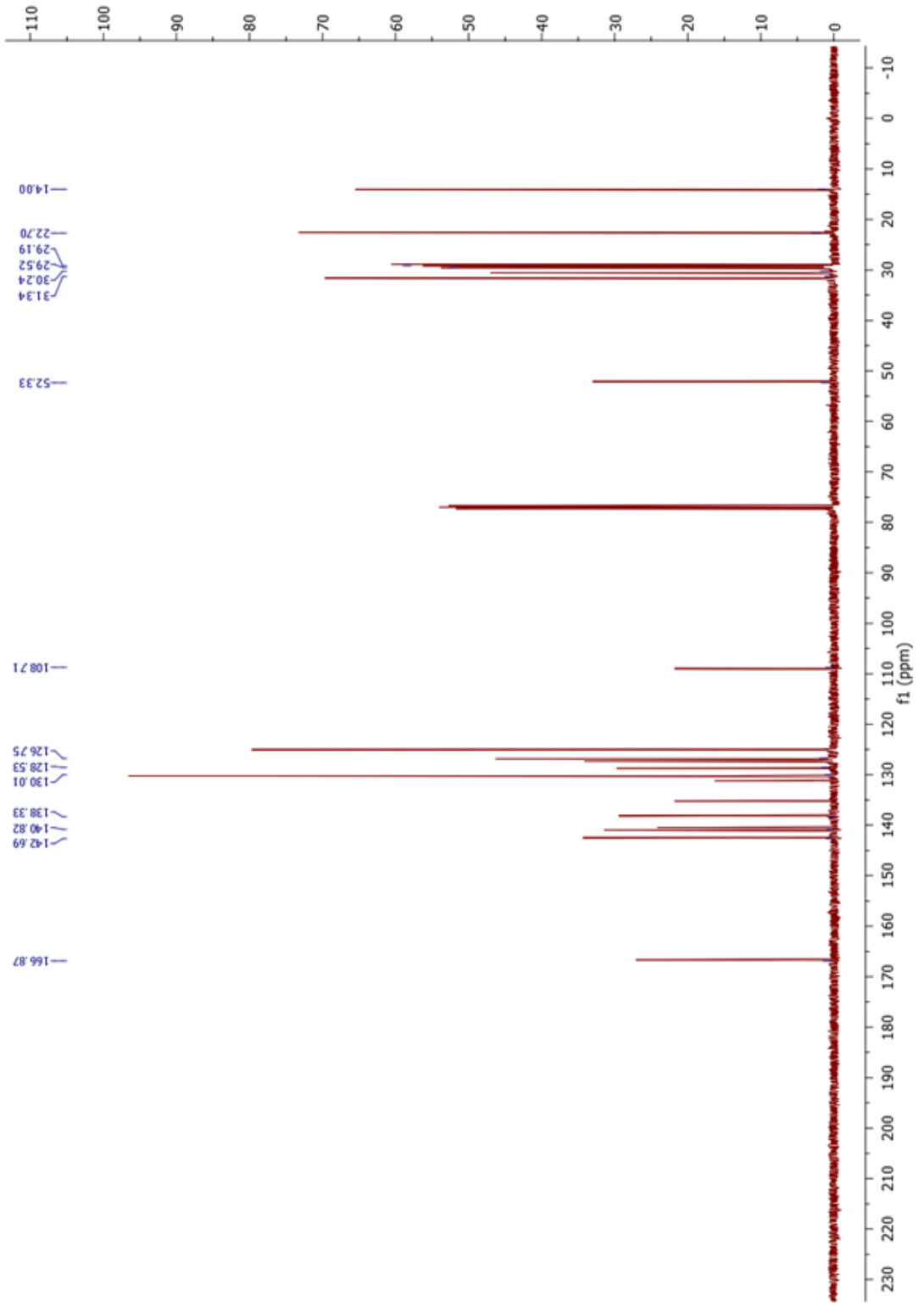

3-) (EA41) ^{1}H NMR of 4-(5'-bromo-3,4'-dihexyl-[2,2'-bithiophen]-5-yl)benzoic acid

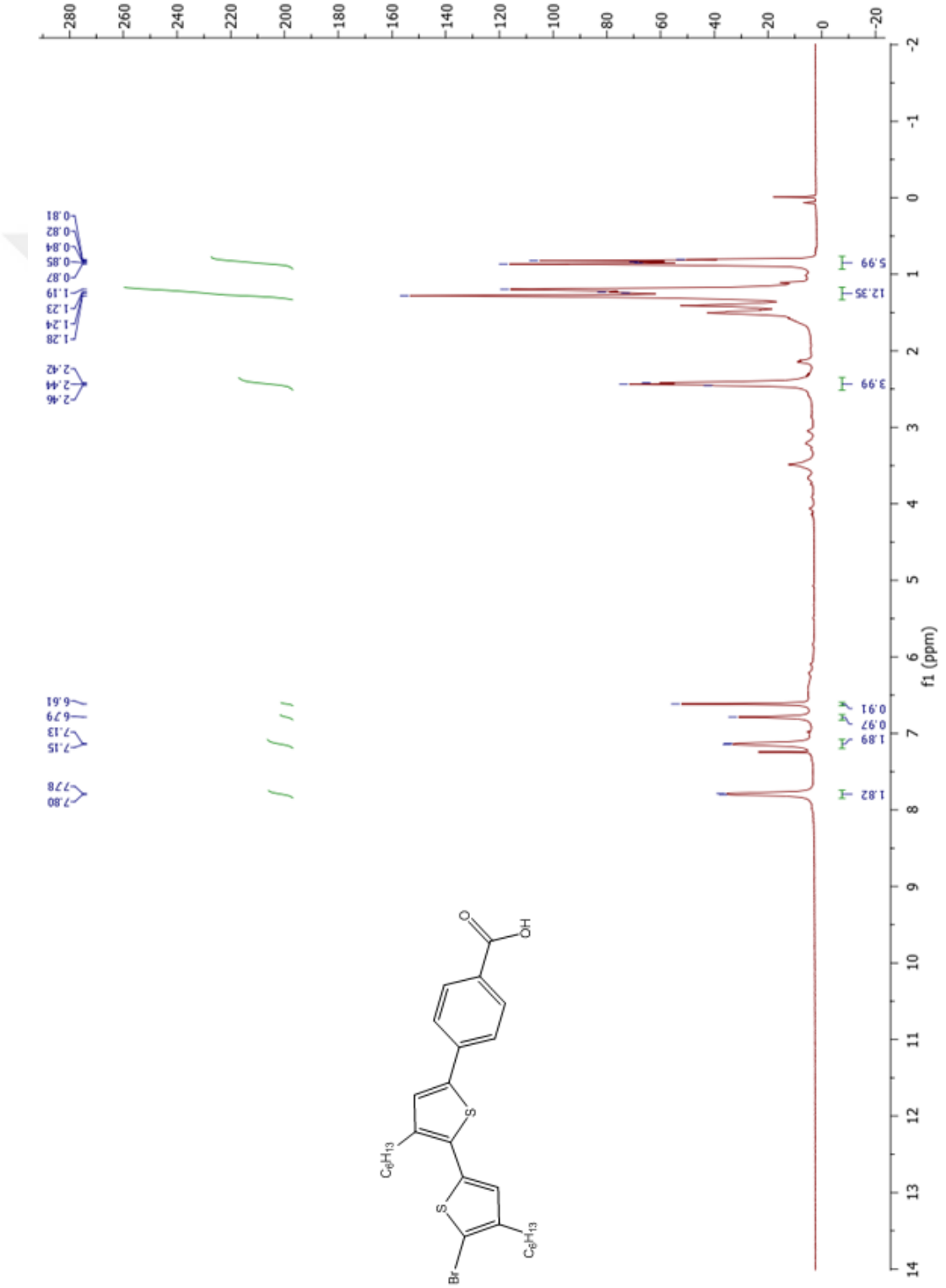

4-) (EA41) ^{13}C NMR of 4-(5'-bromo-3,4'-dihexyl-[2,2'-bithiophen]-5-yl)benzoic acid

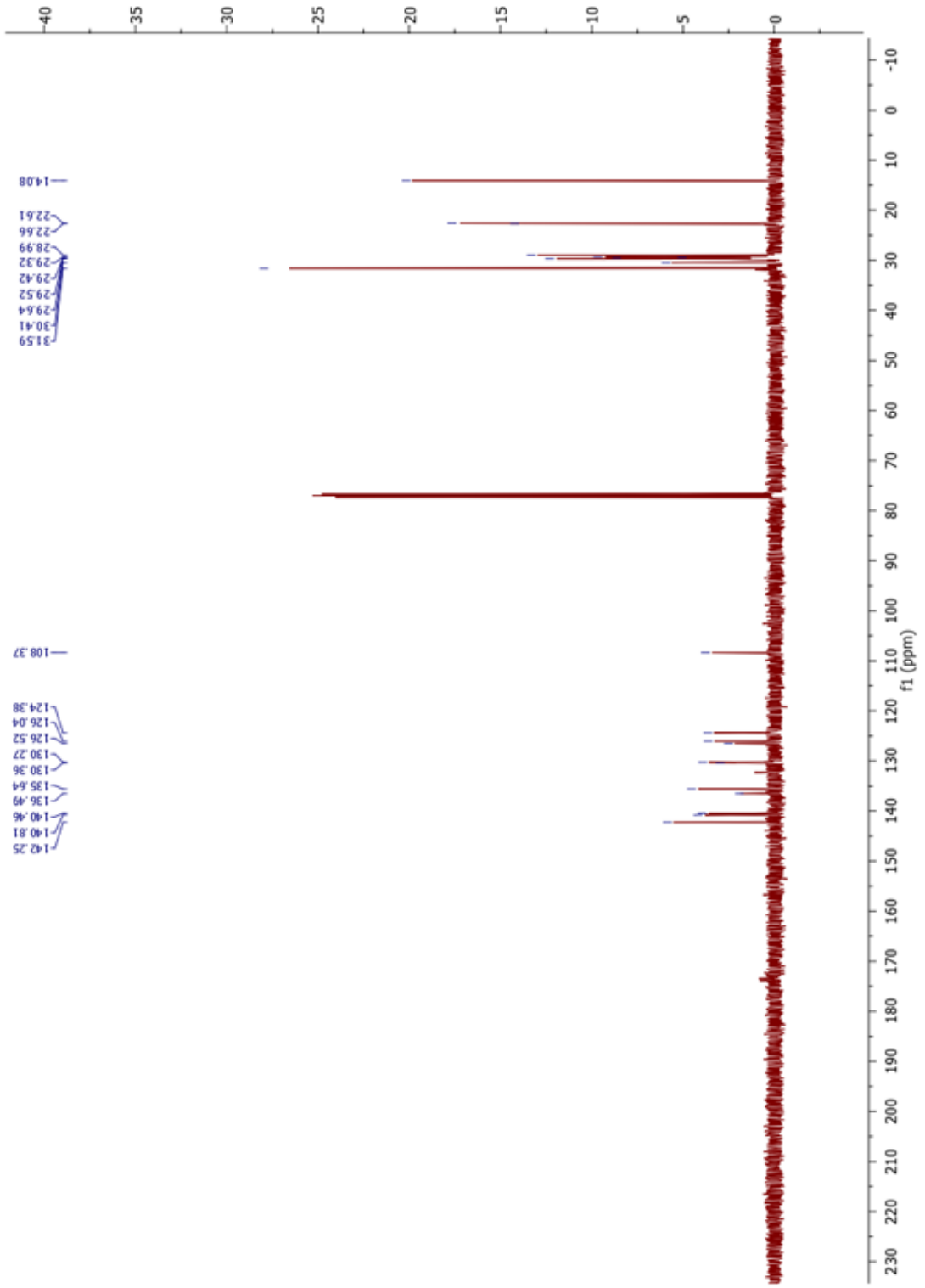

5-) ^{1}H NMR of methyl 4-(3,4'-dihexyl-5'-(3,4,5-trimethoxyphenyl)-[2,2'-bithiophen]-5-yl)benzoate

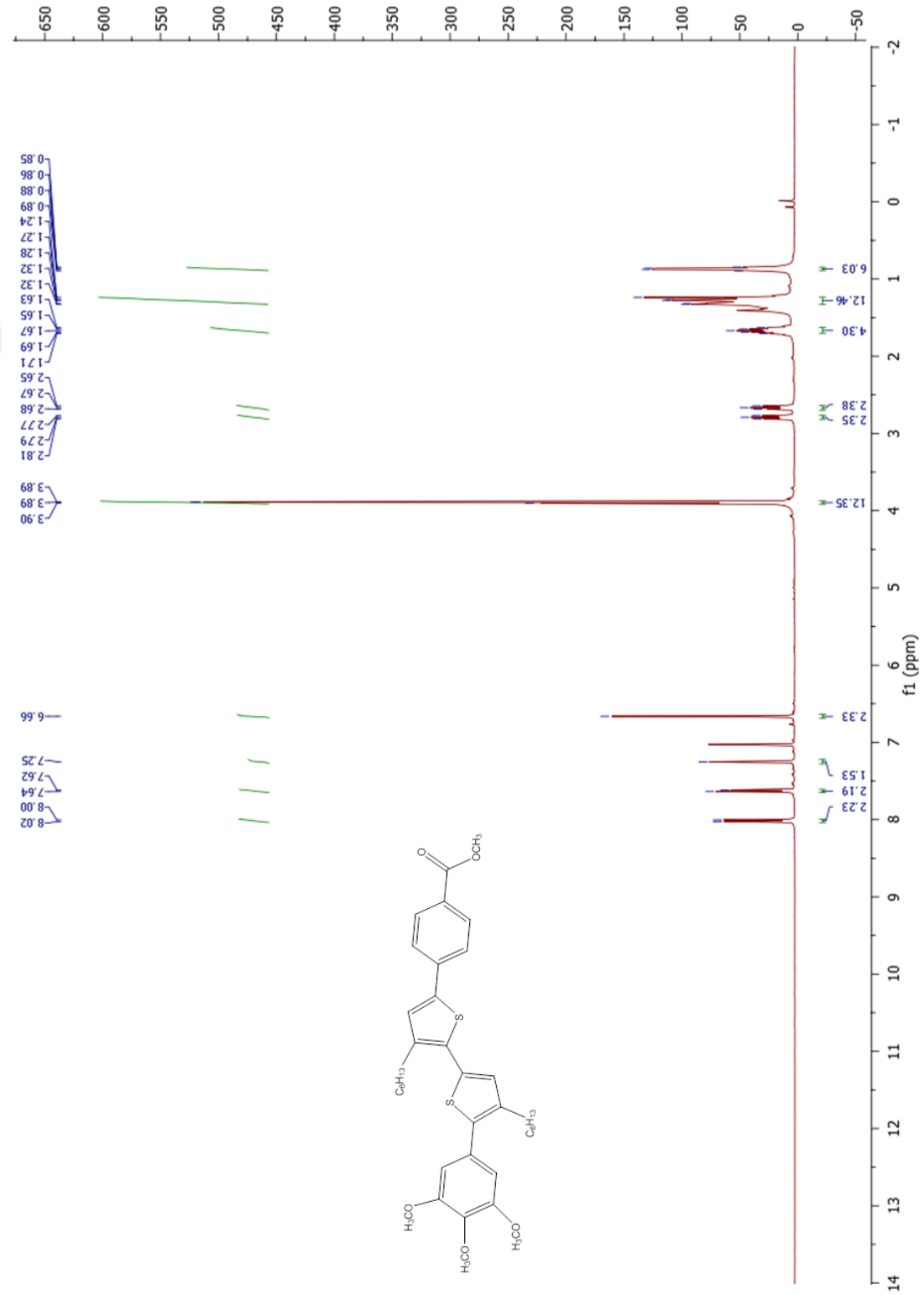

6-) ^{13}C NMR of methyl 4-(3,4'-dihexyl-5'-(3,4,5-trimethoxyphenyl)-[2,2'-bithiophen]-5-yl)benzoate

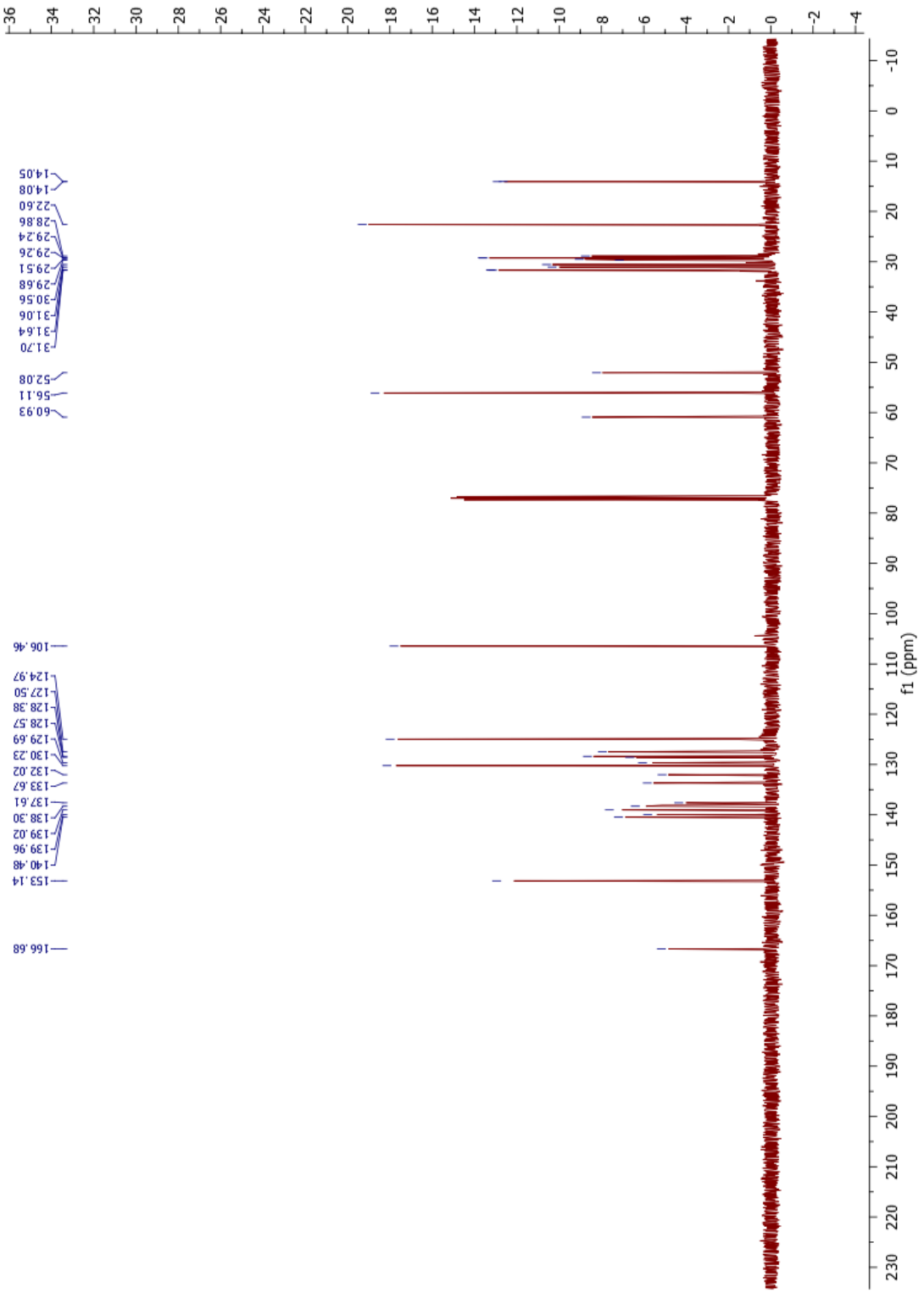

7-) ^{1}H NMR of 4-(3,4'-dihexyl-5'-(3,4,5-trimethoxyphenyl)-[2,2'-bithiophen]-5-yl)benzoic acid (EA-46)

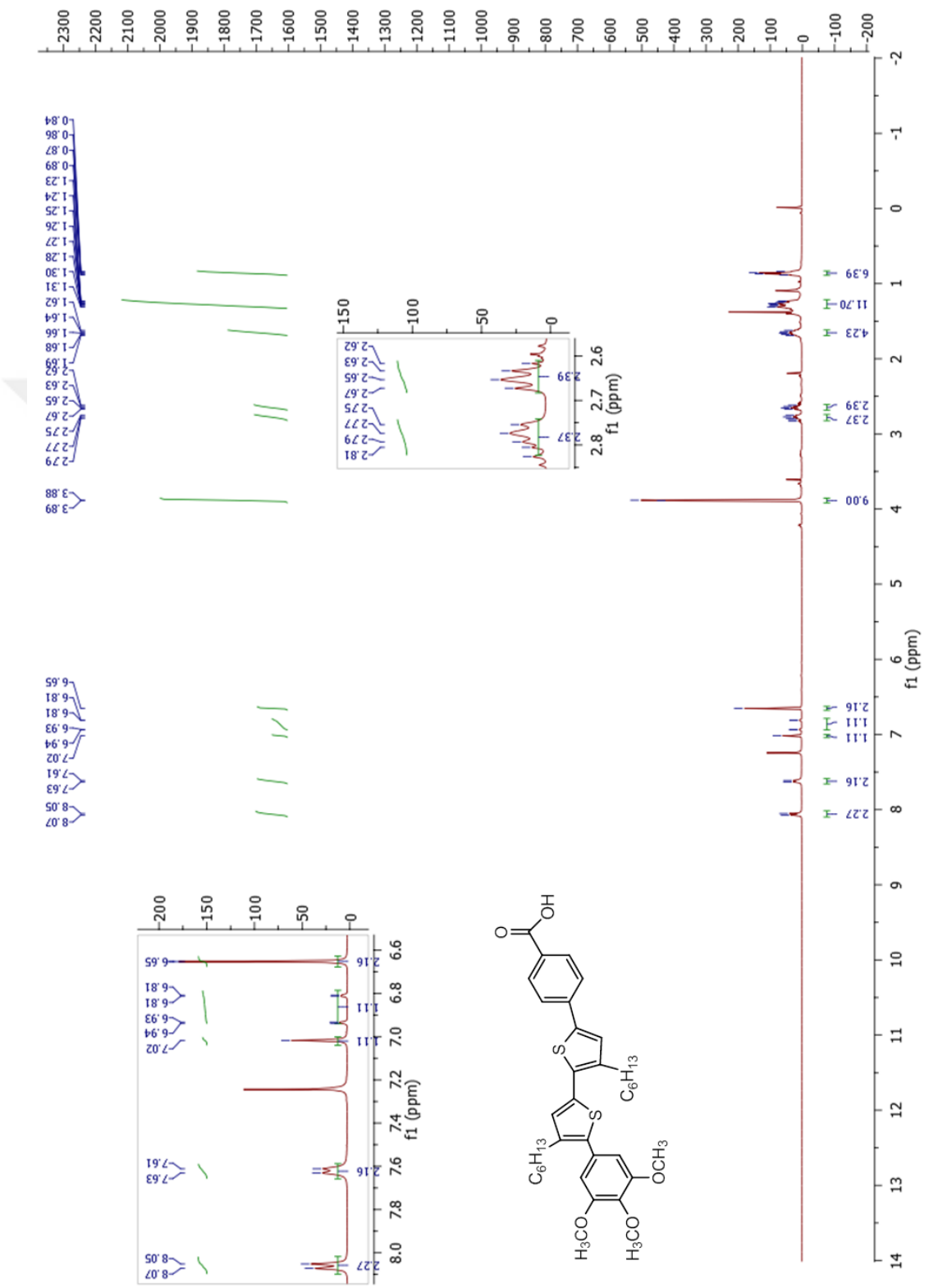

8-) ^{13}C NMR of 4-(3,4'-dihexyl-5'-(3,4,5-trimethoxyphenyl)-[2,2'-bithiophen]-5-yl)benzoic acid (EA-46)

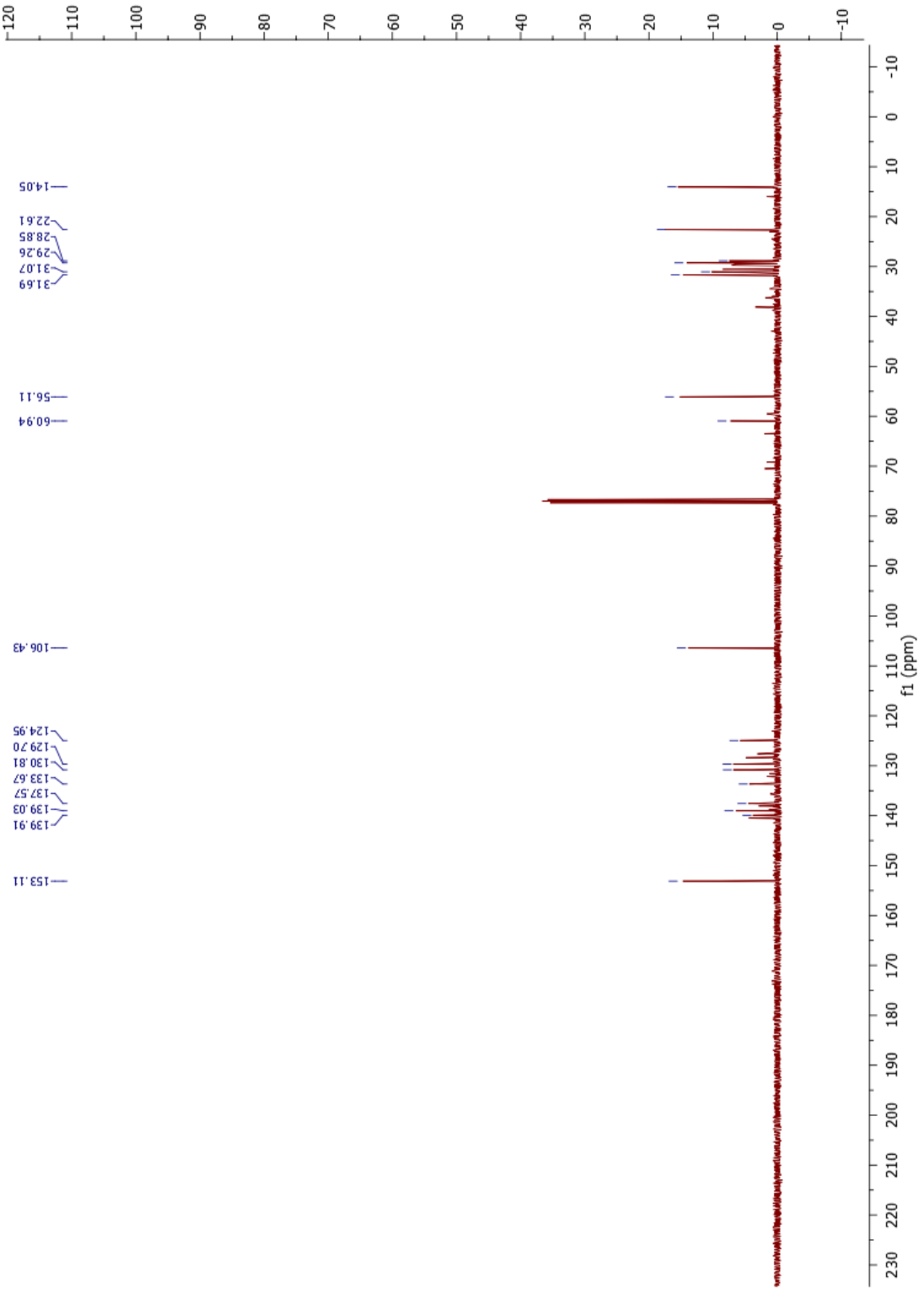

9-) ^{1}H NMR of methyl 4-(5'-(3,5-dimethoxyphenyl)-3,4'-dihexyl-[2,2'-bithiophen]-5-yl)benzoate

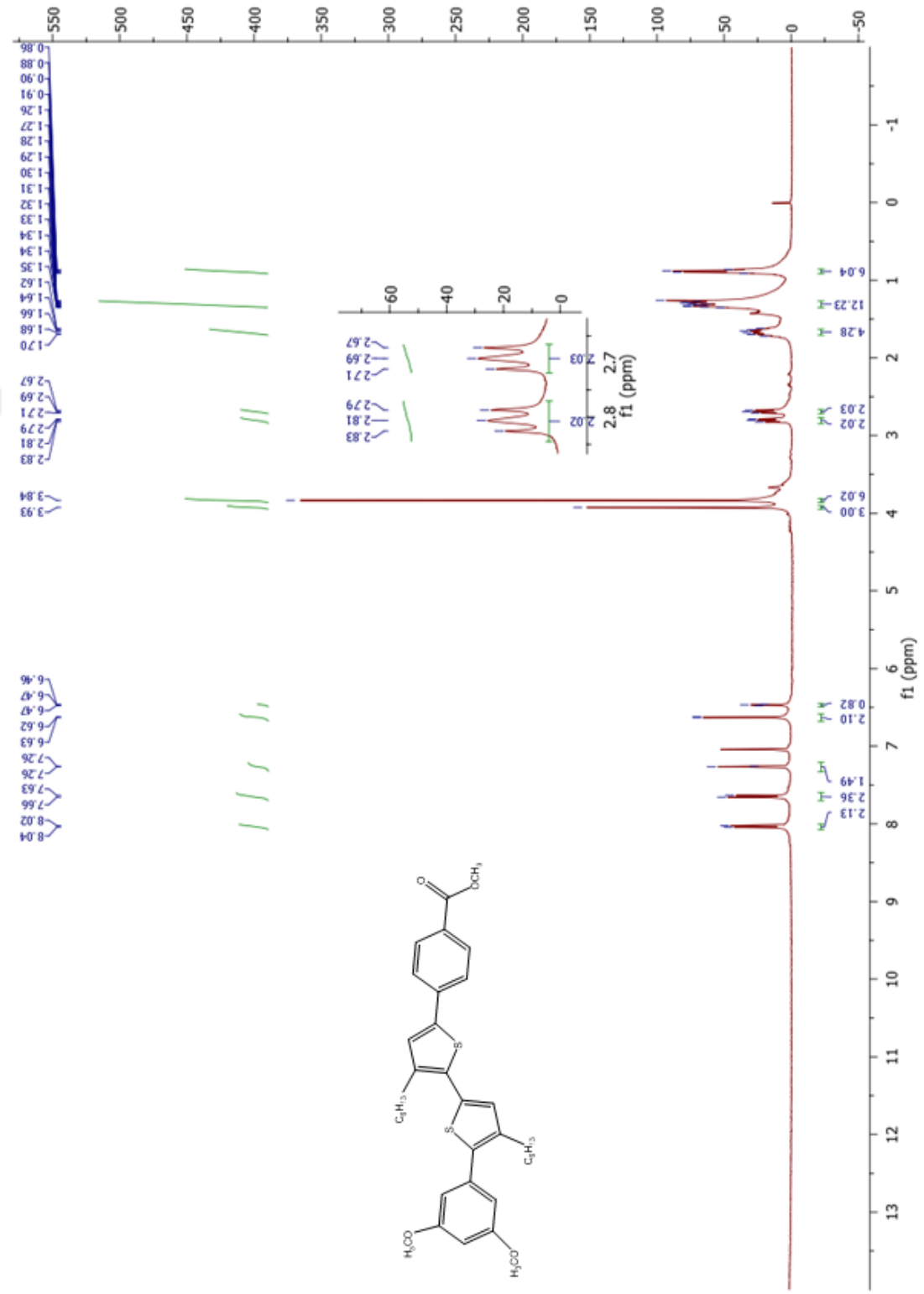

10-) ^{13}C NMR of methyl 4-(5'-(3,5-dimethoxyphenyl)-3,4'-dihexyl-[2,2'-bithiophen]-5-yl)benzoate

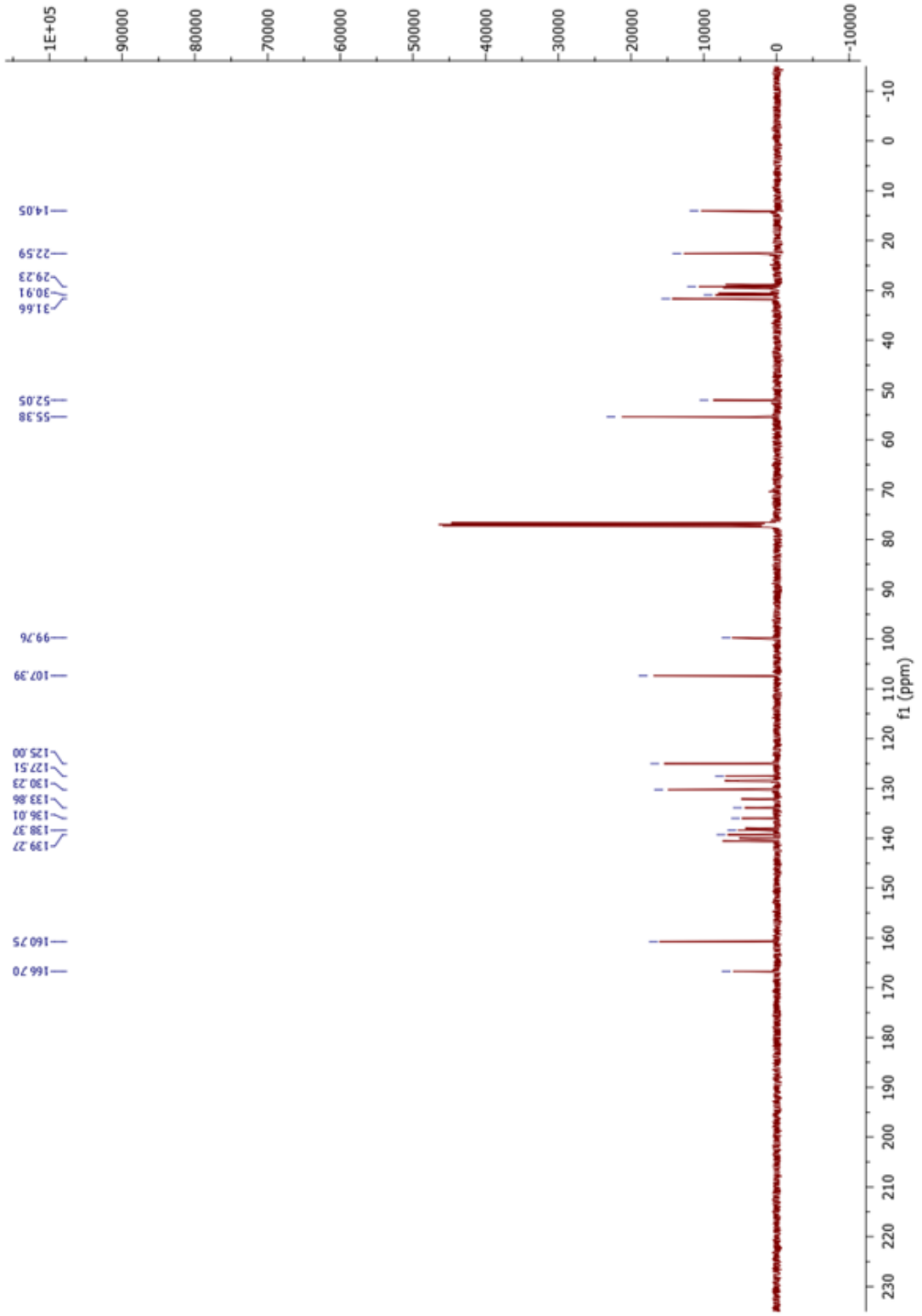

11-) (EA49) ^{1}H NMR of 4-(5'-(3,5-dimethoxyphenyl)-3,4'-dihexyl-[2,2'-bithiophen]-5-yl)benzoic acid

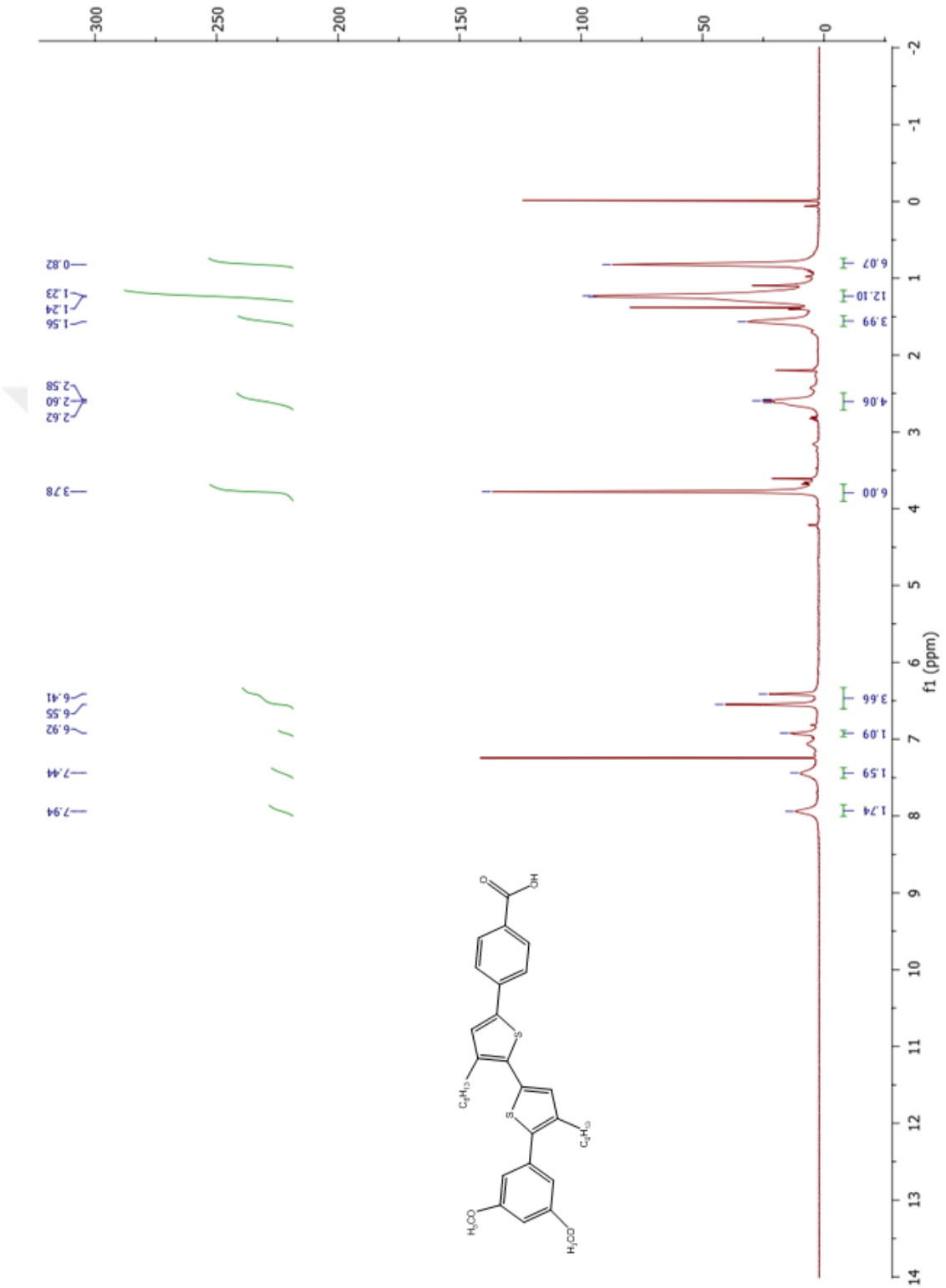

12-) (EA49) ^{13}C NMR of 4-(5'-(3,5-dimethoxyphenyl)-3,4'-dihexyl-[2,2'-bithiophen]-5-yl)benzoic acid

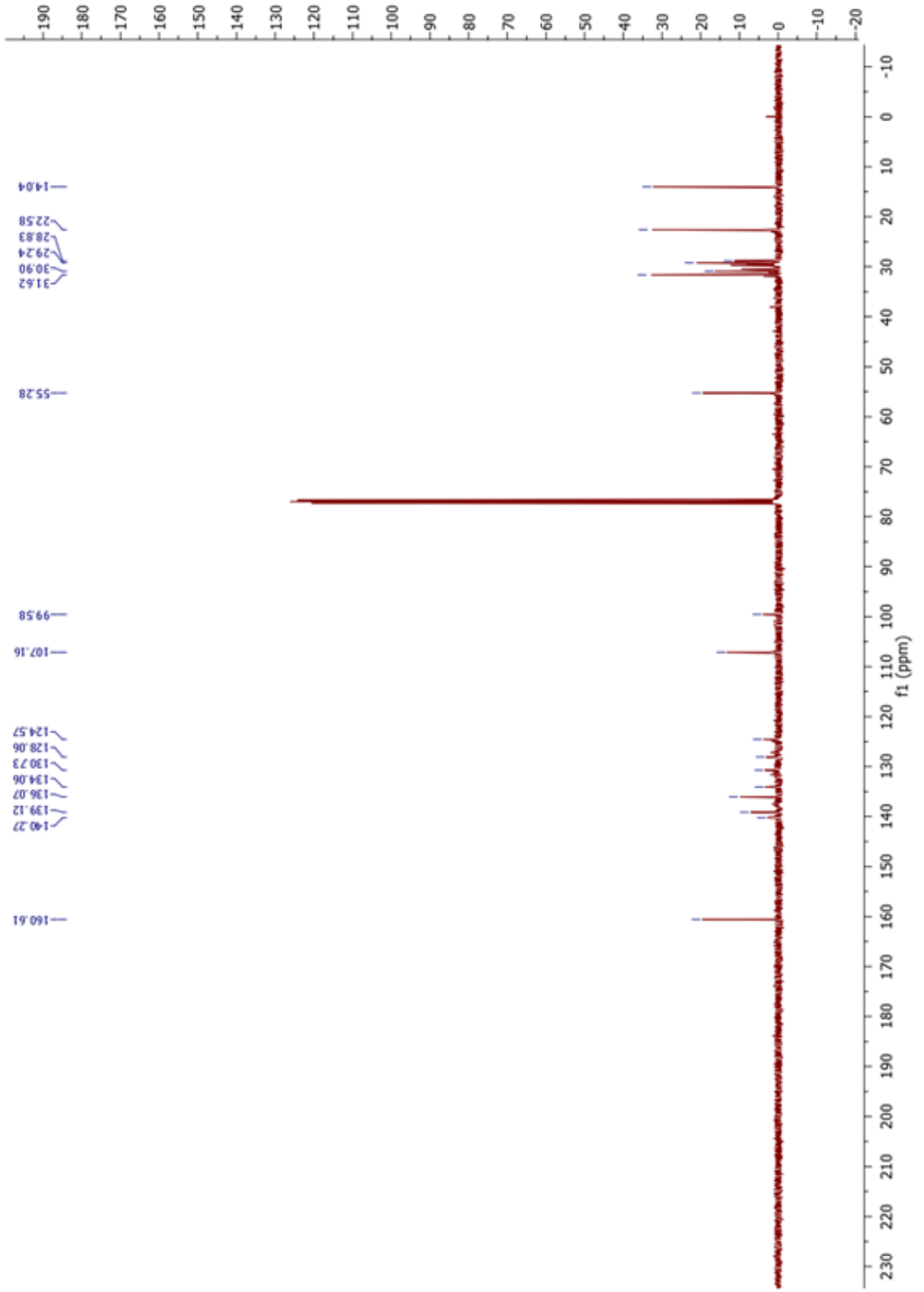

13-) ^{1}H NMR of methyl 4-(3,4'-dihexyl-5'-(3,4,5-trifluorophenyl)-[2,2'-bithiophen]-5-yl)benzoate

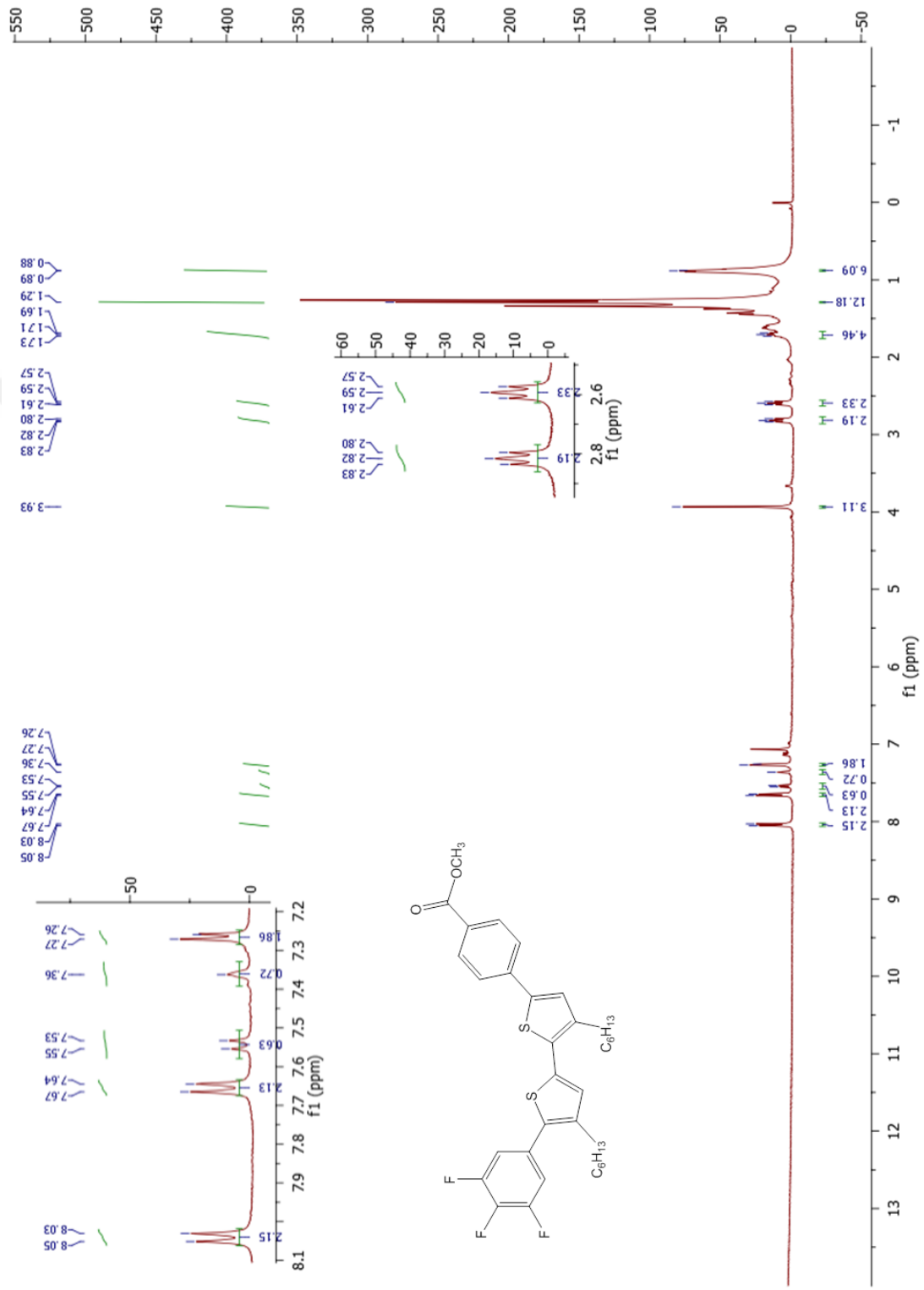

14-) ^{13}C NMR of methyl 4-(3,4'-dihexyl-5'-(3,4,5-trifluorophenyl)-[2,2'-bithiophen]-5-yl)benzoate

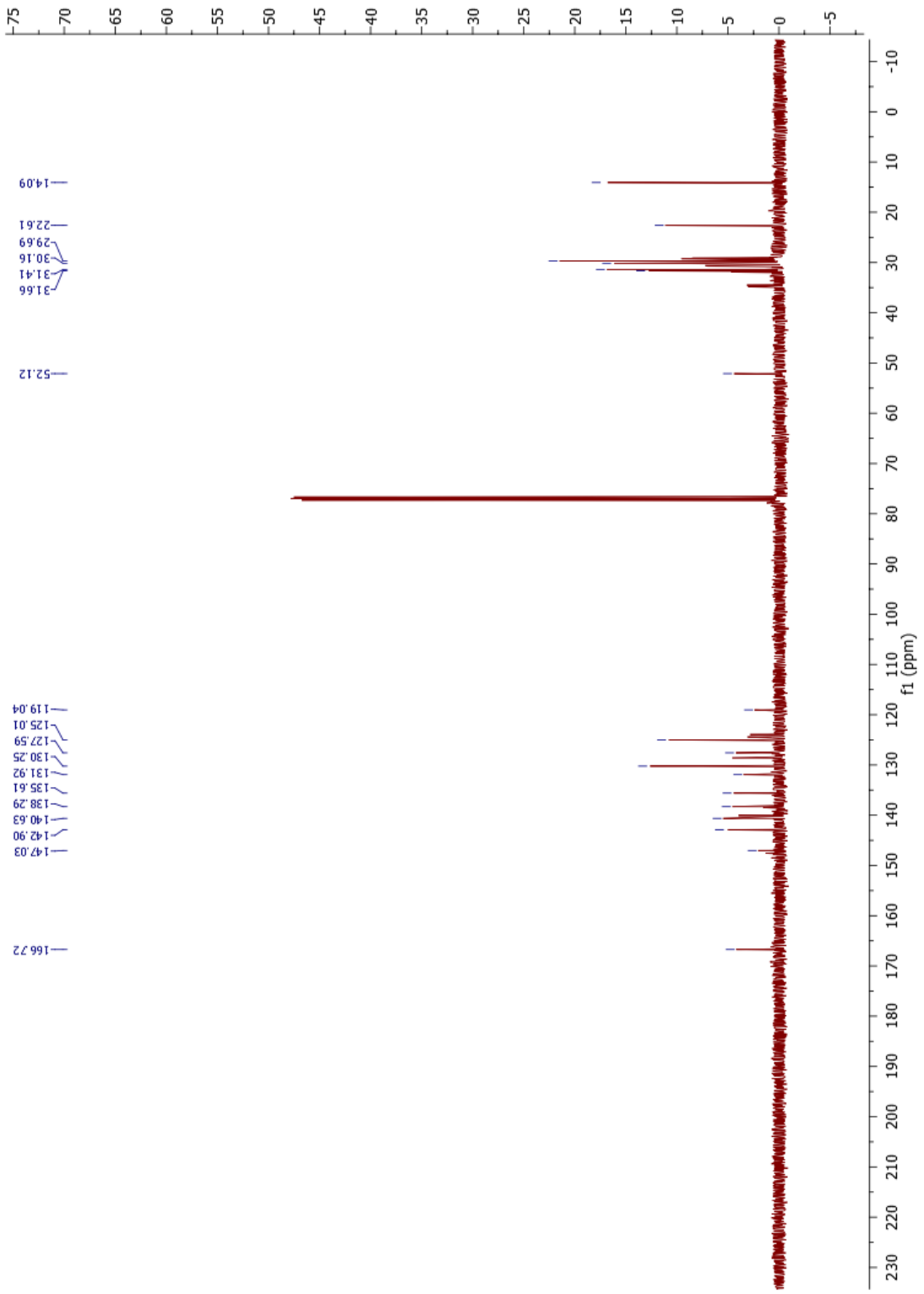

15-) ^{1}H NMR of 4-(3,4'-dihexyl-5'-(3,4,5-trifluorophenyl)-[2,2'-bithiophen]-5-yl)benzoic acid (EA50)

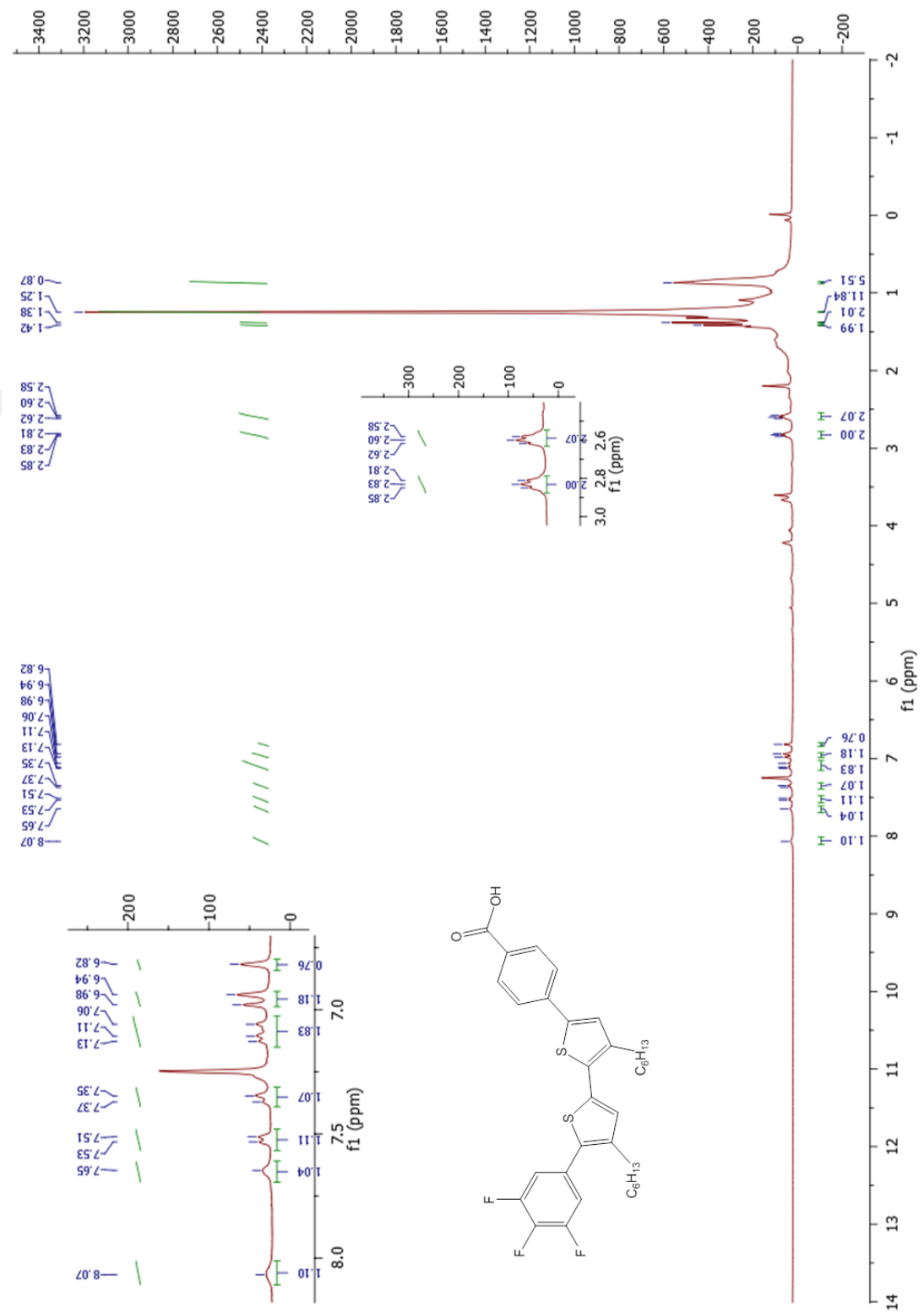

16-) ^{13}C NMR of 4-(3,4'-dihexyl-5'-(3,4,5-trifluorophenyl)-[2,2'-bithiophen]-5-yl)benzoic acid (EA50)

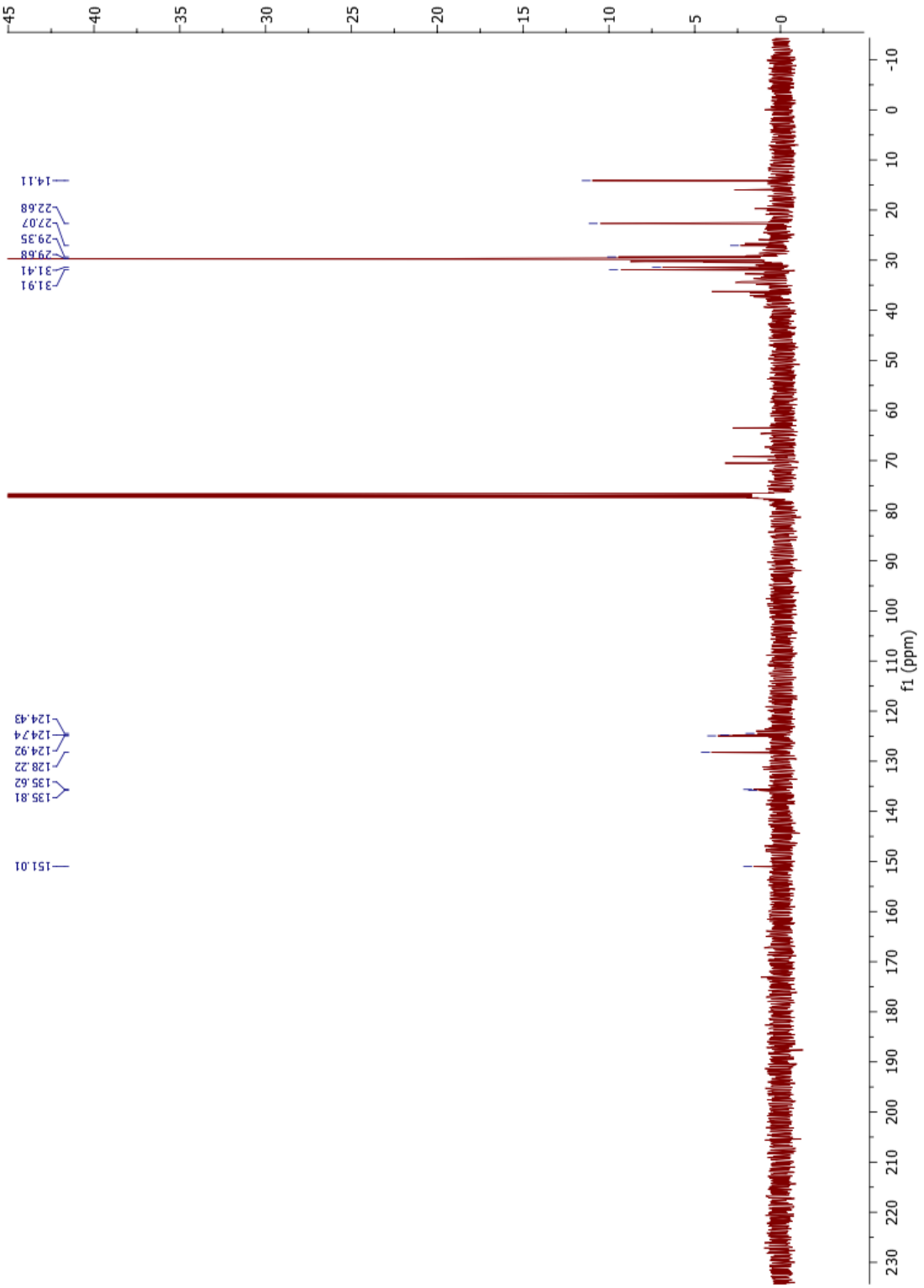

17-) ^{1}H NMR of methyl 4-(5'-(3,5-difluorophenyl)-3,4'-dihexyl-[2,2'-bithiophen]-5-yl)benzoate

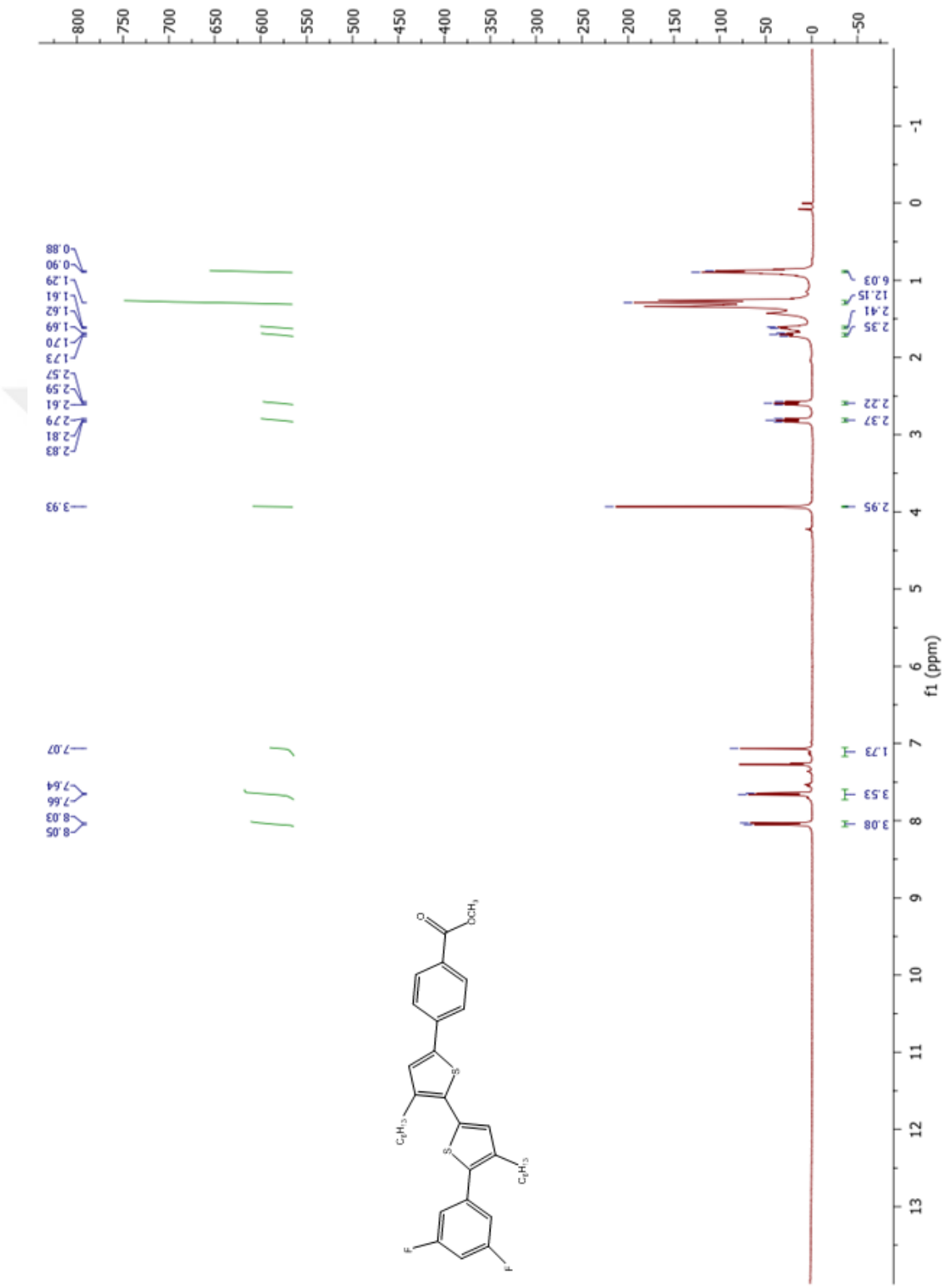

18-) ^{13}C NMR of methyl 4-(5'-(3,5-difluorophenyl)-3,4'-dihexyl-[2,2'-bithiophen]-5-yl)benzoate

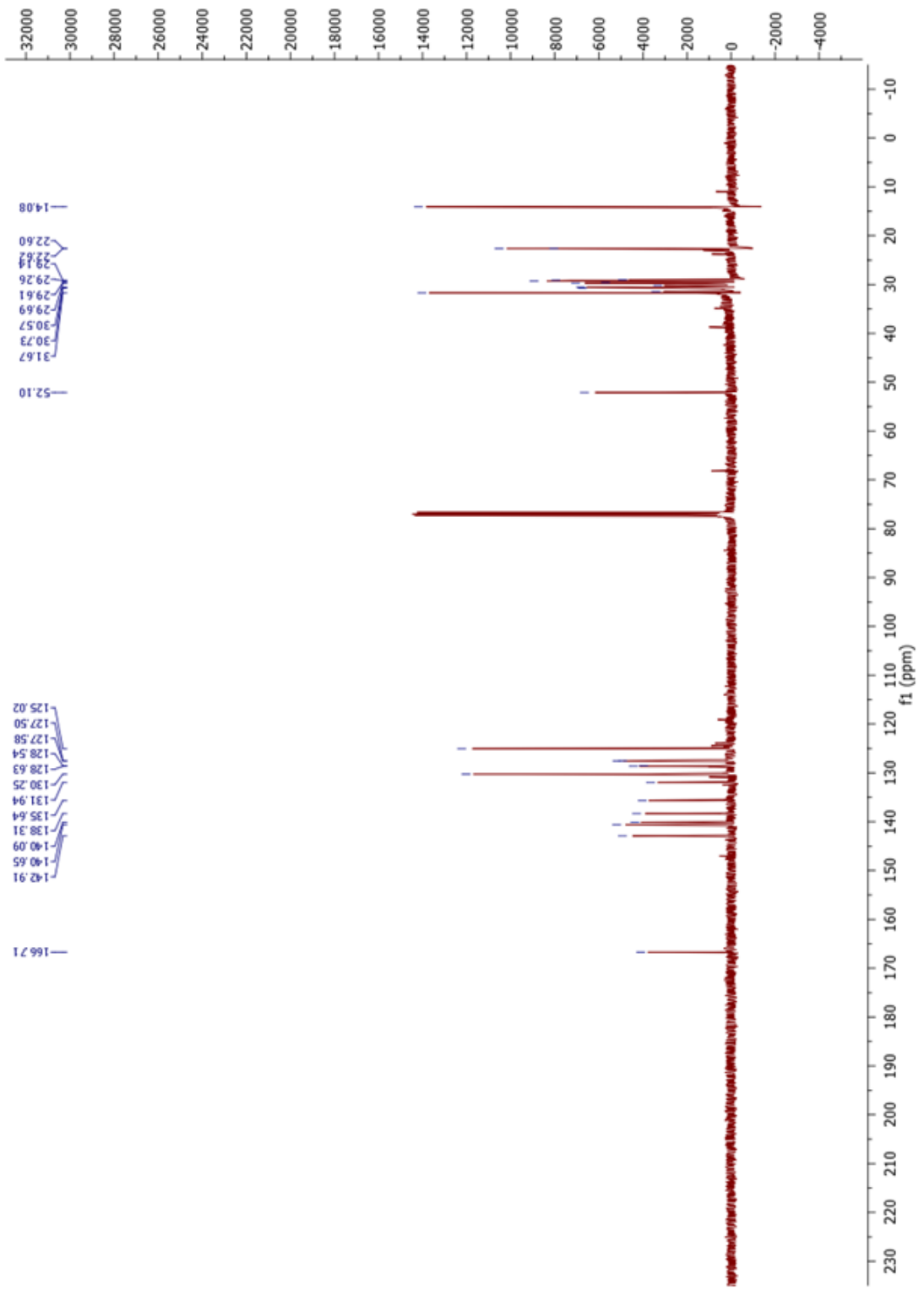

19-) (EA56) ^{1}H NMR of 4-(5'-(3,5-difluorophenyl)-3,4'-dihexyl-[2,2'-bithiophen]-5-yl)benzoic acid

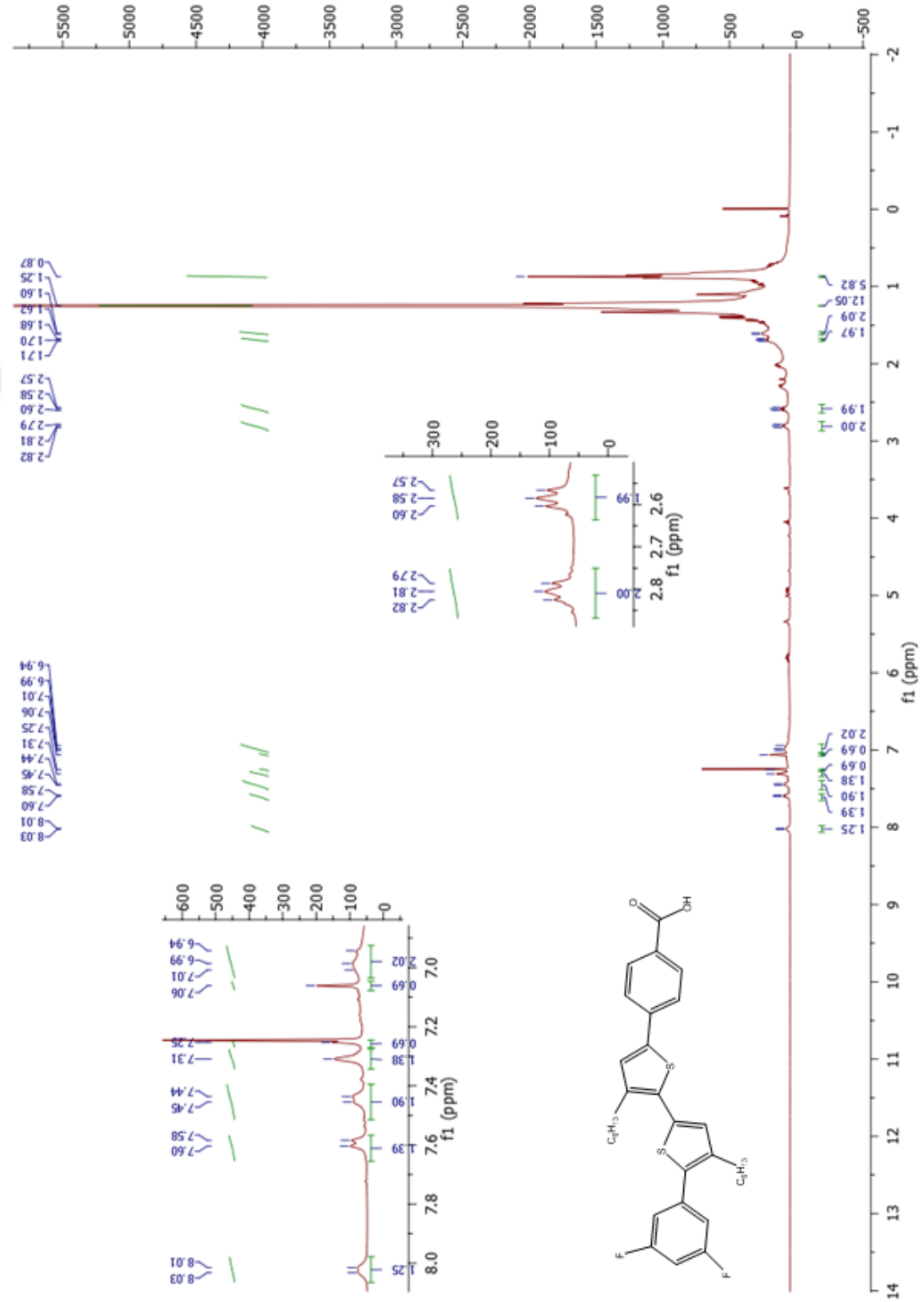

20-) (EA56) ^{13}C NMR of 4-(5'-(3,5-difluorophenyl)-3,4'-dihexyl-[2,2'-bithiophen]-5-yl)benzoic acid

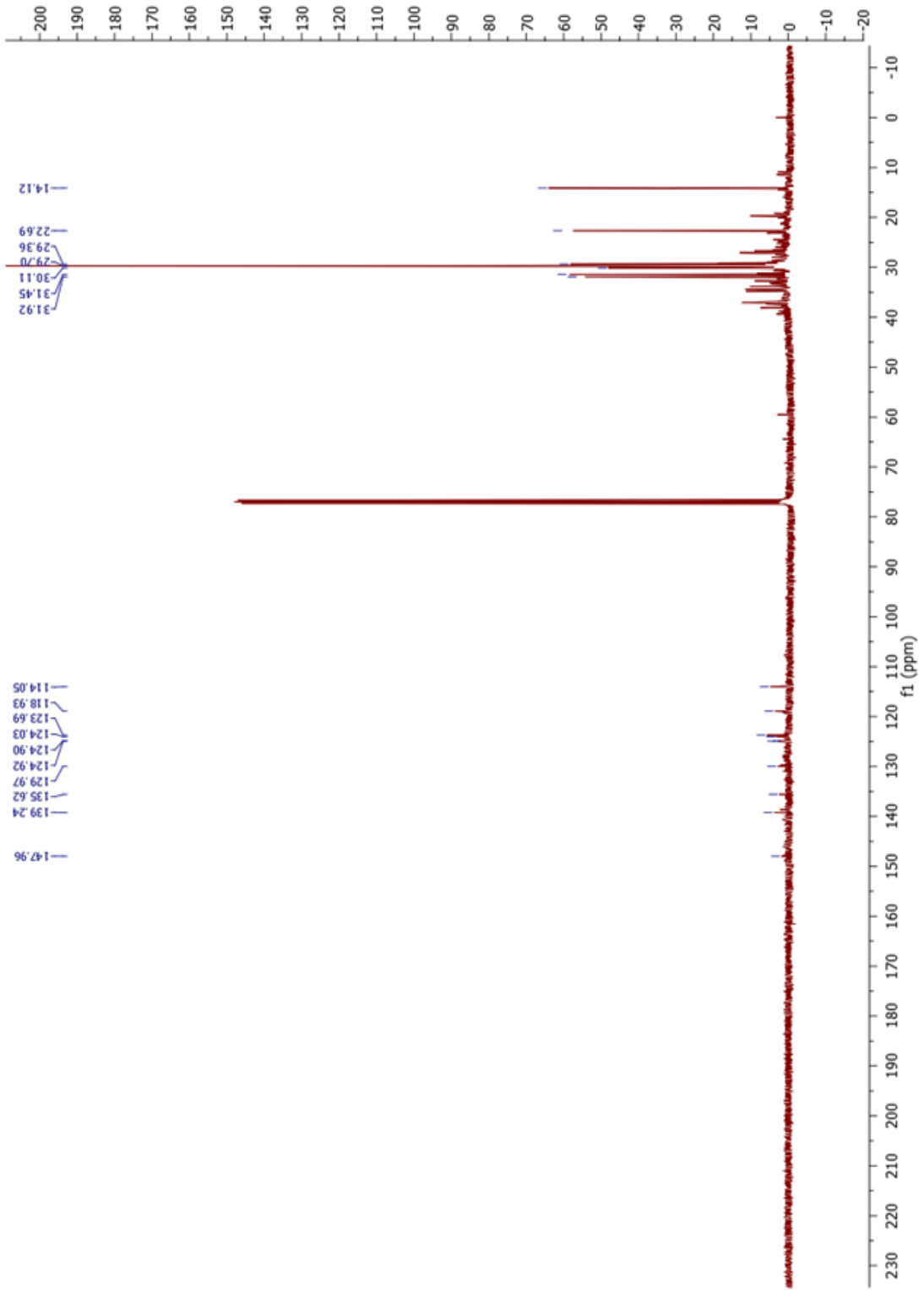

21-) ^{1}H NMR of methyl 4-(5'-(4-(bis(4-methoxyphenyl)amino)phenyl)-3,4'-dihexyl-[2,2'-bithiophen]-5-yl)benzoate

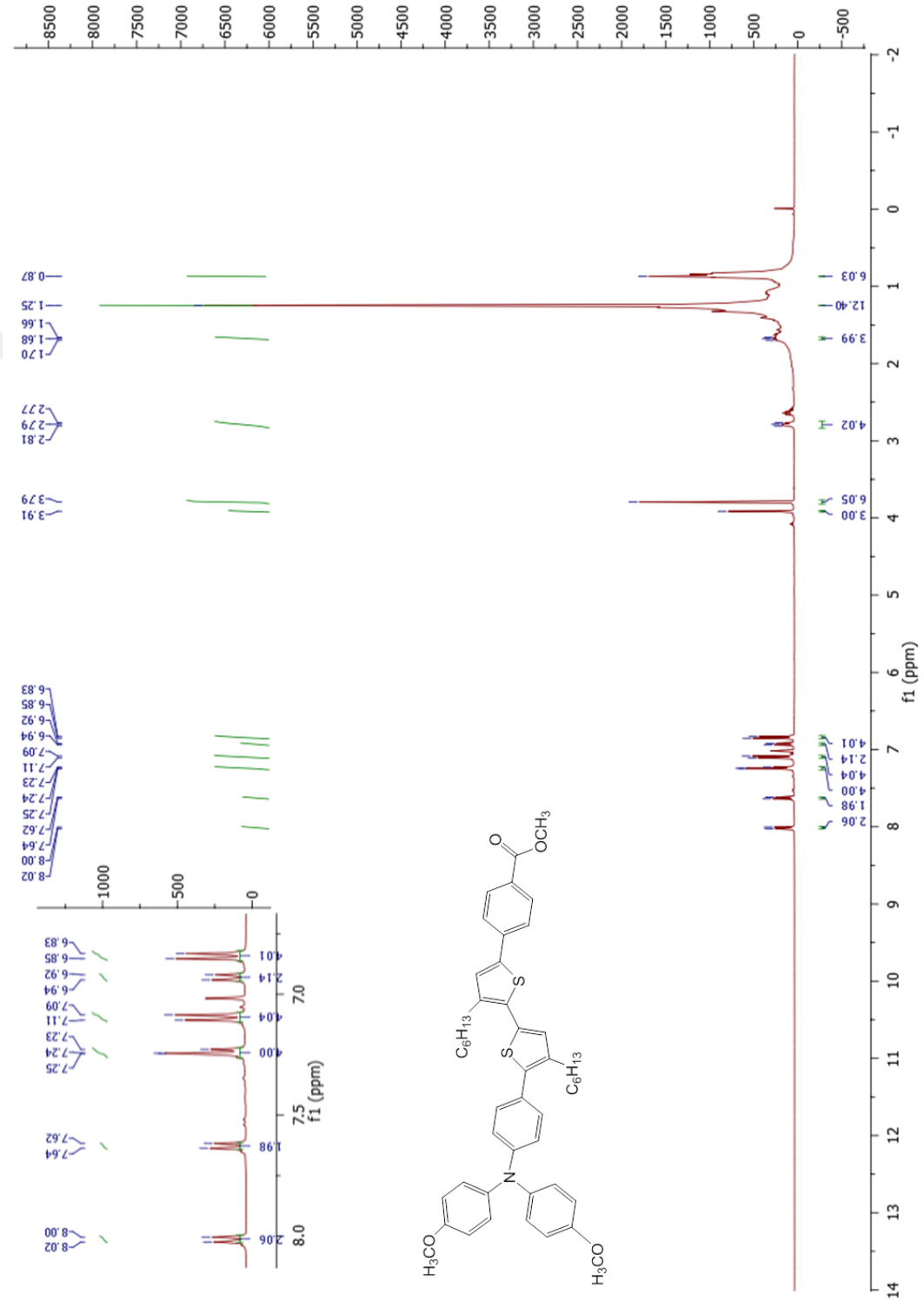

22-) ^{13}C NMR of methyl 4-(5'-(4-(bis(4-methoxyphenyl)amino)phenyl)-3,4'-dihexyl-[2,2'-bithiophen]-5-yl)benzoate

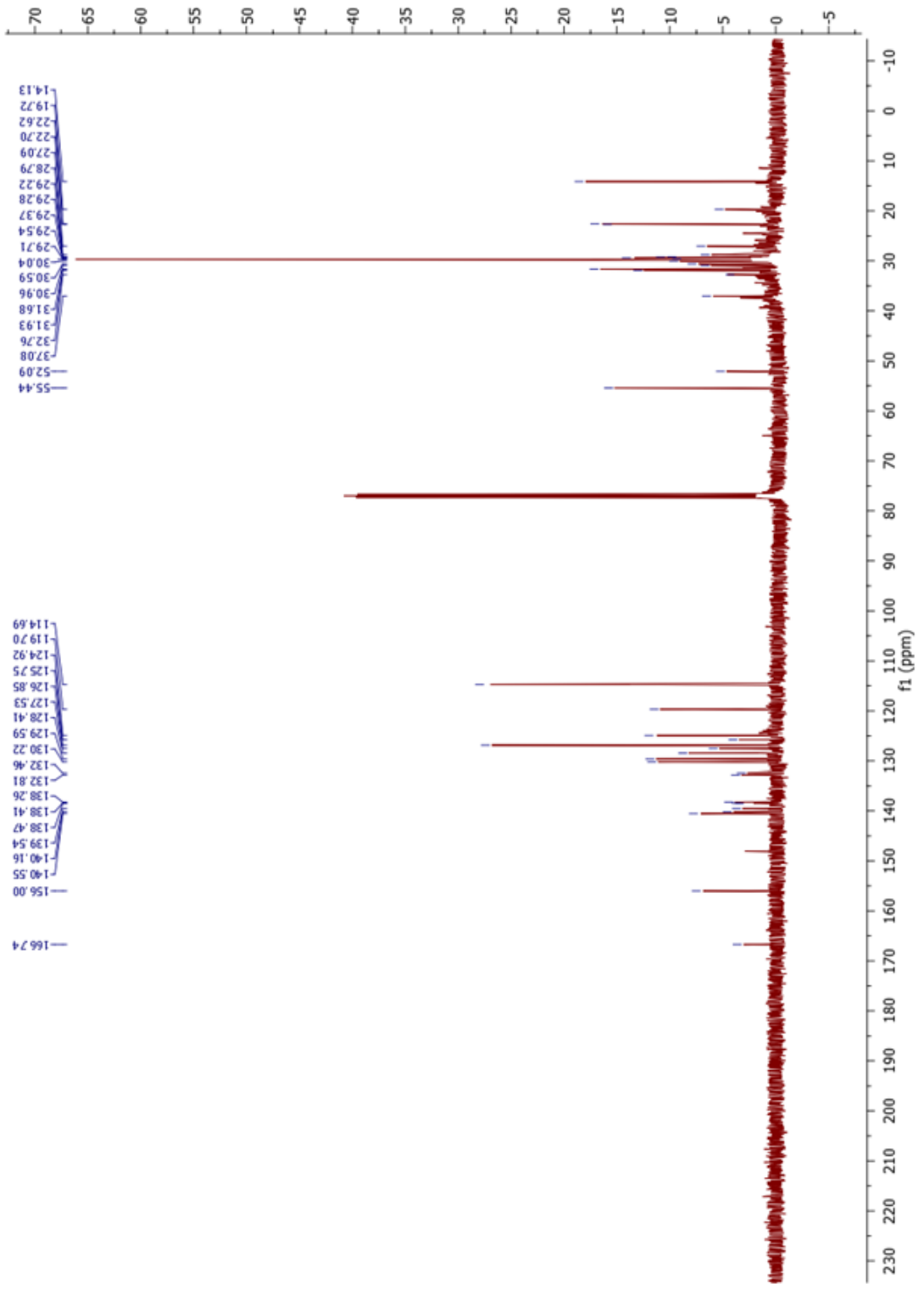

23-) (EA58) ^{1}H NMR of 4-(5'-(4-(bis(4-methoxyphenyl)amino)phenyl)-3,4'-dihexyl-[2,2'-bithiophen]-5-yl)benzoic acid

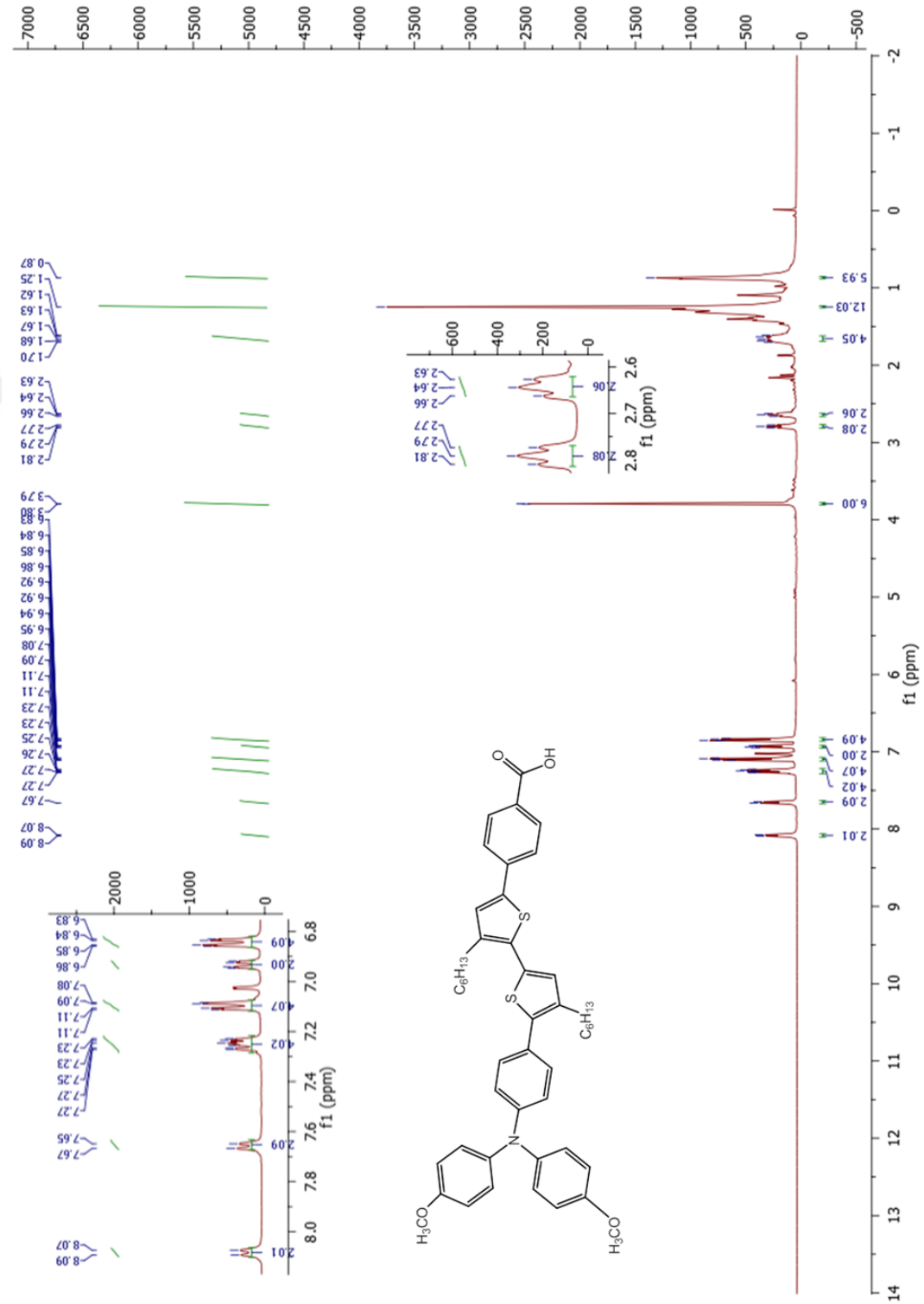

24-) (EA58) ^{13}C NMR of 4-(5'-(4-(bis(4-methoxyphenyl)amino)phenyl)-3,4'-dihexyl-[2,2'-bithiophen]-5-yl)benzoic acid

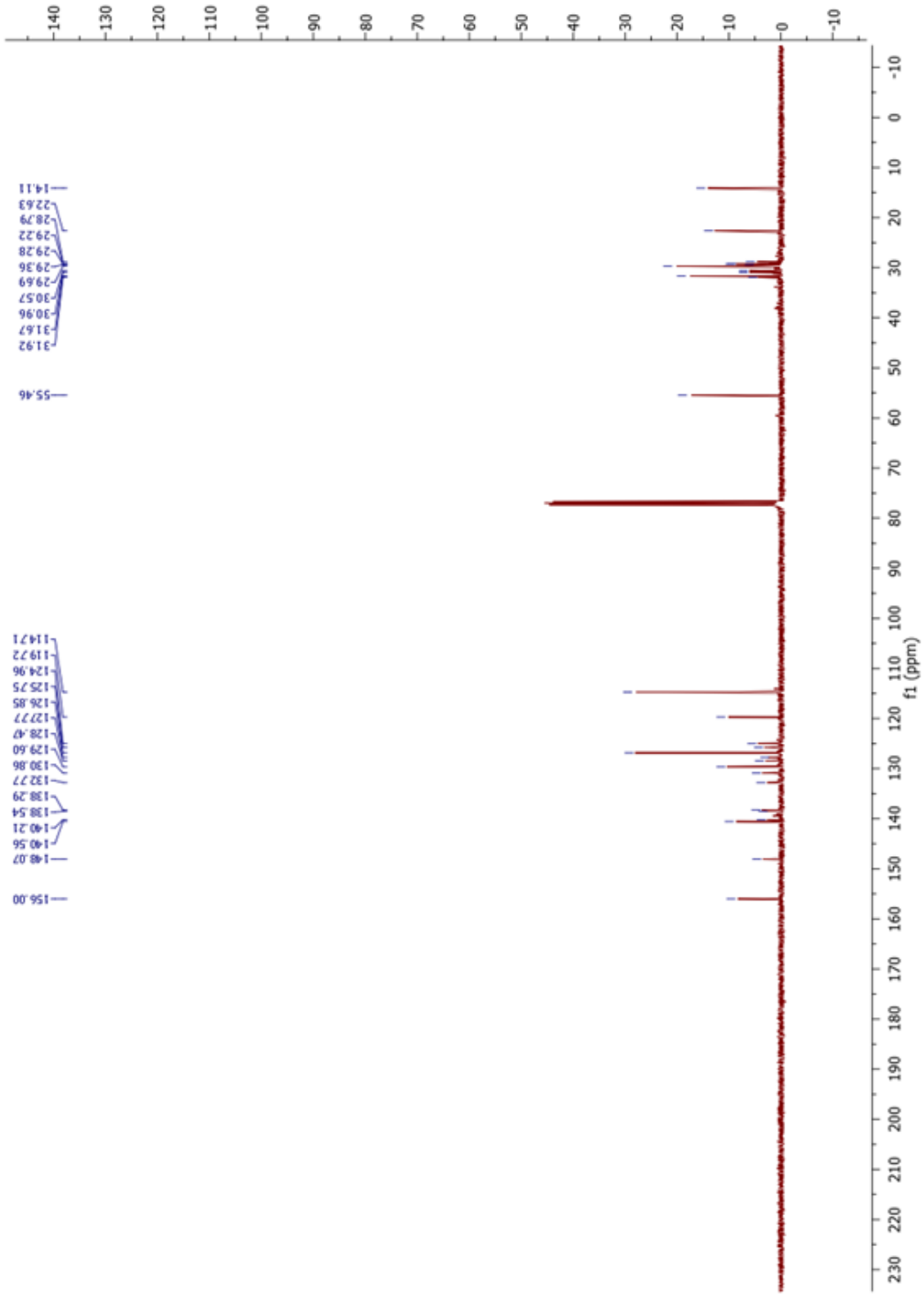

CURRICULUM VITAE

Emre ARKAN

List of Publications:

1. Electrospinning of $Cu_2ZnSe_{4-x}S_x$ Nanofibers by Using PAN as Template DOI:10.1016/j.matlet.2014.10.132
2. Fabrication of Quaternary Cu_2FeSnS_4 (CFTS) Nanocrystalline Fibers Through Electrospinning Technique DOI: 10.1007/s10853-014-8637-x
3. Earth-Abundant Cu_2CoSnS_4 Nanofibers for Highly Efficient H_2 Evolution at Soft Interfaces DOI: 10.1002/cnma.201500113
4. Water Affinity Guided Tunable Superhydrophobicity and Optimized Wettability of Selected Natural Minerals Accepted by Journal of Coatings Technology and Research, DOI: 10.1007/s11998-018-0115-y

Seminars& Symposiums:

1. Investigation of Tunable Wetting Properties of Modified Natural Mineral Powders - Porous Powders Materials (PPM) Izmir-TURKEY (17 September 2015)
2. Poster Presentation: Design and Synthesis of Carbazole & Phenotiazine Derivatives and Evaluation of Their Anticancer Activity (27PB-pm155) The 135th Annual Meeting of the Pharmaceutical Society of Japan Kobe-JAPAN (25-28 March 2015)
3. Poster Presentation: Novel Hole Transport Materials for Perovskite Solar Cells International Workshop on Flexible Bio- and Organic Printed Electronics (IWOBEO), Selcuk University Konya-TURKEY (1-3 May 2014)
4. Poster Presentation: Modified Silica Sols as Emulsifiers - Frontiers of Silica Research, Chalmers University of Technology and EKA Chemicals AB Gothenburg-SWEDEN (15-16 March, 2011)